Politecnico di Torino

MSc in Automotive Engineering

Model-based vehicle dynamics control system and states estimation for 4WD Formula SAE electric vehicle track performance assessment

Candidate: Andrea Masoero

Supervisors: Prof. Andrea Tonoli
Eng. Raffaele Manca

Academic Year 2024/25

Contents

List of Figures

List of Tables

dedicated to

Abstract

Yaw Control is an interesting topic especially when applied to 4WD electric vehicles. Given the high number of degree of freedom, the torque distribution can be performed according to many ways, both with good engineering practices or with numerical optimization strategies. The need of a validated Yaw Controller for Squadra Corse PoliTo has become important since the level of the competition in Formula Student is increased in the last years. This controller is meant to help the driver both during tight turns, by make the car to rotate faster, and high speed cornering, with a stabilizing effect.

To make proper advantage of the Yaw Control, vehicle sideslip angle information should be used as a safety measure. An Extended Kalman Filter and a combined estimation strategy was implemented in past works, but was lacking of reliability and some measure had been taken in order to properly validate this system.

This work aims to propose a validation method, with a track performance assessment of both the Yaw Controller and the sideslip angle estimation, also presenting state-of-the-art methodologies for Yaw Controllers, estimators and model validation techniques. Moreover, a deeper detail description of SC vehicle control system is performed, giving some hints based on the last years experience of how it can be evolved. In the end some strategies for different estimation strategies blend, between dynamic,kinematic and combined, are suggested based on the experience and on the possible working condition of the vehicle.

The work has been divided into two main moments: data acquisition and data processing, which comprehends the sideslip estimation enhancement. Data was acquired in a dedicated test session, comparing passive vehicle and controlled performance. The controller was flashed on a dSpace MicroAutobox2 that is usually employed by the team as VCU. Sideslip angle measurement is performed, via a Kistler SF-Motion sensor, to provide the information to the controller and retrieve data for the sideslip estimation validation. During data processing, important KPI analysis is performed to evaluate the behavior of the controller and estimator, while tire temperature information has been used to enhance the performance of the EKF.

The results show that the controller is very effective, also in the low grip conditions in which has been tested, with a reduction during a Double Lane Change maneuver in $IACA_{\delta}$, from 37.15 deg to 14.13 deg, and $\delta_{SW,max}$, from 104.3 deg to 35.0 deg with the vehicle in passive mode that was running at an entry speed of 53 km/h, while 54 km/h is kept during TV ON tests.

The performance of the EKF has been enhanced for all the test maneuvers, and Especially during DLC and slalom maneuvers. The GOF(NRMSE) value lowered from 1.2 up to 0.44 for a DLC and from 0.84 up to 0.39.

1 Introduction

Electric sport cars are intrinsically more dependent on vehicle dynamics control systems due to the high instant possible torque that can be delivered to the single wheel or to the differential. Being the electric motor widespread across the automotive population, mounted on mostly hybrid cars, but also BEV, the demand in advanced control systems architectures raised in the last decades, passing from the traditional traction control and ABS up to more innovative solutions of torque vectoring. If the vehicle is equipped with 4 electric motors driving one wheel each, the engineer has much more freedom compared to a 2WD car, leading to complex solutions but a final result in terms of performance that is much more satisfying. These controls can be applied both for racing performance, to increase the effective grip of a vehicle, or for road use mainly to increase the safety of a vehicle.

Form the 60's, in a parallel way to the automotive industry, was also expanding the field of mathematics and statistics that concerns the filtering and the estimation of a real quantity based on a set of measures, science of which Rudolph E. Kalman is the father with its well known in literature Kalman filter. Today, with the increasing cost of the materials, the automotive industry is much interested in replacing the actual physical sensors with 'virtual' sensor or estimators: mathematical recursive algorithms capable of estimating a variable of a dynamic system without directly measuring it, hence saving the cost of the physical sensor. The aim of this work is to present both these two aspects of current automotive industry and research field, with practical application that have been implemented in Squadra Corse, FSAE team of the Politecnico di Torino.

1.1 Formula Student

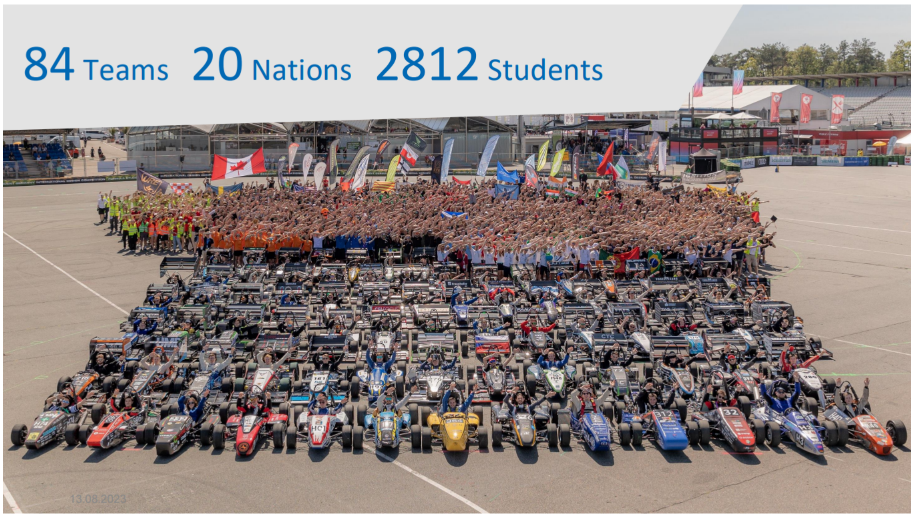

Figure 1: Formula Student Germany teams picture at the Hockenheimring

Formula Student is an engineering competition organised by the Society of Automotive Engineers in which teams more than 200 teams form all over the world challenge themselves and other by building a race vehicle and competing in major circuits situated in mainly Europe. The main objective of this championship is to train engineering students in a highly demanding, competitive and dynamic environment before entering professional environments.

To this competition can participate internal combustion engine vehicles, hybrid vehicles or fully electric vehicles, and all of them can compete in a manual driving mode category or in a Driverless Cup, in which the car becomes completely autonomously driven. ICEs and EVs compete in different categories while driven in manual mode but they compete against each other when driven in autonomous mode.

Each race is composed by different events that are evaluating the team and the car at 360 degrees. Among the events there are two major categories: static events and dynamic events.

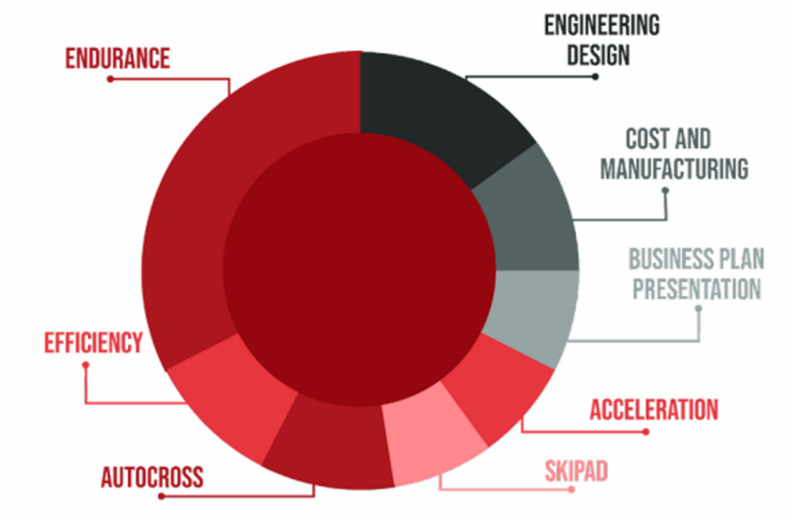

Figure 2: Formula Student race events

Static events are three: Engineering Design, Business Plan Presentation, and Cost and Manufacturing.

The engineering Design consists of presenting the design choices made during the season and the development of the prototype. Each category of the score has one or more judges that based on their experience in the automotive industry will give a mark to the work done by the division.

The Cost and Manufacturing has the target of explaining and justifying the team's costs of the current season, all related to the manufacturing of the vehicle, with a focus on the environmental impact and carbon footprint of the production of a particular vehicle subsystem.

Business Plan Presentation consists in a simulating a real business plan case study. The target is to find the best innovative business idea to sell the car or a a service relative to the car. An entire financial analysis is needed, from the idea, to the product one, passing from market forecast, marketing and future trends. The most appreciated ideas can come from the renewable field of energy, like reusing car parts to generate energy of any type or to guarantee high tech services like vehicle fleet command, communication and so on.

Dynamic events are four: Acceleration, Skidpad, Autocross and Endurance & Efficiency.

Acceleration event consists in a straight acceleration of 75 m, the lower the time and the higher is the score. In this events are truly important the weight repartition of the car and the automatic controls like traction control and launch control so that the driver has just to accelerate and control possible reactivity of the car without thinking about the actual grip.

In the Skidpad event the car has to run in a track formed by two symmetric circles, with a track width of 3 m and a diameter of about 18 m. This is done to test the lateral grip of the car. In this event it is crucial to have a light car, equipped possibly with 4WD and torque vectoring. The limit between a good result and a failure is very thin since all the teams are very near in performance because usually it is a test case during design to optimize car performance.

Autocross event consists in a complete lap around a cone delimited track with minimum corner radius of 4.5 m, slaloms and straights with maximum length of 80 m. They are very tortuous with tight turns and fast bits. The key for a good lap is a confident driver, capable to put the car on the limit with cold tires and only helped by traction control during strong accelerations and torque vectoring for the tight sections.

Endurance event is the most important of the race, in 3[1], since it consists in running a total of 22 km with a driver change in between of 3 minutes held after 11 km. Even this short distance is a challenge for the vehicle equipped with a low capacity battery pack compared to road vehicles (around 7 kWh against at least 45 kWh of a road vehicle). Moreover this vehicles have usually a low reliability due to the advanced technologies implemented and the inexperience of the team members. During the endurance a mid-high pace must be held in order to not overheat critical parts, save battery but also lower the energy consumption because points are awarded also for the efficiency of the vehicle.

(a) Engineering Design

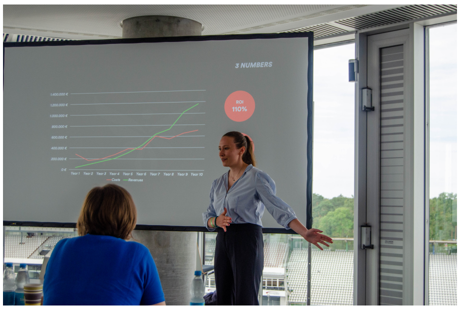

(b) Business Plan Presentation

(c) Autocross

(d) Endurance

Figure 3: some representative FSAE events

[1] © Formula Student Germany, wintermantel, seizinger

The races are held in the main circuits around Europe. For safety reasons the car are not driven on the actual track but on some of its section delimited by cones, in order to slow down the cars and guarantee minimum risk to the drivers.

Figure 4: Main formula student races of the championship

The most important races are considered to be the ones held in Germany, held in the Hockenheimring, and Austria,held in the Red Bull ring, followed by all the others. The Italian race is held in Varano de' Melegari, at Dallara test track.

1.2 Competitors

Among all the teams, being the turn over of the people involved in the project very high, there is not always a fixed winner or a more frequent winner in the years. To win in formula student a team must have a validated and reliable architecture, both for the team composition and the car. Good documentation must be produced each year to trace different examined solutions, document faults and possible solutions.

The rule book allow to the engineers a lot of freedom concerning the design of the vehicle, so that the students can come up with innovative ideas that are sometimes a test bench for real road applications in the case of a collaboration with an OEM.

On this topic, in the last years, in Formula student has been more and more frequent the implementation of active suspensions, starting from a decoupled configuration, to control roll and pitch. This is particularly useful during the German race in which the track is particularly bumpy.

Another technical advancement that increases exponentially the performance of these vehicles is the utilization of active aerodynamics, especially high power solutions, up to 20kW fans where used to push or suck the air at the floor level increasing by almost twice the aerodynamic down force. This feature is a game changer because in this way a car of this type, that usually can have a maximum speed of 140 km/h and an average speed during a lap in a FSAE circuit of 60-70 km/h, can express a much higher grip at lower speeds by exploiting the aerodynamic features already at 30-40 km/h by generating an air speed under the body of over 100 km/h. It is also possible to supply the power fan directly from the HV battery pack without the risk of exceeding the 80 kW power request since the power ground effect can be progressively switched off when the car becomes more and more power-limited instead of grip-limited at increasing speed. Due to the high performance gap and the increasing volume an power and thus the voltage and speed of the fan, this solution has been limited to a max power of 500 W.

Active aerodynamics and active suspensions are very efficient if implemented together due to the high sensitivity to the ground high of a car that exploits aerodynamic power ground effect. A car that can dynamically adjust its ride heights to have a very stable platform for the aerodynamics is therefore a very high performance vehicle.

All the previously mentioned features, combined with a weight without the driver of less than 180 kg, 10 inches tires, proper suspension kinematics and an advanced torque repartition control can make these vehicles to achieve blistering performances: 0-100 km/h in less than 2.5 s, maximum lateral acceleration of over 3 g, maximum longitudinal deceleration of 4 g.

The performance benchmark in 2024 is established by some teams like FS Team Tallinn, from Tallinn University of Technology and Tallinn University of Applied Science, AMZ racing, from ETH Zurich, TU Graz racing from Technical University of Graz and Yohanneum Racing Graz from University of Applied Sciences of Graz.

(a) ETH Zurich

(b) TU Graz

(c) UAS Graz

(d) UAS and TU Tallinn

Figure 5: Top FSAE teams

This vehicles are equipped with 4 in-wheel electric motors, a carbon fiber monocoque, full aerodynamic package, active suspensions for roll and heave control and active aerodynamics and all of them have a weight of about 170 kg without the driver. The cars from Tallinn and Zurich can run also in fully autonomous mode, hence provided with superior control system strategies.

1.3 Squadra Corse PoliTo

Squadra Corse is the FSAE team from Politecnico di Torino, competing in the EV class. Founded in 2004, the team raced in the first event in 2005 with the first internal combustion prototype SC05.

Figure 6: Squadra Corse past prototypes

From that moment, a constant evolution has been brought to the prototype:

- in 2009 the first hybrid prototype was built, the SC08H, world title winner.
- in 2012 the first completely electric powertrain was introduced with the SC12e.
- in 2013 the first carbon fiber monocoque is manufactured.
- in 2014 the first complete aerodynamic package is studied with the SC14.
- in 2017 and 2019 the car won the Italian race in Varano.

In 2023 the team decided to not take part at any race event and the season was devoted to a testing session that lasted more than 40 days, successfully completing more than 300 km that were useful to enhance the reliability of the car, update and test all the control systems and test the sensitivity to tire setup angles and pressures.

1.4 SC24 prototype Overview

In 2024 Squadra corse raced in Austria, Germany and Italy with the last prototype, SC24, named Andromeda.

Figure 7: Squadra Corse 2024 prototype: Andromeda

Main vehicle data	
Mass without driver	207 kg
Front mass repartition	45%
Wheelbase	1.525 m
Track	1.202 m
Center of gravity height from ground	0.28 m
Tires	185/40 R14 slick
Rims	R13 magnesium alloy
Aerodynamic lift coefficient	4.8
Aerodynamic drag coefficient	1.5
front aerodynamic balance	58%
Nominal HV battery pack capacity	7.7 kWh
Nominal HV battery pack voltage	564 V
0-100 km/h	2.6 s
Maximum speed	122 km/h
Maximum lateral acceleration	2.5 g
Powertrain type	Electric 4WD
Maximum motor power by data sheet	35 kW
Maximum regenerated power	40 kW
transmission ratio	14.69
Autonomous mode	not available

Table 1: SC24 vehicle data

This vehicle had some reliability problems in the first part of the season due to high sensibility to magnetic interference and water infiltration during heavy rain in FSG. Apart from these episodes, showed both performance and resilience under heavy rain in FSATA and allowed the team to retrieve the data for this work. In general is characterized by an inefficient static weight repartition, that creates undesired understeering behavior at low speeds and a oversteering behavior at high speed that will be solved in future projects.

1.5 SC24 Vehicle Control System

SC24 control systems have 5 macro-sections: MCB and HVCB CAN communication, inverter CAN communication and control, Control Systems, Global Parameters and dSpace Log.

1.5.1 MCB and HVCB

The main can bus is responsible for the communication between the ECU and the low voltage electronic boards that acquire and condition the signals from sensors. In the MCB is included the board that governs the status of the TSAL (tractive system active light), fundamental component for the safety of the vehicle since it indicates if the powertrain is effectively energized and ready to run or not.

The state machine that determines the state of the vehicle itself is implemented here. The car can be in 5 states: LV ON, Precharge, HV ON, RTD, Discharge.

In LV ON state the powertrain is not energized, the car is safe to touch and the TSAL is steady and green since the voltage across the DC bus is lower than 60 V. After a first push of the RTD button, one of the two AIRs (accumulator insulation relays) and the precharge relay close to allow the voltage across the DC bus to progressively equalize the one at the output of the HV battery pack, this is the precharge state. When 60 V are reached across the DC bus the TSAL starts flashing red to warn people before touching the car. The Precharge state ends when the other AIR is closed too, thus the car enters HV ON state. In this state the car cannot move but the inverters and the motors are supplied with high voltage. This is the worst case for electromagnetic interference since the lowest control level embedded in the AMK inverters is switching at extremely high frequency to obtain an ideal duty cycle of 0. This problem can be solved by feeding the inverters only when a torque request is actually coming from the vehicle control system section, but this was not done for a lack of testing facility.

To definitely turn on the car, according to the rule book a simultaneous actuation of the brakes and the push button must be done, to prevent in case of errors, bugs or faults that the car starts moving immediately after entering the RTD (Ready To Drive) state, the TSAL is red flashing and the motors can actually give torque and respond to the accelerator pedal. When the car is switched off again or has some kind of fault, the powertrain is progressively de-energized and the voltage across the DC bus is lowered while the car enters in the Discharge state. The discharge state should end after a maximum time following the rules.

This state machine directly influences the state machine used in the inverter can communication

Signals coming from the BMS (HVCB) are also processed here and are mainly used for two things: error detection and measurement of bus voltage and bus current. These last two will be particularly useful for the SOC estimation.

Other important signals used in the section are the steering sensor signal, the brake line pressure signal, the two throttle signals, many temperature signals coming from both LV battery and HV battery, IMU signals, GPS signals.

In this section can be commanded the switch on of the pumps and fan for the main cooling system and the fan for the battery cooling system, as well as the brake light switch on.

1.5.2 Inverter CAN communication

In the car there are 2 more can bus, related to front inverters and motors and rear inverters and motors. The split between the two buses was performed for reliability reasons in case of a failure on one line, at least the car is able to continue to run at lower power to complete an event.

In this section, each inverter is controlled at high level by a FSM that has the main objective to manage possible errors arising in the inverters during the operation. 4 out of the 6 states mirror pretty well the states of the car state machine that was described in 1.5.1, only in state 4 the inverter can make a current request to actuate a torque. State 5 and 6 are error states named 'soft error' and 'hard error'. An intermediate error can be reset without an external intervention and can be due to a minor fault like the loss of supply. A hard error is latched until a manual reset is done by performing a power cycle of the low voltage system.

The motors are speed controlled because it is easier to implement with respect to a torque control, since once the target speed is reached automatically the inverter lowers the motor torque to not overcome the target speed. It is important to remind that the vehicle control system is a dynamic control system, not a kinematic control system. Thus, it produces torque requests that will be used as torque limits in the lower level speed control of the motor to reach a target speed equal to the maximum of 20000 rpm, in case of positive torque request, or 0 in case of commanded regenerative braking. This is also good from the safety point of view since the motor cannot spin in reverse, thus the vehicle cannot go rearwards, that is in effect banned by the rule book.

The behavior of the lower level controller can be checked by looking at the two feedback current signals from the inverter, the torque current and the magnetizing current using the well known eq.1 that links the dqframe currents to the torque in an IPM motor

$$T_e = \frac{3}{2}p\lambda_m i_q + \frac{3}{2}p(L_d - L_q)i_d i_q = K_t i_q + \frac{3}{2}p(L_d - L_q)i_d i_q \tag{1}$$

Where p is the pole pair number,λ_m is the flux linkage, K_t is the torque constant given by the manufacturer, $L_{d,q}$ are the coil inductance in dq frame given by the manufacturer, i_d is the magnetizing current and i_q is the torque current. The motor speed control characteristic is shown in fig.8

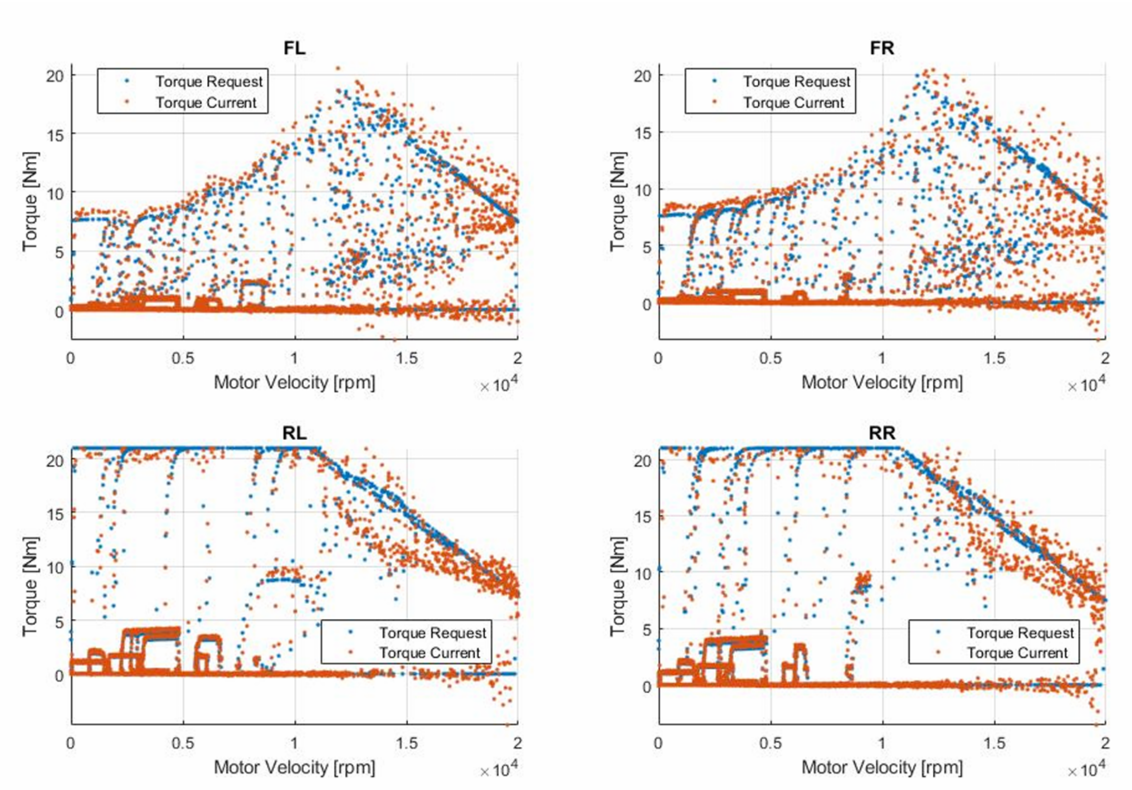

Figure 8: motor speed control characteristic

This figure shows how the torque request signal is followed by the motors output torques with a sufficient precision. The blue dots represent the requested torque while the orange dots represent the output torque from the torque current signal. Both the signals are plotted in function of the motor speed. The good overlay between the two signals show the correct functioning of the motors speed control, since the motors return what the Control System asks them.

1.5.3 Global parameters

In this section, all the possible internal parameters of the control system are initialized. This parameters contain vehicle major characteristics and tuning parameters related to Power Control, Launch Control, Traction Control and Torque Vectoring.

Grouping all these parameters in a single control subsystem is particularly useful with real time interface programs, when the control system has been compiled and flashed on the ECU, so that, being a specific location is chosen to be equal among all these constants, it is much easier to access to that constant and change its value in ControlDesk. A more efficient way to do this, is to load the parameters into datastore memory initialized in the Matlab workspace at code generation time.

1.5.4 dSpace Log

The used ECU is a MicroAutobox II, by dSpace, a general purpose ECU commonly used for control testing and rapid prototyping environment. This ECU gives the opportunity to log a maximum of 250 signals sampled at 100 Hz, single format. In this section, among the logged signals we can find some sensor signals, some error message and code from the inverter CAN and HVCB, some internal control system signal useful for debug purposes and many others.

1.5.5 Control Systems

In Control Systems section can be found a cascade architecture of Power Control & Launch Control, Torque Vectoring and Traction control in parallel with a Velocity estimator, longitudinal slip estimator and vehicle sideslip estimator as in fig.9.

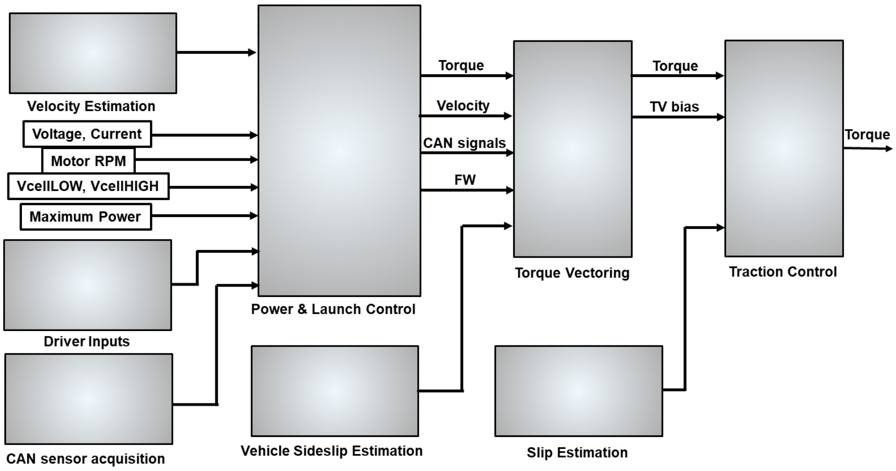

Figure 9: SC24 control system architecture

1.5.6 Power Control

The Power control is divided into two subsystems: Feedback and Feedforward.

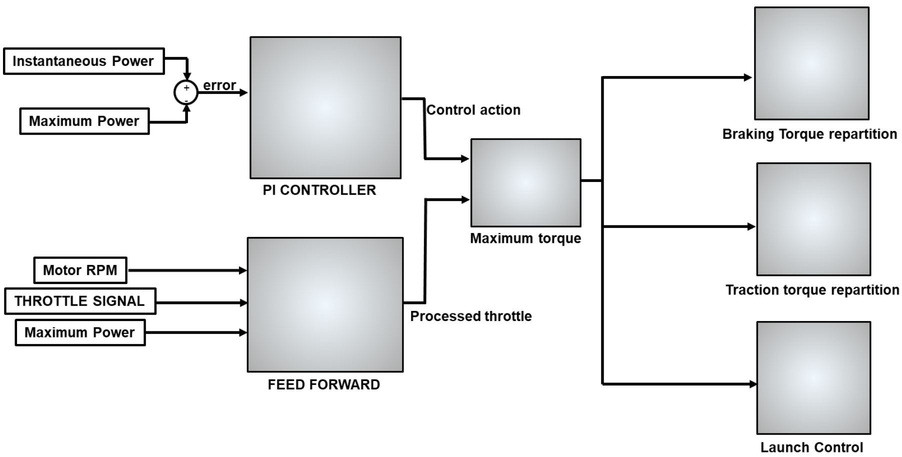

Figure 10: Power Control architecture

The Feedback control is made by a discrete PI controller based on the error between a moving average of the actual power required at the DC link and the maximum power. The controller output is saturated to negative values so that it will not increase the power request when a low throttle is applied. Due to the architecture of the controller and the high responsiveness of the electrical system of the car, a lot of power fluctuations where common. The power limit had to be set to 75 kW since the overshoot on the moving average of the signal was circa of 5 kW, this was done to ensure rule compliancy until 2023 (power limit of 80 kW). In the end this controller provides perfect tracking at steady state conditions due to the integrator, but it is inefficient in the compromise between reactivity and overshoot, since 5 kW were lost at steady state to compensate the overshoot during transients. Take into account that fast power transients are happening only in case of wheel slipping, due to the high peak rotational velocity.

The Feedforward calculates what is the reduction in the throttle signal such that, assumed equal and mean the rotational velocity of the 4 motors and efficiency of the powertrain of 0.8, the throttle signal output is translated in a total torque on the 4 motors that multiplied by the mean rotational velocity and divided by the efficiency it does not overcome the maximum power. The feedforward was added to the previous architecture in order to keep the same reactivity of the controller without limiting the maximum power to 75 kW. To the feedback control is then given the duty on fast transients, since it limits the power looking at the wheel or motor speed a priori.

One problem of this whole architecture encountered during Acceleration disciplines, is that after about 2 s in which a motor is giving 21 Nm, the lower level AMK control raises an error code and lowers its power output for thermal protection. This spoils the high level architecture since it is completely lost power tracking at steady state due to the fact that the Feed forward controller commands an impossible torque on the rear wheels, that is just saturated by the lower level controller. This resulted in a power loss at the end of the acceleration of about 10 kW, not acceptable.

The final solution that brought to a complete, stable tracking of a maximum power of 79 kW, was to deactivate the feed forward controller when the error code arises, that is fine since after 2 s the steady state was well reached, and let all the control duty to the feedback only. In this way the feedback control can increase the torque con the front wheels instead of giving more on the rear wheels in order to match the power reduction due to lower level protection mode from AMK.

The whole system has been validated in 2024 early season. Some work should be done to correctly join the power control during regenerative mode, that has the aim to avoid overvoltage or overcurrents on the DC bus and during an endurance increase the power that can be regenerated via a one-pedal drive mode.

1.5.7 Launch Control

Launch control is engaged during straight accelerations to correctly split the torque between front and rear axle. It is again a combination of two subsystem: feedback and feedforward.

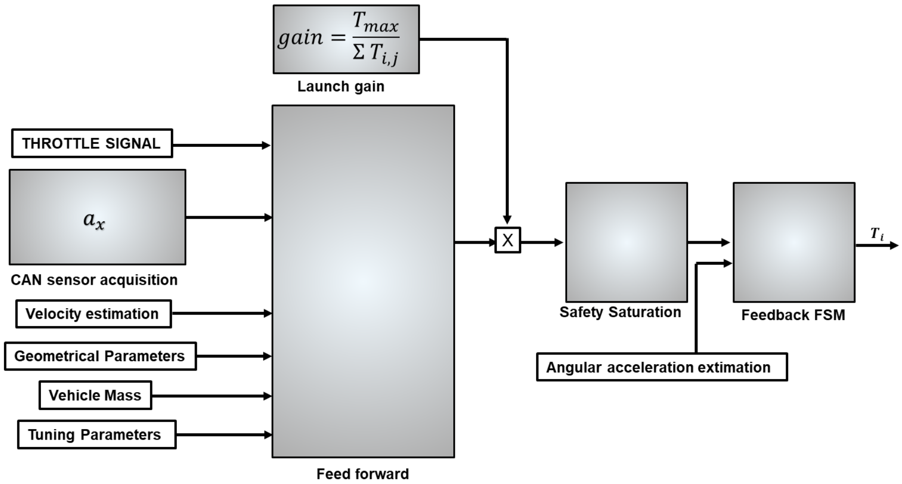

Figure 11: SC24 Launch Control architecture

The feed forward contribution is a model based torque distribution algorithm that estimates the maximum torque that can be commanded on one wheel to exploit the maximum longitudinal force guaranteed by the grip, taken from tire data, and the estimated vertical force. This subsystem do not guarantees the stability at steady state and is particularly susceptible to low grip conditions found with low tire temperatures or damp track.

The feedback contribution has the duty only to reduce the torque in case of slipping. It is implemented by a 4 state FSM in StateFlow, a slip controller specifically tuned for longitudinal application only, and it is independent of the tire or vehicle model, thus guarantees stability also in low grip applications.

The whole system has been validated in the 2024 season, with the opportunity also to extend this logic to the lateral and combined application in the lower level Traction Control.

1.5.8 Yaw Control

The Yaw Control is responsible for the torque repartition between left and rear sides and partially also on front and rear. It is composed by a reference calculation, a feedback controller a feedforward controller and a torque allocation function.

For more information about the validation in simulation of this architecture refer to [3] and [4].

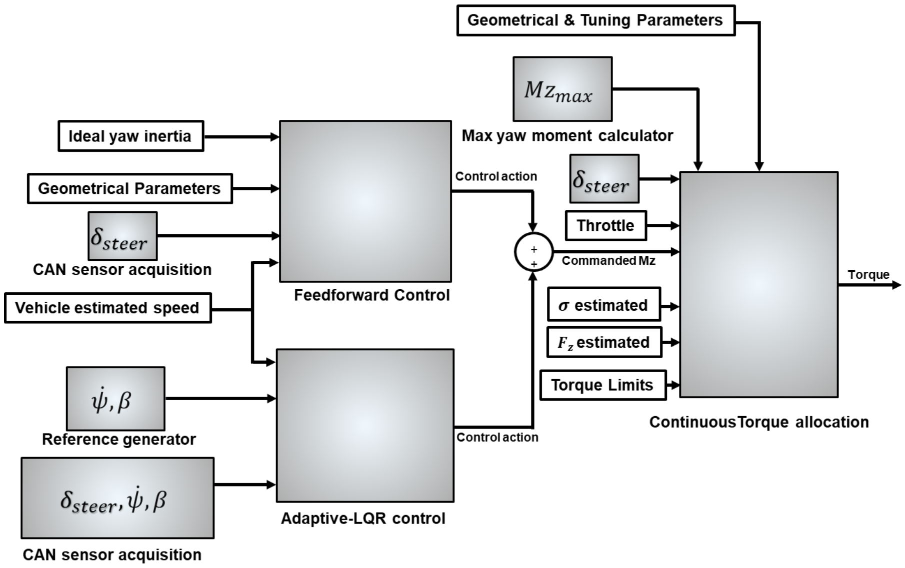

Figure 12: SC24 Yaw Control architecture

The reference generator produces the target yaw rate and vehicle sideslip to be fed as references to the yaw controllers.

To get the yaw reference, it uses the speed of the vehicle and steering angle to calculate the neutral behavior yaw rate as in eq.2.

$$\dot{\psi}_{ss} = \frac{V_x \delta}{K_{yr} l (1 + K_{us} V_x^2)} \tag{2}$$

This reference is saturated according to the lateral grip limit and so the lateral acceleration limit of the vehicle as in eq.3 and eq.4.

$$\dot{\psi}_{max} = \frac{\mu g}{V_x} \tag{3}$$

$$\dot{\psi}_{ref} = \dot{\psi}_{max} tanh(\frac{\dot{\psi}_{ss}}{\dot{\psi}_{max}}) \tag{4}$$

in these equations, μ is a tuning parameter as well as K_{yr}, to obtain the desired reference, more oversteering or more understeering, depending on vehicle characteristics.

The saturation ensures that a car already at the grip limit is not destabilized by a yaw rate reference that is not reachable due to its dynamic limits.

To get the sideslip reference, it uses the the measure or estimated sideslip of the vehicle in order to reduce it in case it exceeds a variable maximum value as in eq.5 and eq.6.

$$\beta_{ref} = \beta_{max} tanh(\frac{\beta}{\beta_{max}}) \tag{5}$$

$$\beta_{max} = 0.02 \mu g \tag{6}$$

In these equations, μ is the actual grip of the vehicle and can be a function of vehicle speed due to aerodynamics, but can be tuned as well to increase or decrease the maximum sideslip angle allowed by the controller.

1.5.9 Feedforward controller

The model based feed forward controller has the task of making the car more reactive due to its open loop contribution. It works in parallel with the feedback controller that instead guarantees steady-state stability.

The concept behind its design is to make the actual car to rotate like another ideal vehicle with a different yaw inertia, that can be tuned via a parameter. The ideal vehicle must have lower inertia if the wanted real vehicle behavior should be more oversteering and vice versa. The internal model of this controller is a linear bicycle model, with constant cornering stiffness. A more advanced model can be introduced taking care of possible oscillations in the output of the controller.

The transfer function of the controller is presented in eq.7 and eq.8.

$$FF(s) = \frac{M_{z,FF}(s)}{\delta_f(s)} = \frac{G_{des}(s) - G_{nom}(s)}{G_P(s)} \tag{7}$$

$$G_{des}(s) = \frac{\dot{\psi}_{des}(s)}{\delta_F(s)}; G_{nom}(s) = \frac{\dot{\psi}(s)}{\delta_F(s)}; G_P(s) = \frac{\dot{\psi}(s)}{M_{z,FF}(s)} \tag{8}$$

Where G_{nom}, G_{des} and G_p are all transfer functions, respectively between nominal vehicle yaw rate and steering input, desired vehicle yaw rate and steering input and nominal vehicle yaw rate and yaw moment input.

The magnitude of the output of the controller depends basically on two things: the difference between the ideal inertia and the vehicle inertia and the frequency of the steering input, hence its velocity. The faster the steering input, the higher the magnitude of the commanded yaw moment. This is very useful, but needs first of all a lot of driver training to be properly exploited. As an example, this controller is usually switched off because a driver that is not used to it would be scared of the reactivity of the car at high speed, since generally the higher the speed and the faster should be the steering wheel input by a proper racing driver. It must be noted that a parameter of the bicycle model is the speed of the vehicle, so the actuation of the controller increases when vehicle speed increases.

In order to mitigate this, two strategies can be actuated. A soft switch depending on vehicle speed can be implemented easily to progressively switch off the controller at high vehicle speed, but is not a clean model-based solution. Another solution can be to implement an internal model of the controller that takes into account the actual grip limit of the car and not only the linear cornering stiffness, for example by using a model in which the cornering stiffness saturates at high sideslip angles. This strategy would require an estimation of vehicle sideslip to retrieve the front and rear sideslips.

1.5.10 Feedback controller - ALQR

The feedback controller is a model-based Adaptive LQR and has the aim to guarantee steady state tracking. The internal model is based on a linear bicycle model with time-varying parameters as described in eq.9.

$$\dot{\mathbf{x}} = A\mathbf{x} + B_u\mathbf{u} + B_d\mathbf{d} \tag{9}$$

In which A,B_u and B_d are the continuous-time, time-varying matrices of the system, while $\mathbf{x}$ is the state vector composed by the sideslip angle of the vehicle and the yaw rate. This system has one control input u, that is the yaw moment M_z, and a disturbance, that is the wheel steering δ_w.

$$A = \begin{bmatrix} \frac{-C_F - C_R}{mV} & \frac{-C_F a + C_R b - mV^2}{mV^2} \\ \frac{-C_F a + C_R b}{J_z} & \frac{-C_F a^2 - C_R b^2}{J_z V} \end{bmatrix} \tag{10}$$

$$B_d = \begin{bmatrix} \frac{C_F}{mV} & \frac{C_R}{mV} \\ \frac{C_F a}{J_z} & \frac{-C_R b}{J_z} \end{bmatrix} \tag{11}$$

$$B_u = \begin{bmatrix} 0 \\ \frac{1}{J_z} \end{bmatrix} \tag{12}$$

$$x = \begin{Bmatrix} \beta \\ \dot{\psi} \end{Bmatrix} \tag{13}$$

The cornering stiffness used in this model is not constant but is derived from the lateral Pacejka model of the mounted tires. This model has some advantages compared to a symbolic Jacobian calculation. For example, there is a split between the Pacejka model that influences only C_f and C_r, this allows deeper understanding of the internal model and helps separating the effects of different parameters. It is a easy to understand, easy to analyze and very portable, flexible to a possible future change in tire model. Other tire models that can be implemented are, for example, a combined longitudinal-lateral Pacejka model, to improve the behavior in case of longitudinal ground forces (strong braking and acceleration), or a strongly different architecture like a FIALA tire.

Using the vertical forces on the tires and the sideslip angle of the tires, we can retrieve through the Pacejka model the cornering stiffness of all the tires.The cornering stiffness of two tires on the same axle are then summed up to obtain the cornering stiffness of the axle. This model takes into account both the possibility to have different sideslip angles between inner wheel and outer wheel due to toe angle setup or due to Ackermann steering geometry and also the vertical load transfer due to lateral accelerations, still keeping a linear-like computational effort.

This very same model is also implemented inside the dynamic estimation of the sideslip angle of the vehicle, inside the EKF.

The cost function minimized by the LQR is showed in eq.14.

$$\int_0^t (\mathbf{x}'Q\mathbf{x} + \mathbf{u}R\mathbf{u})dt \tag{14}$$

Q and R are weight matrices defined in literature as in 15 and 16.

$$Q = \begin{bmatrix} \frac{1}{\beta_{max}^2} & 0 \\ 0 & \frac{1}{\dot{\psi}_{max}^2} \end{bmatrix} \tag{15}$$

$$R = \frac{1}{Mz_{max}^2} \tag{16}$$

$M_{z,max}$ is the maximum possible yaw moment that can be obtained by commanding maximum positive torque on one side and maximum negative torque on the other. It can be assumed constant, with straight front wheels and generated by the longitudinal ground force caused by the maximum torque of the motor, in this case a maximum of around 2000 Nm can be obtained.

In reality the maximum traction torque is function of the state of the vehicle, depending on the speed the motor can run in flux weakening operation and thus the maximum torque is heavily reduced. About the regenerative torque instead, it might not be available in the first instant of the maneuver due to the possible high SOC of the battery, any commanded regenerative torque will increase the voltage on the DC bus due to the internal resistance of the battery and if the SOC is too high it may cause an overvoltage error, causing a DNF (Did Not Finish) for any discipline in the race.

1.5.11 Torque allocation

The feedback and the feedforward controllers give as output a yaw moment M_z, it must be translated into the torques of the electric motors such that the longitudinal forces at the ground level give rise to that moment. To do this, a Matlab function is used, implementing an heuristic local optimization method. It takes as inputs: M_z, the reference sum of the 4 torques, the flux weakening limits, the vertical estimated forces on the wheels, the estimated longitudinal wheel slips, the steering angles of the front wheels and two additional parameters s_1 and K.

The reference sum of four torques is directly commanded by the power control, it is crucial to not overcome this limit both during traction, because of disqualification, and during regenerative braking, to avoid overvoltages on the DC bus and the DNF. The torque split between left and right is then actuated such that both the reference sum of the four torques and the Mz are respected considering the front steering angles and a steady state condition in which the car is not accelerating. Take into account that, if we don't look at the vertical forces on the tire, the front wheels have much more potential to express a yaw torque due to the steering. In fact, when the two wheels are steered, the lateral component in vehicle reference frame of the longitudinal tire force can cause a yaw moment up to 8 times higher than the one expected if all the calculations where done without considering the steering angle. This is due to the fact that the over-mentioned component of forces have concord direction between left and right wheels and have an efficient lever arm with respect to the center of gravity of the vehicle. While this might be useful during traction, it is pretty disadvantaging during braking, since a longitudinal negative force with the turned steering wheel will result in an understeering moment.

The torque split between front and rear axle is done taking into account both the vertical force on the wheel and the slip of the wheel. The more a wheel is vertically loaded and the higher is the given torque, while the higher is its slippage ,the lower its given torque. To merge the vertical force and the wheels slip to obtain an actual 'weight', in the optimization meaning of the term. At low wheel slip values the vertical force is taken more into account, while at high slip values only the slippage is taken into account. This was done to promote a better collaboration between Torque Vectoring and Traction Control, that is in our interest since the TC would cut out the torque in case of wheel slippage but will not take into account the loss in yaw moment, while if we try to avoid wheel slippage already with the torque distribution then the risk of having it to be cut out is lower. As a last step, the torque is saturated to the flux weakening limits or the control limits. Due to this, the recommendation during a skidpad maneuver is to limit the power of the vehicle to 30 kW, to make it more drivable at the low speeds imposed by the event, but to keep a high possible limit torque of about 15 Nm out of the 21 at disposal. In this way, the throttle request will produce a total torque that can be distributed without the risk of cutting it, thus reducing the efficiency of the Yaw Control.

It must be pointed out that if the two wheels on the same side are slipping at the same rate, then this distribution will not have any effect since the total torque to be done one one side is already decided by the previous step and so for equal slippage at front and rear on the same side, then the torque will be more or less even distributed between front and rear.

The tuning parameters can partially modify the repartition between front and rear, taking into account that the car in question is a sport car and thus a mainly RWD must be implemented to avoid understeering behavior due to the torque request on the front axle. The target torque repartition between front and rear ranges between 40%f-60%r and 30%f-70%r.

This function is suitable for our application because is simple, efficient, has a continuous output and its reliable in most of the circumstances, in the sense that the actual yaw moment at the ground is coherent with the command yaw moment from feedback and feedforward controllers. While this function works pretty well in steady-state applications, as in a skidpad event, it is not optimal in case of high angular acceleration of the wheels since it overestimates the ground force. The ground force is lower in case of strong accelerations because of a higher contribution of the inertia of wheel and motor, thus a higher part of the commanded torque is accelerating the wheel and is not discharged at the ground. This effect is very hard to quantify but is in general minor.

A better solution for this application might be the implementation of a real-time proper optimization problem solution algorithm. An optimization problem formulation is characterized by an objective function and a set of constraints. In the standard form of such a problem, the function is a minimization function as in eq.17 and the constraints are a set of equalities as in eq.18.

$$min \quad f_{obj}(\mathbf{x}, s_i) \tag{17}$$

$$b = A \begin{Bmatrix} \bar{\mathbf{x}} \\ s_i \end{Bmatrix} \tag{18}$$

where $\bar{\mathbf{x}}$ is the vector of the optimization variables (in this case are the motor torques), s_i is a set of slack or surplus variables useful to convert constraint inequalities into equalities and b the vector of the known terms. Among the constrain equation, should be encoded the torque limits for each motor and the total reference torque limit from the power control. The final formulation of the problem depends wether if we want to minimize the error between the actual Mz and the commanded from the controllers, or wether M_z is taken as a constraint and in the objective function the slip and vertical forces are taken into account.

It must be pointed out that the best optimization strategy should take into account also the elliptical model of the tire, to avoid unwanted oversteering or understeering due to lateral grip loss as a consequence of longitudinal force exploitation. Moreover, a real-time optimization problem solver has a computational cost that is orders of magnitude higher than the simple function previously described, hence it couldn't be implemented since it is not available for code generation on the MicroAutobox II that is at team's disposal.

A partial solution to this problem can be the implementation of a fully connected part of a neural network. Neural Networks are much more computationally efficient than the recursive real-time optimization problem solver, they can be trained offline with the results gained from the optimizer and then loaded on the ECU for online applications. In this way the Neural Network can partially mimic the much more complex solver.

1.5.12 Traction Control & ABS

Traction Control and ABS have the aim of avoiding wheel slippage during acceleration or deceleration, to maximize lateral and longitudinal ground forces. The solution implemented in the vehicle uses a Fuzzy Logic controller as in fig.13.

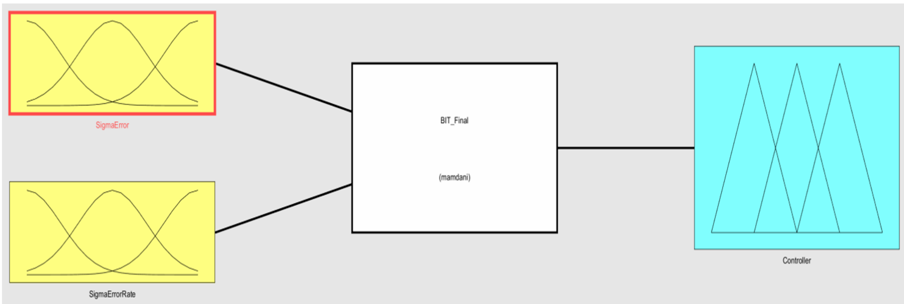

Figure 13: Fuzzy Logic controller structure

Each fuzzy logic controller takes as input the slip error and its discrete derivative and outputs a value between [0-1]. This value indicates the percentage of torque that must be subtracted to the input torque to obtain the desired behavior.

Talking about Traction Control, it is optimized in two conditions, straight acceleration and acceleration in turn. This requires the implementation of two fuzzy logic controllers per each wheel. Four level of slip error were identified, each represented by a membership function: Low Error (LE), Medium Error (ME), High Error (HE) and Maximum Error (MAXE). Six levels, instead, have been defined for the slip error rate: Negative High Error Rate (NHER), Negative Medium Error Rate (NMER), Negative Low Error Rate (NLER), Positive Low Error Rate (PLER), Positive Medium Error Rate (PMER) and Positive High Error Rate (PHER).

The controller MFs define the controller action. Also these MFs work between 0 and 1, since the goal of the control action is to reduce the input torque: at most it will be reduced of its entire quantity, with a controller action equal to 1. Five controller MFs have been defined: Low Control (LC), Medium Low Control (MLC), Medium High Control (MHC), High Control (HC) and Maxium Control (MAXC). For more detailed information about how the tuning was performed, see [5].

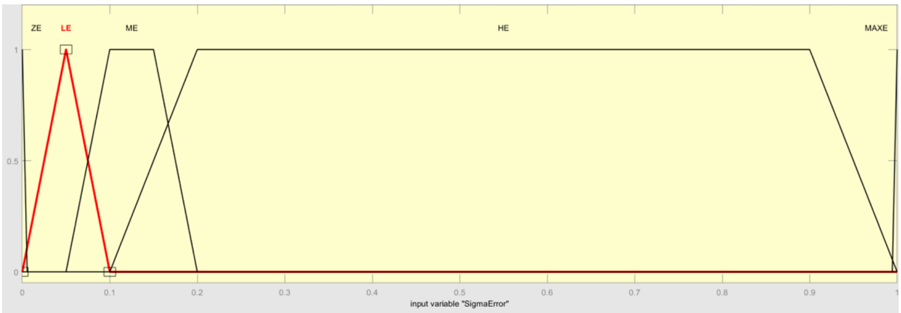

Figure 14: Error membership functions

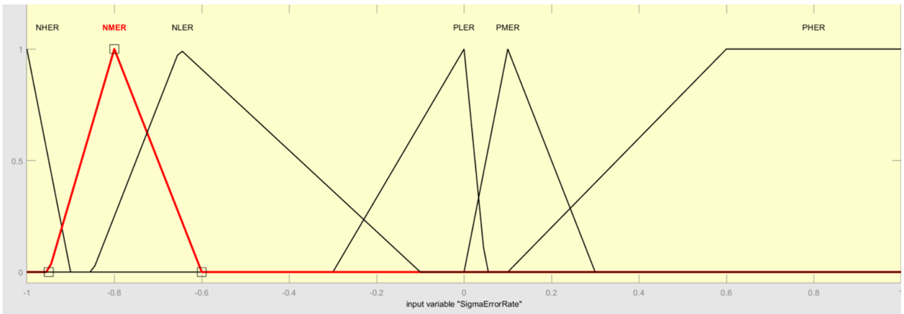

Figure 15: Error rate membership functions

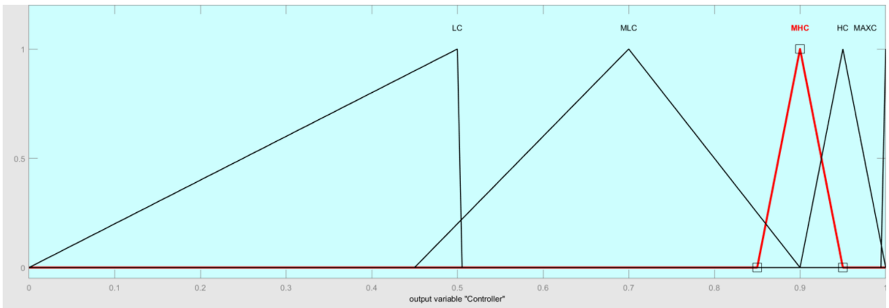

Figure 16: Controller membership functions

Talking about ABS, it is optimized in two conditions, straight braking and corner entry. It must be pointed out that an ABS system on a road vehicle works in a completely different manner with respect to what is implemented on SC car. In a road vehicle the ABS acts directly on the pressure inside the brake line, releasing it when wheel locking is detected. In SC vehicle the ABS is implemented only from the regenerative braking point of view since the control system commands the motor torques. To sum things up, ABS is less effective than Traction Control, while traction control is a life saver when a wheel starts slipping, we cannot tell the same for ABS when a wheel is locked. What can be said is that ABS can be essential in case of a one-pedal drive mode when maybe there is a difficulty from the driver in controlling the actual negative torque request.

Mechanical ABS is not allowed by the rules since the brake system is a safety critical system. The car in fact has to pass a technical inspection called 'brake test' in which the powertrain is deactivated while the vehicle is moving at a reasonable speed and the driver must press the brake pedal in order to lock all 4 wheels simultaneously. The test cannot be passed if mechanical ABS is embedded in the vehicle, because it would prevent the locking of the wheels. This inspection is meant to test the mechanical capability of the brakes and their correct functioning in case of panic braking, take into account that the trend in Formula student is to reduce as much as possible the size of the brakes and let the regenerative torque do the majority or sometimes all the job, in order to increase the efficiency of the vehicle. The effect of this trend is that majority of teams are under-dimensioning the brakes in order to just pass the inspection and save weight. This is not applicable to SC car, given its weight and faster SOH (State Of Health) decrement that a HV battery pack undergoes if high charging currents are commanded, that would require a complete rebuild of the battery pack every year if not multiple times during the same season.

About the activation of TC or ABS, they cannot be active simultaneously on the same wheel. The activation of one with respect to the other depends on the input torque, if that is positive then TC activates and vice versa.

1.5.13 Vehicle Sideslip estimation

The model chosen to perform sideslip angle estimation is a dual track model as in fig.17.

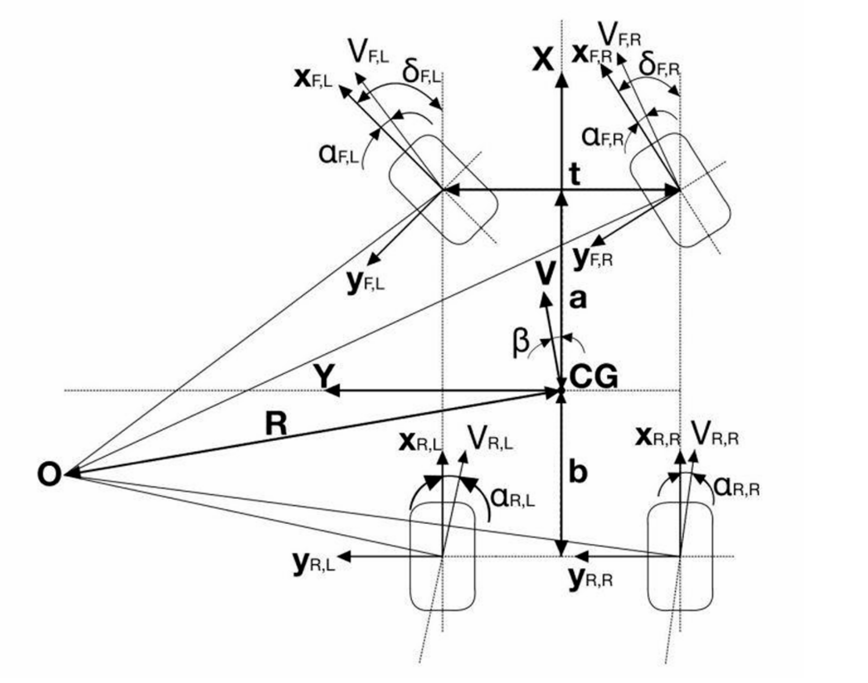

Figure 17: Dual track model [1][2]

The usage of this model is justified by the fact that FSAE vehicle undergoes to high lateral acceleration, thus the load transfer has a worsening effect on the total grip of the vehicle that cannot be ignored. Moreover, some of the assumptions behind simpler models (linear bicycle models) are not met during the vehicle normal working, since the track length of about 1.2 m is not negligible with respect to the radius of a skidpad of 9.125 m or even worse with the minimum turn radius during an Autocross of circa 5 m. The cornering stiffness of the tires are found according to a Pacejka model. The problems and the solutions related to this model will be further discussed in section 4.

The architecture consists in a kinematic sideslip angle derivative estimation, a dynamic estimation performed by an Extended Kalman Filter, merged together after being filtered with two low-pass filters.

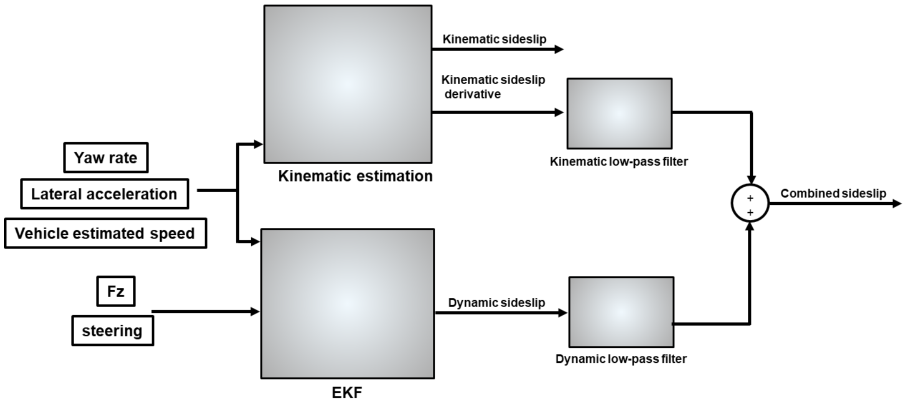

Figure 18: Vehicle sideslip angle estimation architecture

The kinematic contribution is meant to give good results in cases in which the internal model is not satisfactory in performance or sufficiently close to the real system. The EKF instead must guarantee the stability and convergence of the estimation at steady-state.

For more information about the validation in simulation of this architecture refer to [3] and [4].

The covariance matrix of the EKF has been tuned with a trial and error procedure, as well as some fine tuning of the filters.

1.5.14 Vehicle Speed estimation

Vehicle speed estimation subsystem is responsible for estimating the vehicle speed by taking into account the rotational speed of the motors and the accelerations from the IMU. It is implemented via a fuzzy logic system as in fig.19 from [6].

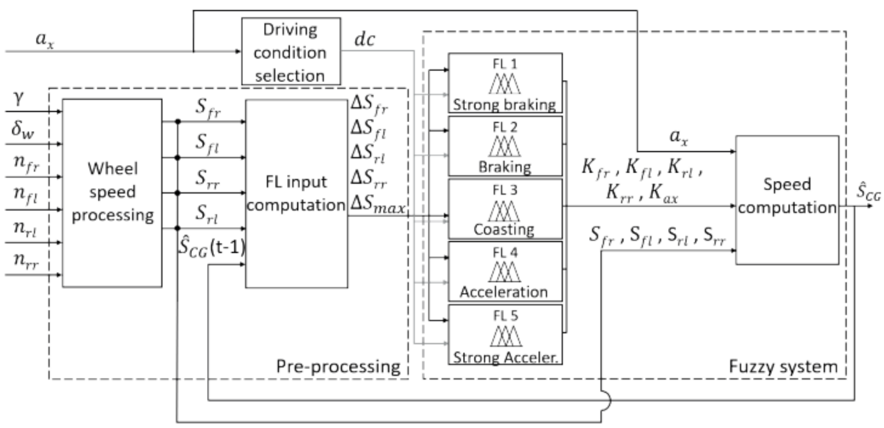

Figure 19: Fuzzy velocity estimation architecture

The linear speed of the wheel can be computed looking at the speed of the motor and the wheel radius. Assuming to have already an estimate of vehicle speed, it can be compared to the linear wheel speed to understand if a wheel is slipping, locking or neither of those.

A driving condition selection block is fed with the measurement of the longitudinal acceleration and allows identifying five different conditions: strong braking, braking, coasting, acceleration, and strong acceleration according to acceleration value.

According to a Fuzzy controller, tuned as in [6], to each wheel is given a weight stating how much reliable is its linear speed when it will be used to compute the vehicle speed as a weighted average.

A reasonable objection can be raised if this speed is used to calculate then the slippage of a wheel to be fed into the Traction Control or the ABS. To have a better vehicle speed estimation, less dependent on wheel velocities, GPS speed can be used.

This estimator has been validated in 2023 comparing its estimation with the measure of the the sideslip angle and speed sensor Correvit S-Motion by Kistler.

1.6 Thesis Outline

This work is structured as follows:

- Section 2 presents the State of the Art for vehicle State Estimation and Yaw Control Systems;
- Section 3 presents the track validation of the feedback part of the previously presented architecture for Yaw Control;
- Section 4 presents an enhancement proposal for the sideslip estimation EKF.

2 State of the Art

2.1 Yaw Controllers

Yaw controllers are widespread to improve vehicle handling in limit condition. With the advent of hybrid and electric powertrain this has become an even more interesting topic given the possibility to have multiple powertrain and different torque distribution. The goal of these algorithms is to compute a yaw moment Mz needed to reduce a yaw rate error with respect to an arbitrary reference. Usually it is computed with the neutral and kinematic characteristic of a bicycle model, as stated in section 1.5.8. Yaw Controllers can be implemented also for vehicle sideslip angle control as a safety measure to avoid too large angles at high speeds. We must remember that the larger is the sideslip angle and the higher is the non-linearity in the behavior of the vehicle and a normal human driver can find difficulties in controlling the car in such a situation.

The following categories are implemented for high level controllers, to which other two control layers must be complemented: a torque repartition layer and a lower level torque control of the motors.

2.1.1 PID controllers

The simplest method consists in a Proportional-Integral-Derivative (PID) controller, based on the yaw rate reference error and/or the sideslip angle error. The law governing the output of a PID controller is reported in eq.19 and a possible control architecture is reported in fig.20.

$$M_z = K_P e(t) + K_I \int_0^t e(t)\,dt + K_D \dot{e}(t) \tag{19}$$

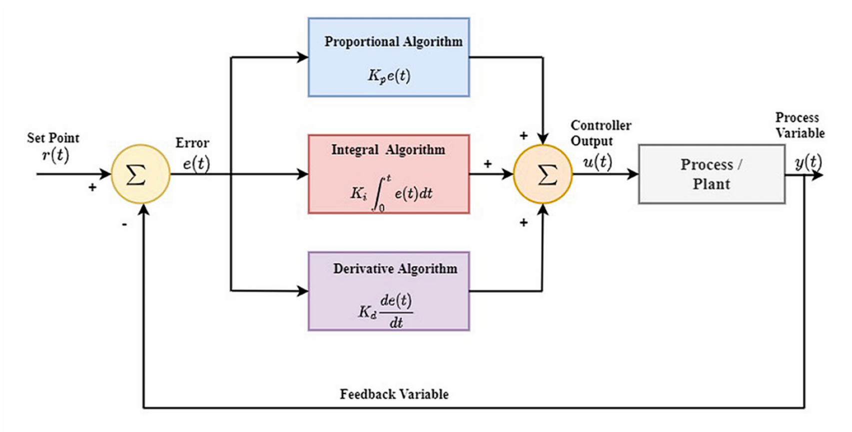

Figure 20: PID controller structure

PID controllers are simple and easy to tune, their behavior is linked to the gains K_P,K_I and K_D that can be tuned according to tab.2 and to tab.3, that reports the Ziegler–Nichols' method.

Parameter	Rise time	Overshoot	Steady-state error	Stability
K_P	Decrease	Increase	Decrease	Degrade
K_I	Decrease	Increase	Eliminate	Degrade
K_D	Minor Change	Decrease	No effect in theory	Improve if small

Table 2: Effect of the PID parameters on the system

We can start from a P controller. Let K_u be the value of K_P at which the closed-loop system oscillates with a constant amplitude. Let T_u be the oscillation period.

Controller	K_P	K_I	K_D
P	$0.5K_u$	-	-
PI	$0.45K_u$	$1.2\frac{K_P}{T_u}$	-
PD	$0.8K_u$	-	$\frac{K_pT_u}{8}$
PID	$0.6K_u$	$2\frac{K_P}{T_u}$	$\frac{K_pT_u}{8}$

Table 3: Effect of the PID parameters on the system

It is possible to tune this controller looking at the resulting damping ratio, since the whole system will behave like a mass-spring-damper setup.

PID controllers are robust against external disturbances, noise and change in plant parameters. Optimality of the control output is not guaranteed. The drawback of PID controller is that they are effective if the plant is LTI (Linear Time Invariant) meaning that the dynamic equations of the plant are linear differential equations characterized by fixed parameters with respect to time. The linear model of a vehicle, the bicycle model, is not properly time invariant since the A and B_d matrices reported in 10 and 11 have elements that depend on the vehicle speed. If speed is assumed to be constant, then the model is LTI. In this application this cannot be assumed, so the a PID controller with fixed gains is not a possible solution. A possible solution to this problem consists in a gain-scheduling approach, tuning the gains at different speeds for the wanted response and interpolating for intermediate speeds with a LUT (Look Up Table)

Generally, the controller is reduced to a PI only, since the derivative component has the effect to amplify error noise that is detrimental for stability. If the derivative term is considered, the error is usually conditioned with a discrete low-pass filter, this configuration is called PIDF controller.

2.1.2 LQR controllers

LQR controllers fall into the category of optimal controllers. Differently from the PID, they require an internal model of the vehicle which reliability affects the effectiveness of the controller itself.

LQR stands for Linear Quadratic Regulator, meaning that it minimizes a quadratic weighted cost function that includes the vehicle state and the control input, in this case the torque vectoring actuation of M_z. The minimization is usually referred to the weighted *Energy* of a signal, another name to call the weighted squared L_2 norm. In general, the objective is to minimize the summation between the weighted energy of the state vector, with nonzero weights on the Q matrix corresponding to the variables that are under control, and the energy of the control input. It is possible to reformulate the internal dynamic model of a plant in order to have the state error vector as new state vector, in this case LQR controller would minimize the Energy of the error.

Being a state feedback controller, the control gain is obtained by solving the Riccati equation. The equation is usually solved offline if the plant is LTI. If the plant cannot be assumed as LTI, the equation can be solved online, with some more computational effort, but with an adaptive model as in the case explained in 1.5.10, becoming an Adaptive LQR controller and showing much better performance in an extended range of speed. The architecture of such a controller looks like the one depicted in fig.21 from [7].

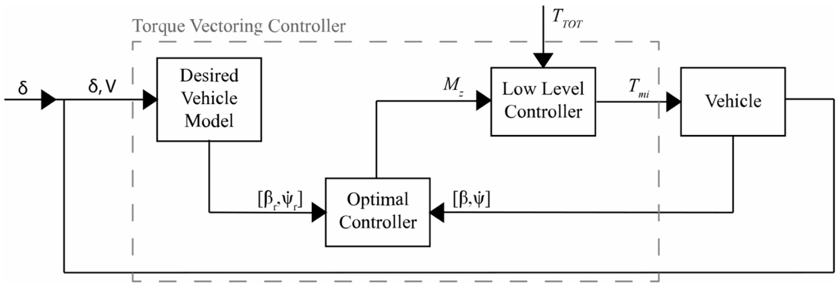

Figure 21: LQR controller structure

2.1.3 FeedForward controllers

This category of controller act in open loop, thus they cannot operate to ensure steady state stability. For this reason, their operation is much faster with respect to a closed loop control and are usually employed in systems like the one showed in fig.22 from [7], in which they are coupled with a state feedback controller of any sort and their aim is to improve the responsiveness and the reactivity of the whole control architecture, without spoiling the steady state stability.

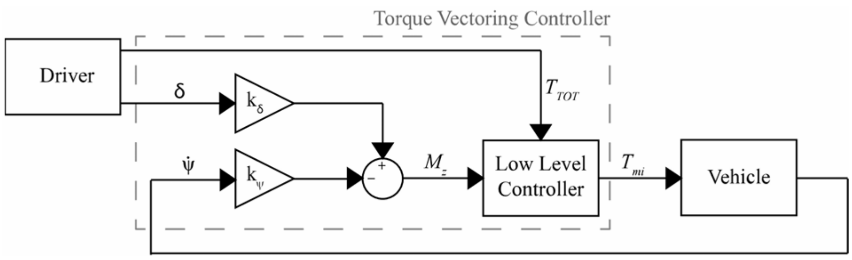

Figure 22: Feedforward controller structure

In fig.22, the feedforward branch is implemented via a Proportional controller on the steering angle imposed by the driver, K_δ, that is summed to the feedback contribution. An advantage of this solution is that it is extremely easy to tune and very drivable. Considering the perspective of the driver that has to handle the car on the limit, knowing that the more steering angle and the higher the yaw moment is very intuitive. The limit of this approach is that it is not adaptive with respect to the car speed, or in general it does not adapt to the vehicle state.

Another possibility is to have a transfer function instead of a simple gain, in this way the system has the possibility to react differently depending on the frequency of the input or depending on the system state, as implemented in 1.5.9.

2.1.4 Sliding Mode controllers

Sliding mode controllers are Variable Structure Controllers [8]. The output of this controller is binary, low or high, usually implemented with a sign function. The high control output (can be positive or negative) is meant to bring the state of the plant as close as possible to a state surface, composed by working points in which it is more convenient to operate the plant. After having reached this state surface, the plant will work while 'sliding' on it. In this formulation, the SMC gives rise to chattering phenomena when the plant is near the target surface, attenuated via low-pass filters. The advantage of this solution is that it is completely unaware of the plant characteristic, thus also unaware of plant and model discrepancies.

Evolutions of this architecture can be considered:

- SMC with boundary surface: The target surface has a thickness in which the control action is continous. Avoids control discontinuities but chattering is still a possible problem.

- SOSM Second Order Sliding Mode: The controller defines the control action first order derivative with the switching function, suppresses the chattering behavior.

- ISM integral Sliding Mode: Starts immediately with sliding motion, without the requirement of the reaching phase in which the system dynamic is not the ideal one.

2.1.5 Fuzzy Logic Controllers

Fuzzy Logic controllers is an approach regarding the design of control systems for strongly non linear systems for which the competence and experience of the designer prevails about the controlled plant is much more robust than the actual mathematical modeling. This logic do not rely on some deep mathematical theory or complex models, but on three main blocks: *fuzzification*, *inference engine* and *defuzzification*.

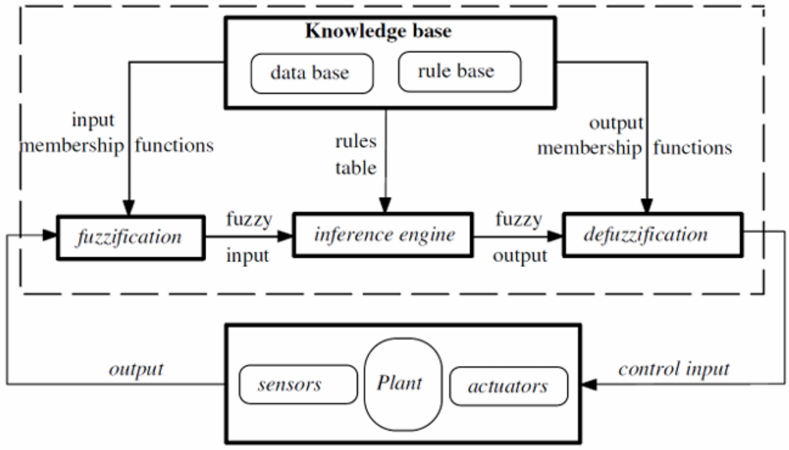

Figure 23: Fuzzy Logic controller structure

Fuzzification happens with the Input Membership Functions, where the yaw rate error, sideslip angle error and possibly their rates are the numeric variables and are converted into classes or language variables, A single numeric variable can belong to multiple classes with different importance.

The *inference engine* is a table of rules, in which the classes are combined to decide possible control rules. Since more classes for the same numeric variable can be activated, then more rules with different importance can be activated as well.

Defuzzification has the job of converting the activated rules into a numeric control output with the Output Membership Functions. The most used algorithm is the CoG method.

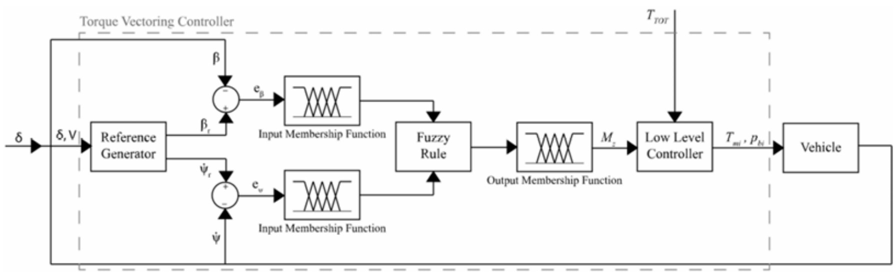

Figure 24: Fuzzy Logic torque vectoring controller structure

The tuning of such a system is much more effective if it is performed on the real system, given the uncertainties in the model, but this means that has a limited portability between systems.

2.1.6 NMPC controllers

Numerical Model Predictive Control is a widespread control strategy for strongly nonlinear systems, for which is defined a constrained control problem [9]. The difference between LQR and NMPC lays in the fact that NMPC optimizes the behavior of the vehicle in a finite time horizon, differently from LQR in which the optimization is ideally defined up to $t = \infty$. With NMPC controllers, at each time instant the cost function that takes into account the trajectory in the state space is minimized through the computation of a suitable control trajectory along the time horizon, but only the first element of the control trajectory is applied. It is easy to understand that this is substantially more computational expensive with respect to traditional strategies.

This controller gives the opportunity not only to optimize the squared L_2 norm of the state vector, but also to limit the operational domain of the plant by prohibiting or limiting some states, by performing what is called constrained optimization.

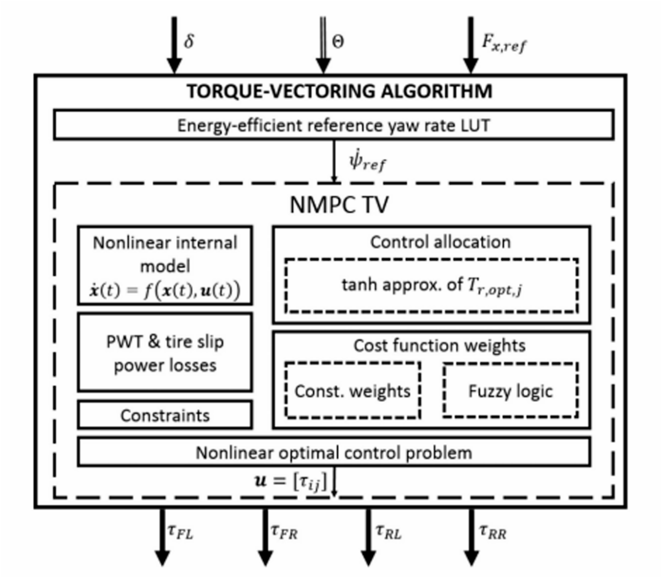

Figure 25: NMPC torque vectoring controller structure

A controller of this type can take into account powertrain layout limits in torque and power and overcome them with a suitably studied control strategy

Given the importance of the model in this strategy, the inconsistency between model and real vehicle can spoil the algorithm characteristics.

2.1.7 Neural Networks

Neural networks are the new frontier in control system strategies. They are the opposite of what is usually called 'model based' approach, since their performance is based on previously produced data on which the training is performed. These can be used in multiple ways:

- Internal models of other control architectures. NN can be trained to mimic the behavior of a physical system, let it be a model or a real system hat produce synthetic or real data.

- Real time tuning of other control system architecture parameters as reported in[10].

- Mimic the behavior of more complex and computationally expensive algorithms such as NMPC controllers. The Neural network can be tuned offline with the results coming from a NMPC that is not able to run in real time.

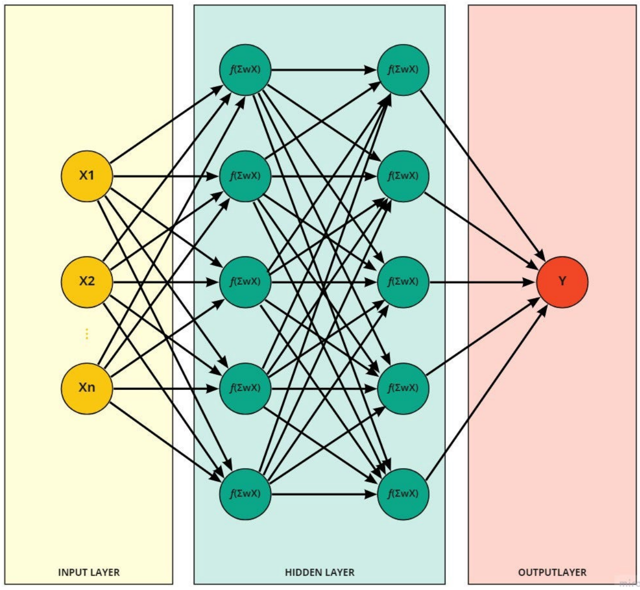

Figure 26: Fully connected Neural Network structure

2.2 Side slip angle estimation

The implementation of a Yaw Controller requires signals that are generally not available in a vehicle equipped with medium-low cost sensors. Among these missing sensors are present:

- Tire load sensor/ push-rod load sensors. Useful to have a better view of load transfer repartition during real operation, without using dynamic equilibrium equations and a better estimation of tire ground forces;
- Tire longitudinal and lateral forces load sensors. Useful in order to validate tire models in post-processing and use those models for suspension optimization;
- Tire temperature and pressure sensors. These would be useful to validate thermal models and to monitor in real time the proper functioning of the tires with respect to the camber angle setup;
- Sideslip angle sensor. This is extremely useful for proper handling control.

Some of the previous signals can be roughly estimated. For example front and rear axle total lateral force can be found with the lateral equilibrium of the bicycle model, while vertical forces can be estimated using IMU accelerations and vehicle estimated speed.

The sideslip angle of a vehicle can be measured in 2 ways:

- Two-antenna GPS system: the two points for which the GPS position is known provide both the speed vector in the inertial reference frame and the yaw direction of the vehicle, hence the sideslip angle can be derived as the angle between the yaw direction and the speed vector in global coordinates. While the two absolute positions measure can be relatively inaccurate, up to 5-10 m of inaccuracy, the fact that there is a fixed distance between the two can give accurate results when estimating the yaw angle as stated in [11]. The cost of this system can be up to €500.

- Optical sensor: Some optical sensors are available on the market. Their working principle is based on comparing two frames of the tarmac texture, taken at a known ad calibrated distance. The relative position of the two frames indicates the spacial movement, hence the speed and the direction. The cost of this system can be up to €15.000.

In order to make the yaw control of the vehicle satisfactory, sideslip angle estimation must be performed if direct measure is not available.

2.2.1 Kinematic estimation

One way to estimate the sideslip angle of a vehicle is by using the kinematical relationship of slip angle velocity, yaw rate, lateral acceleration, longitudinal velocity and road bank angle reported in eq.20 and the estimation can be performed as in eq.21.

$$a_{y,meas} = (\dot{\beta} + r)V_x - g\ sin(\phi_r) \tag{20}$$

$$\hat{\beta}_{kin} = \int \dot{\hat{\beta}}\ dt = \int (\frac{a_{y,meas} + g\ \phi_r}{V_x} - r)\ dt \tag{21}$$

With r that is the yaw rate and V_x is the longitudinal speed. For our specific application, the road bank angle is assumed to be null.

This method is of course robust against discrepancies between a vehicle and its model, tire model and track grip, since it is based on measured variables only. The problem of this approach is that the integral will for sure diverge due to bias errors in the sensors, no matter how limited it is.

2.2.2 Dynamic estimation

Dynamic estimation methods are robust in case of sensor errors, with proper tuning of the parameters the estimation should be stable and will not diverge. The problem of these approaches is that their accuracy depends a lot on accuracy of the internal model, on road condition, on the overall grip and so on. One of the most relevant dynamic estimation method is for sure the Kalman filter.

2.2.3 Kalman Filter

The Kalman filter is the best possible (optimal)estimator for a large class of problems and a very effective and useful estimator for an even larger class [12], and consists in a recursive procedure of prediction and correction. A possible problem for which the Kalman filter can be a solution is the *observer design problem*, in other words determine the internal state of a system looking only at its outputs. In the assumption that the system in question works with a linear stochastic difference equation like eq.22

$$x_k = A\ x_{k-1} + B\ u_k + w_{k-1} \tag{22}$$

and its outputs are described like eq.23

$$z_k = H\ x_k + v_k \tag{23}$$

where w_{k-1} and v_k are respectively process and measurement noise, random variables, that model both sensor noise and electrical circuit noise. These are assumed to be white and with normal probability distribution. In theory, A,B and H can change in time. The complete algorithm is shown in fig.27.

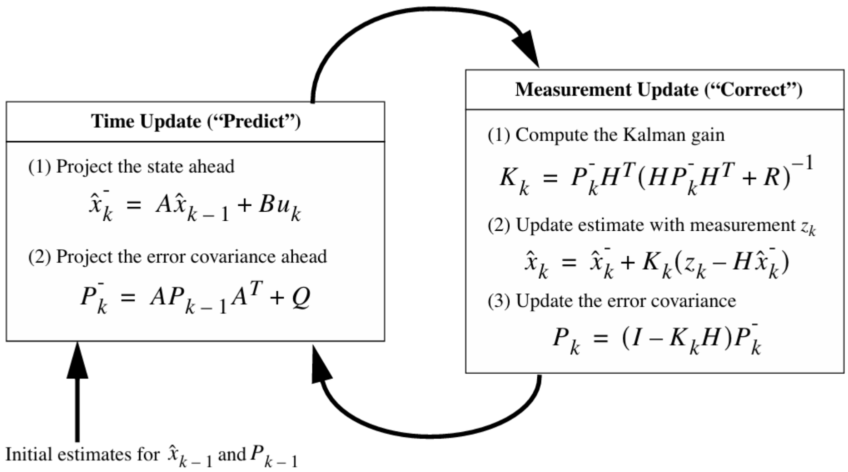

Figure 27: Kalman filter algorithm

2.2.4 Extended Kalman filter

When the plant is not linear, simple Kalman filter equations are no more valid, using a simple Kalman filter for estimating the state of a nonlinear system is not a solution.

The new plant in analysis is characterized by the following difference equation and measurement equation

$$x_k = f(x_{k-1},\ u_k, w_{k-1}) \tag{24}$$

$$z_k = h(x_k, v_k) \tag{25}$$

The solution to this problem is the Extended Kalman Filter, which recursive procedure is reported in fig.28.

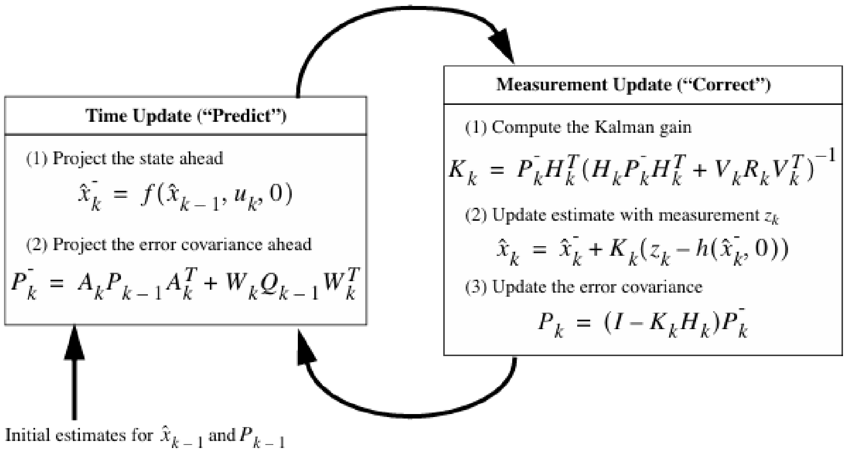

Figure 28: Extended Kalman filter algorithm

where A is the Jacobian matrix of f with respect to the state x, W is the Jacobian of f with respect to w, H is the Jacobian of h with respect to x and V is the Jacobian of h with respect to v.

In the specific case of this work, we have that

$$z = \begin{Bmatrix} r \\ F_{y,F} \\ F_{y,R} \end{Bmatrix} \tag{26}$$

where $F_{y,F}$ and $F_{y,R}$ are the axle side forces that can be estimated as in eq.27 and 28, since IMU signals are reliable these estimated forces can be assumed as measurements.

$$\hat{F}_{y,F} = \frac{m\ a_y\ b + J_z \dot{r}_{meas}}{a+b} \tag{27}$$

$$\hat{F}_{y,R} = \frac{m\ a_y\ a - J_z \dot{r}_{meas}}{a+b} \tag{28}$$

The result of the dynamic estimation is $\hat{\beta}_{dyn}$.

2.2.5 Combined estimation

As analyzed in [11], there is the possibility to join the kinematic and dynamic estimation, trying to keep the best characteristics of the two sides. The law is reported in eq.29.

$$\hat{\beta} = \frac{1}{\tau s + 1}\hat{\beta}_{dyn} + \frac{\tau}{\tau s + 1}\dot{\hat{\beta}}_{kin} \tag{29}$$

At lower frequencies the main contribution is given by the dynamic part, robust against bias errors, while at high frequencies the dynamic change of sideslip is done according to the kinematic estimation.

2.2.6 Neural Networks

The implementation of a Neural network for the estimation of the sideslip angle of a vehicle is becoming more and more common, especially for the latter implementation inside more complex models or inside other controllers. The neural network can be tuned offline with synthetic or real data.

One problem linked to this approach is the complete absence of a physical model, if a parameter of the plant is changed or there is an important mismatch, then the neural network must often be retrained, using time and computational cost.

2.3 Model validation

Model validation is the base for model based control and estimation design. A vehicle model can be validated under a limited number of operational conditions, for example the internal model inside the torque vectoring algorithm exposed in 1.5.10 works better for small values of longitudinal acceleration due to the pure lateral model that is taken into account for the cornering stiffness (no elliptical model is considered).

Another aspect can be related to tire data: if we expect that a vehicle is mostly driven under 'linear' conditions, then a linear characteristic of $C_\alpha(F_z)$ can be considered, if the vehicle will work under strong saturation of the tires and at with high tire sideslip angle the linear characteristic is no more satisfactory and will cause an overestimation of the performance.

The main task of validation is comparing the metrics with the accuracy requirements, these metrics can be vector norms, average residuals with standard deviation, coefficient of correlation, normalized integral squared error, normalized root mean squared error, maximum absolute error and many others.

2.3.1 Tests and data

According to [13], the following five test cases are defined as primary validation maneuvers:

- Steady-state lateral dynamics (low frequency);
- Transient lateral dynamics (wide frequency range steering input);
- Longitudinal acceleration(throttle inputs);
- Longitudinal deceleration (braking);
- Road disruption input (suspension kinematics and ride dynamics)

If the model that is interested by validation is a pure lateral rigid vehicle model, only the first two can be adopted.

The higher number of data and signals is acquired, the better it is. In case of a vehicle it would be ideal to measure:

- F_z, vertical forces on the tires or at the spring, assuming to be in steady-state and knowing the anti-roll and installation ratio of the suspension, it is possible to retrieve the vertical force con the contact patch.

- $F_{y,tire}$, lateral force on the contact patch, retrievable with load cells or strain gauges placed on the suspension control arms. These will be fundamental for tire model validation, since there is no known method to measure the single tire contact patch force starting from the accelerometers on board. Only the axle force can be measured by IMU.

- a_x,a_y and r are usually available from an IMU and Gyro.

- δ_W from a steering angle sensor and the LUT between driver steering input and wheel steering.

- β, from 2 point GPS measurement or optical sensor.

It is important to measure all the possible parameter of a model as well.

The position of the center of gravity, both in longitudinal and vertical can be measure with the weights. Another way to measure the CoG height is to run a turn at different speeds, and so different lateral acceleration, measuring the vertical force on each tire and then retrieving the CoG height by reversing the dynamic equilibrium equation 30.

$$\Delta F_z = \frac{m\ a_y\ h_{CG}}{l} \tag{30}$$

The different speed and lateral acceleration should allow to take different measures to extrapolate a mean value and variance.

One of the most difficult to measure parameters is the yaw inertia of a vehicle. The best way is to measure it on a test dynamic platform. Another way can be to perform a sensorized step steer maneuver, retrieve the lateral and longitudinal forces in vehicle reference frame, translate the forces into moments around the CoG taking into account the wheelbase, track and load distribution, sum all the contributions and divide by the yaw measured acceleration.

The powertrain characteristic must be well known, given by manufacturer or test bench.

Any measured parameter in theory should be provided with its uncertainty values.

2.3.2 Manual procedure

The conventional procedure involving:

- Run a simulation;

- Compare the outputs with real logged data;

- Based on the difference look for the reason;

- Change the parameter that affects that particular phenomenon.

This is repeated for different maneuvers until a suitable and reasonable model is found, ideally within the uncertainty limits of the measured parameters.

2.3.3 Automatized procedure

An automatized procedure for model validation is proposed by [13], reported in fig.29.

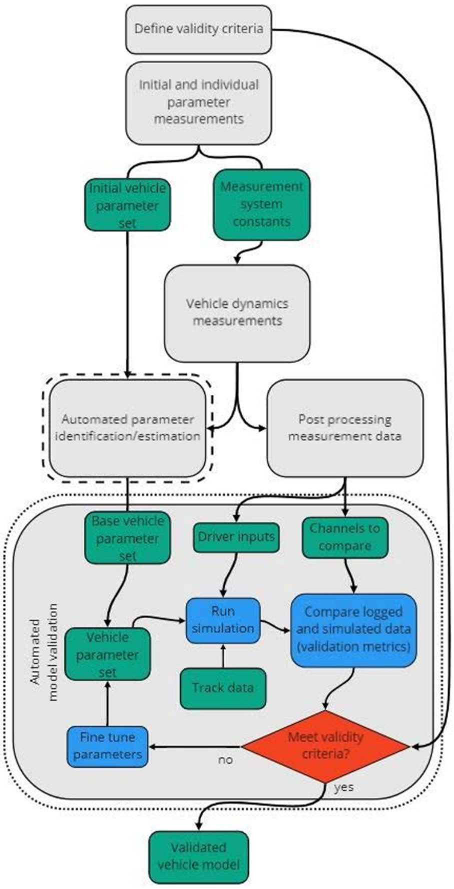

Figure 29: Automatic model validation algorithm

In this algorithm, the job of updating the model parameters is left to a Neural Network specifically trained for this purpose.

Even if the automated procedure might be a nice solution to reduce time and effort, the chosen solution for this work is the manual tuning. The decision was taken considering the fact that the automated procedure needs the interval in which the algorithm can change the parameters, but these intervals were not meaningful since the weight repartition has very low uncertainty while the yaw inertia is not even measure but it is estimated from the CAD of the vehicle. This is due to two reasons: the absence of strain gauge for tire lateral force measure and the impossibility to perform step steer maneuvers.

3 Torque Vectoring - track performance assessment

This section has the aim to present the tests performed to validate the feedback Torque Vectoring algorithm proposed in 1.5.10.

3.1 Test setup

Here is reported the hardware used. All sensors have been properly calibrated before the tests. Apart from the sensors and hardware presented here, many more are implemented in the vehicle, but their description is out of the scope of this work.

We want to remember that each sensor signal comes with a certain amount of noise. IMU and Correvit SF-Motion, presented in the following, will be used in section 4.3.3 to retrieve forces and sideslip angles. A Butterworth filter with a cutoff frequency of 15 Hz is used in post processing to filter-out noise.

3.1.1 VCU - dSpace MicroAutobox2

The Vehicle Control Unit is a dSpace MicroAutobox2,1401/1511 equipped with IBM PPC 750GL processor running at 900 MHz, 16 Mb memory, 16 Mb nonvolatile flash memory containing data recorder.

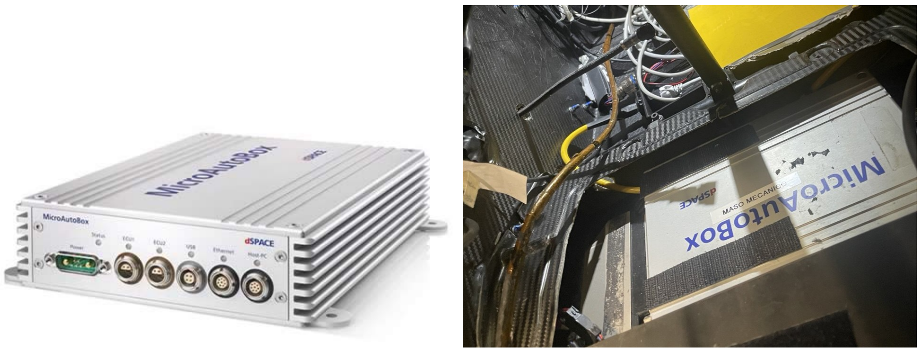

Figure 30: dSpace MicroAutobox II installation

Since all the logics are developed using Matlab/Simulink, also the code generation is done exploiting this software. In fact, Matlab offers together with dSpace, dedicated tools for can communication (both Tx and Rx) and code generation with full-executable, just requiring as input the target dSpace ECU. Moreover, CAN.dbc files are needed to be imported into Simulink before code generation, for proper CAN communication. Once all the parameters are set correctly (CAN communication subsystems, target ECU selected), the C code can be generated autonomously.

3.1.2 IMU - SBG Ellipse-N

This inertial measurement unit is equipped with an internal GNSS receiver, fig.31, and provides data regarding:

- Accelerations
- Roll,Pitch
- GPS position
- Azimuth

The sensor is placed between the front dampers, under the suspension cover. A different position has been found for the GNSS sensor as a consequence of Faraday cage effect. GNSS should be positioned horizontally.

Figure 31: IMU installation

3.1.3 Sideslip angle sensor - Kistler Correvit SF-Motion

The Correvit SF-Motion sensors enable direct, slip-free measurement of the longitudinal and lateral speed as well as the sideslip angle of ground vehicles. Additional measurements, such as the leveled acceleration or the curve radius are already calculated inside the sensor. A conversion of speed to any other point of interest, e.g. the center of gravity or rear axis is possible.

The sensor was placed in the back of the vehicle, perpendicular to ground, in a vertical position as suggested by the data sheet, on the symmetry plane of the car and at a known longitudinal distance with respect to the CoG. The delivered KiCenter software allows an easy sensor configuration. Programmable and standardized signal outputs and interfaces provide direct connection to PC and virtually all data acquisition systems, which makes available all measured state variables.

Extreme attention must be put on the calibration of the sensor: since the sideslip angle ranges normally between -5 and 5 deg, an error of 0.5 deg means a loss of precision by 10%.

The sensor can give as outputs:

- Distance
- Speed vector (x,y)

Figure 32: Sideslip angle sensor installation

- sideslip angle
- accelerations and angular rates
- GPS position and UTC time
- pitch and roll angle

Accelerations and angular rates have been compared to the IMU signals in order to have an indication of goodness of the measurements.

3.1.4 Steering angle sensor - RLS RM08

The RM08 is a compact, sealed, super small, high speed rotary magnetic encoder designed for use in space limited applications. The non-contact two part design removes the need for seals or bearings ensuring long-term reliability and simple installation.

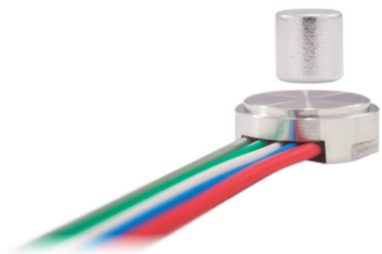

Figure 33: Steering angle sensor

The calibration of this sensor is crucial since the model that will be evaluated using the steering signal is very sensitive to steering input bias errors. Steering angle sensor is generally characterized by a very small amount of noise, thus its output is not filtered.

3.2 Maneuvers

The chosen maneuvers to test the performance of the Torque Vectoring strategy are: Slaloms, Double Lane Change and track laps, held in the old SC test facility. Being on an actual track the maneuvers that can be performed are limited by the available space: ramp-steer, step-steer and sine sweep steer maneuvers are almost impossible to perform because they need much longer straits or much wider tarmac regions for safety reasons.

3.2.1 Slalom

The slalom is performed according to FSG rules, with a port distance of 8 m. The maneuver consisted in arriving at the first port while braking, perform the the slalom in the best of the possibilities using throttle inputs, and steering inputs and accelerate at the exit of the last port.

Figure 34: slalom cone setup

The torque deliverable by each motor to the wheels was set to the maximum torque in traction of 21 Nm, and 10 Nm in regenerative. The maximum power available was set to 30 kW to increase the drivability at low speed but the actual used maximum power was never higher than 17 kW, hence this limit introduced for drivability is not affecting the maximum performance of the vehicle. All the maneuvers had been performed with the same wheel angle setup and on the same date and in the same session, to minimize grip variation and induced errors due to temperature, moreover only the maneuvers characterized by small tire temperature difference where taken into account for this work (the first test were discarded due to tire warm-up). Traction Control is enabled for safety reasons.

A very important thing to point out is that there are three ways to limit an electric vehicle speed: limit the maximum deliverable torque, limit the maximum speed of the motor or limit the maximum power. If we want to limit vehicle performance, it is much more convenient to limit the maximum power, especially if we are testing a torque distribution algorithm. The maximum speed limit has to be avoided because when the motor reaches the maximum speed, the lower level controller presented in 1.5.2 reduces the commanded torque to avoid overcoming the speed limit. As a result, the TV effort would be completely spoiled.

The temperature of the tires was measured after each maneuver and ranges between 23 and 32 °C, temperature at which the tire cannot work properly. This is a more challenging scenario for the vehicle, even if it is compatible with its race utilization, in which tires cannot be warmed up.

3.2.2 Double Lane Change

Double Lane Change is a standard maneuver to assess vehicle stability during emergency situations, its procedure standardized by the norm ISO 3888-1:2018 for passenger cars. The prescribed dimensions from the norm allow too high speed for our test vehicle, putting the driver in danger of a high-speed spin out. Given the limited road width, the test vehicle speed had to be reduced to limit the risk to an acceptable level, hence a non-standard layout has been chosen. This is reported in fig.35.

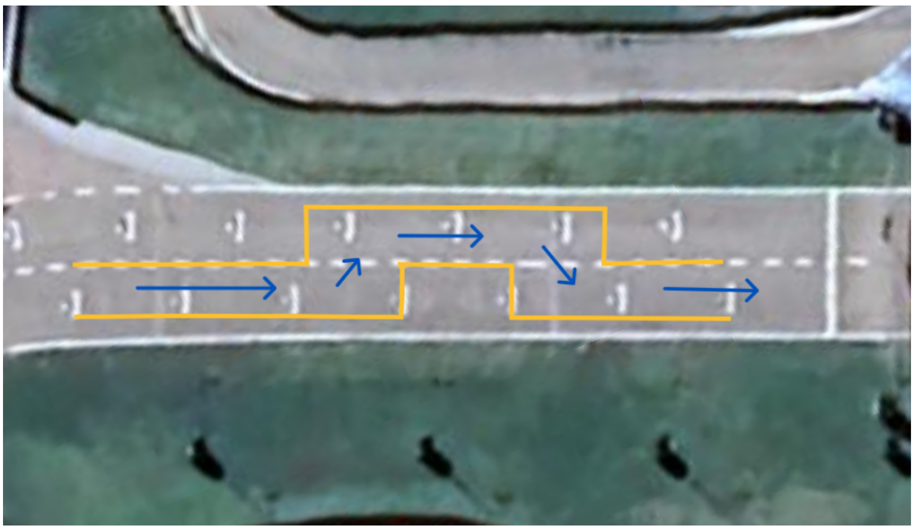

Figure 35: DLC cone setup scheme

This layout is characterized by a track width of about 3.5 m, a port width of about 6 m and a distance between the ports of about 7 m, allowing a maximum speed of the vehicle lower than 55 km/h.

The DLC maneuver is performed as follows:

- The power is limited at about 12 kW, Torque is not restricted.
- The driver accelerates and reaches maximum speed allowed by the maximum power before the entry of the first turn.

- The driver performs the maneuver while keeping 100% throttle.

The choice of having the throttle pedal always pressed has been driven by the willingness to separate as much as possible the power delivery problem joined with the driver behavior and the vehicle dynamics control problem. The possibility of adjusting the throttle actuation is given during slalom maneuvers.

The maximum power at which the maneuver is performed is found with a trial-and-error procedure, in which an initial power, thus an initial maximum speed, is set. If the maneuver is successful, the power is increased iteratively until the test becomes impossible to perform. The maximum power is tuned with the torque vectoring control switched off and kept the same for the test with control switched on. Traction control is enabled for safety reasons.

As for the slalom tests, all the maneuvers had been performed with the same wheel angle setup and on the same date and in the same session. The temperature of the tires was measured after each maneuver and ranges between 22 and 26 °C, taken after each test.

3.2.3 Tack Lap

The layout used for track test has been chosen among the all the possibilities in order to have a lot corners, especially low speed. This layout has a length of approximately 450 m and a maximum speed of 80 km/h. The laptime for this configuration with the imposed maximum power ranges from 28 s up to 34 s depending on grip condition.

Figure 37: track for complete laps upper view

The maximum power of the vehicle was limited to 50 kW in order to preserve the HV battery pack, the maximum torque was set to 15 Nm in traction an 10 Nm during regeneration. Traction Control was always enabled for safety reasons.

As for the previous maneuvers all the laps were performed in the same session, the first laps were not taken into account for the analysis since tire warm-up took

Figure 36: DLC photo sequence while TV is off

between 4 and 5 laps. The steady-state working temperature of the tire were extremely low even after the warm up, between 45 and 55 °C, due to cloudy weather conditions and low air temperature of 16°C. Again. this is an important proving ground for the vehicle since the low grip conditions.

3.3 Results

For each test type, a couple of maneuvers were selected, one with activated Torque Vectoring and the other completely passive (Traction Control switched on). Results are presented in terms of plots of notorious signals versus distance and a table with KPI in tables 4,5 and 6.

The analyzed signals are:

- Driver steering input δ_{SW}
- Vehicle longitudinal measured speed from Correvit SF-Motion sensor V_x
- Lateral acceleration from IMU sensor a_y
- Yaw rate from IMU sensor $\dot{\psi}$
- Sideslip angle β
- Yaw moment M_z commanded by Torque Vectoring
- Motor torques commanded during Torque Vectoring T_{mot}
- GG-plot is presented for the track lap

The analyzed KPI are the following:

- $IACA_\delta$ as described in eq.31, to measure steering effort.

$$\frac{1}{t_{fin} - t_{in}} \int_{t_{in}}^{t_{fin}} |\delta_{SW}| \, dt \tag{31}$$

- Maximum steering angle value $\delta_{SW,max}$
- Maximum lateral acceleration $a_{y,max}$
- Maximum sideslip angle β_{max}
- Yaw rate reference maximum error $\dot{\psi}_{err,max}$
- Yaw rate reference RMS error $\dot{\psi}_{err,rms}$
- Laptime, only for track laps, T_{lap}

TV	$IACA_\delta$ [deg]	$\delta_{SW,max}$ [deg]	$a_{y,max}$ [g]	β_{max} [deg]	$\dot{\psi}_{err,max}$ [rad/s]	$\dot{\psi}_{err,rms}$ [rad/s]	T_{lap} [s]
OFF	28.82	70.3	1.63	2.27	0.92	0.24	-
ON	24.5	55.7	1.70	5.09	0.63	0.16	-

Table 4: KPI table for slalom maneuver

TV	$IACA_\delta$ [deg]	$\delta_{SW,max}$ [deg]	$a_{y,max}$ [g]	β_{max} [deg]	$\dot{\psi}_{err,max}$ [rad/s]	$\dot{\psi}_{err,rms}$ [rad/s]	T_{lap} [s]
OFF	37.15	104.3	1.69	4.21	1.57	0.67	-
ON	14.13	35.0	1.64	3.19	0.40	0.12	-

Table 5: KPI table for DLC maneuver

TV	$IACA_\delta$ [deg]	$\delta_{SW,max}$ [deg]	$a_{y,max}$ [g]	β_{max} [deg]	$\dot{\psi}_{err,max}$ [rad/s]	$\dot{\psi}_{err,rms}$ [rad/s]	T_{lap} [s]
OFF	26.08	94.0	1.96	8.71	1.28	0.40	32.19
ON	24.52	74.1	2.10	9.46	1.13	0.34	30.79

Table 6: KPI table for track lap

All the maneuvers have in common a reduction in the steering wheel operation, which is good for the driver effort. It is also clear that in all the test cases, when the control is active, the maneuver can be performed at a higher speed. It must be pointed out that the comparison between the maneuvers is not influenced by tire grip, as can be seen from the maximum lateral acceleration values that are very similar for the same test category.

Talking about the slalom maneuver, it is nice to notice that the speed is increased and the peak of needed steering is decreased, this means that the curvature gain characteristic or the understeering factor characteristic versus speed has been enhanced towards a more neutral behavior.

It is possible to notice that in the last part of the maneuver there is an increment of Yaw Rate that is not corresponding to an increment in steering angle or speed, thus an oversteer is present and can be seen also on the sideslip trace, as a little drifting. This near to an optimal behavior since and understeering behavior in the exit of a corner is much more impacting on the laptime than an oversteer. It can be noticed anyway that the controller in that instant acts to stabilize the vehicle, ensuring stability and not only performance. This oversteering is very probably due to the torque request at the exit of a corner, thus this effect can be reduced partially acting on the Traction Control. We can appreciate a reduction in maximum and rms yaw rate reference error, this is very important because of the increment in speed as well: the higher is the speed at fixed steering angle and the harder is to maintain the trajectory [14] [15].

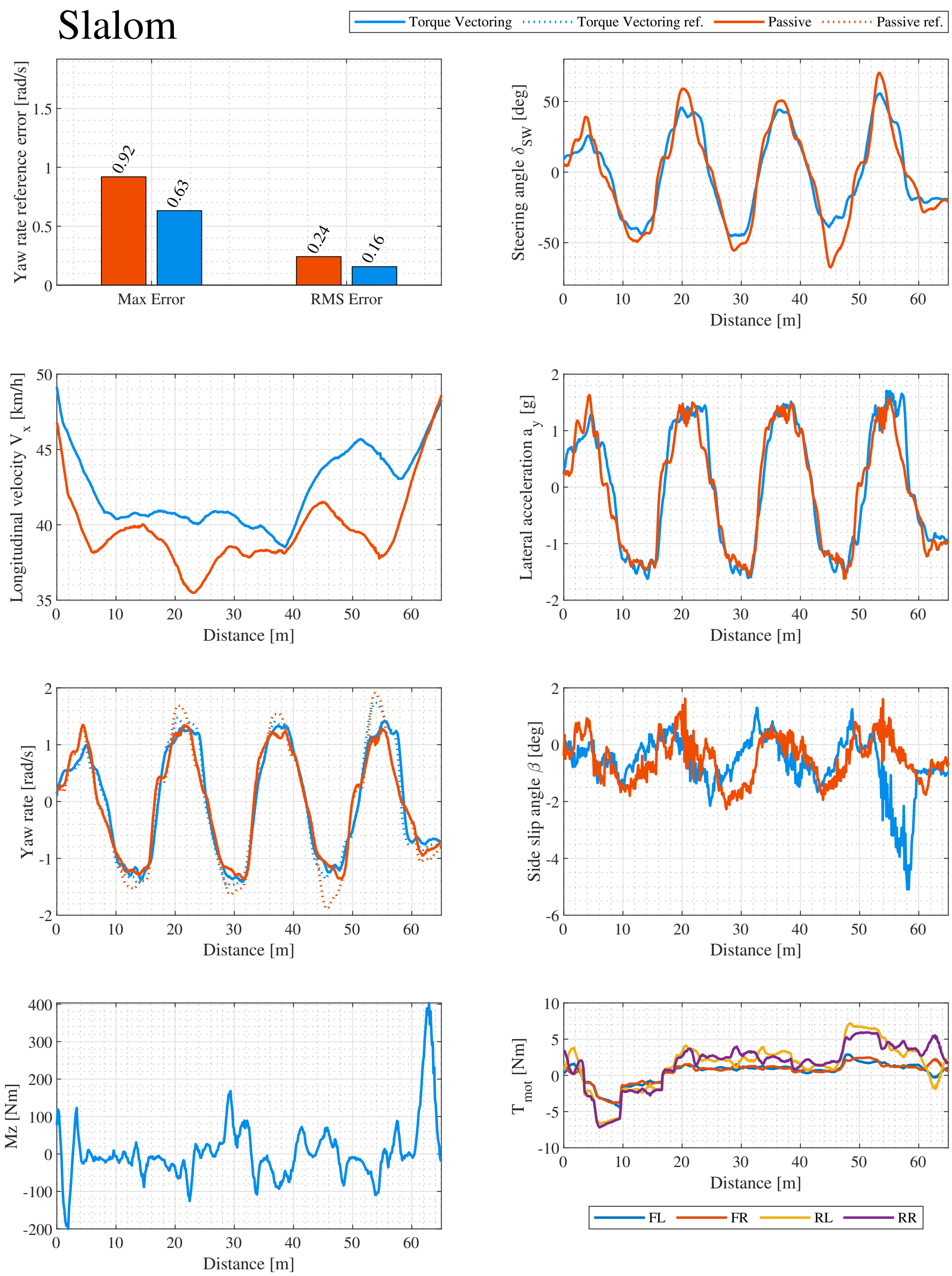

Figure 38: Torque Vectoring validation signals - Slalom

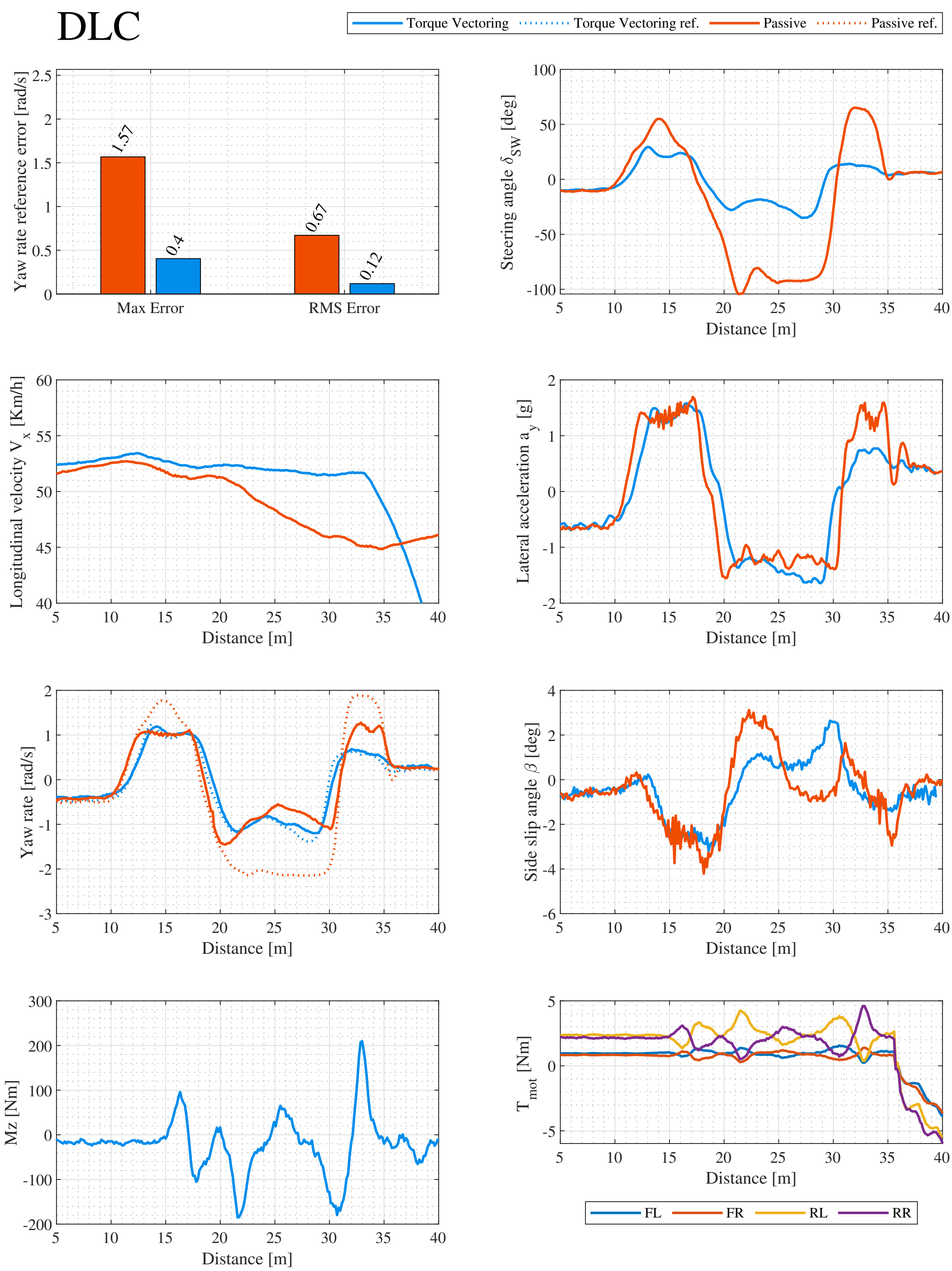

Figure 39: Torque Vectoring validation signals - DLC

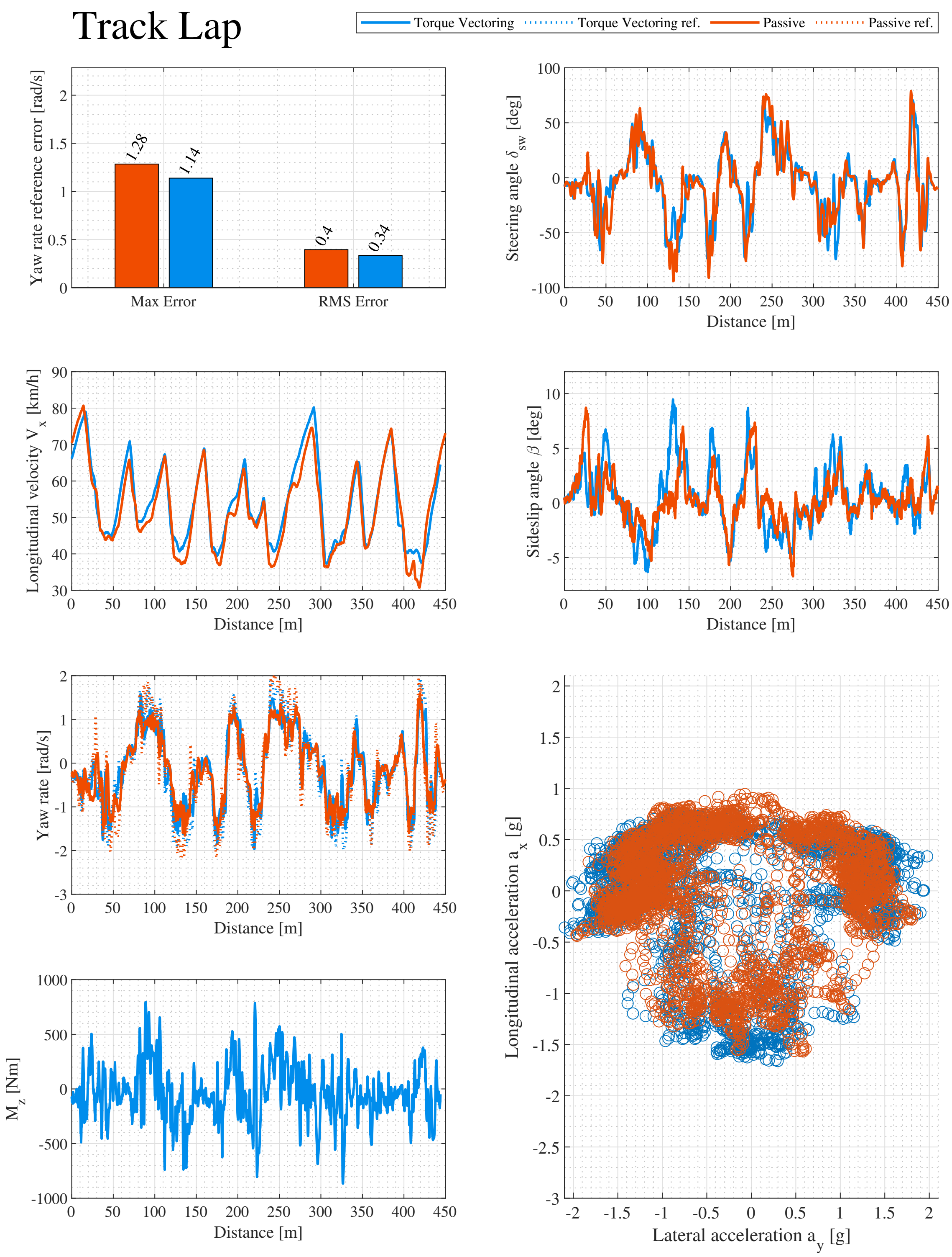

Figure 40: Torque Vectoring validation signals - Track lap

Looking at the DLC it can be said that, with the passive maneuver, due to the high amount of steering needed, the vehicle is slowing due to the longitudinal component of lateral force. Also, some front axle traction force component is needed to provide some yaw moment and it is not able to supply power to maintain constant vehicle speed. The reduction in steering wheel is enormous. The reduction in steering input is good also because the sideslip angle of front tires is reduced, hence the tire behave more linearly and not in strong saturation region.

Considering the Track lap results, it is obvious that the control is beneficial for the vehicle handling and performance since all the minimum speeds of the speed-distance diagram are increased. It is interesting to notice on the GG-plot that the peak lateral utilization region of the vehicle has been extended also at slightly higher longitudinal acceleration (between 0 and 0.5 g): with the intervention of the controller, it is convenient to apply the throttle earlier than before in the corner to give maximum capability to the torque allocation function to distribute the torque without power (throttle) limits. Moreover, with the control it is possible to brake harder due to the decreased risk of spinning that is guaranteed. According to the driver opinion, it is a pleasant sensation to make the car rotate with the throttle input without the risk of spinning the tires. The time gained is impressive, with 1.4 s gained that is around 5% of the total. In perspective of FSG track, with a laptime of around 85 s, that would be a gain of around 4.3 s.

Another benefit of the TV algorithm is that a convenient torque allocation is studied upstream of the TC. This can minimize the wheel slippage and have positive effects also on the energy consumption, effect that is not analyzed in this work.
It must be said that the Torque Vectoring control under analysis takes as input the measured sideslip angle and not the estimated one. This does not spoil the results of this work due to how the reference sideslip angle is computed. During the whole operation the sideslip angle reference has been always equal to the measured sideslip, since the sideslip control is active only in case of very high angles, see 1.5.8.

Figure 41: Test vehicle on a flying lap during testing

4 Sideslip angle estimation - track performance assessment

The Torque Vectoring algorithm can work even without the sideslip angle estimation, in this case only yaw rate tracking is performed. The sideslip estimation is however an important matter for our test vehicle since the sideslip angle sensor cannot be permanently put on the car and a safety measure to prevent high sideslip angles can help avoiding spin out during low grip conditions.

In this chapter the problem of sideslip estimation is addressed, and a possible solution is presented.

4.1 Test setup

Given the limited amount of time and resources, the team parallelized most of the tests necessary to validate the TV algorithm and the sideslip angle estimation, with exactly the same experimental setup. However two additional maneuvers are performed: Sine sweep steering and Constant Radius Cornering

4.2 additional maneuvers

4.2.1 Steering sine sweep

Sine sweep steering maneuver is a common maneuver in vehicle model and control validation since it evaluates the response of the system at different frequencies. If performed correctly and for a broad range of frequencies, it can be processed to give as output the transfer function of the vehicle.

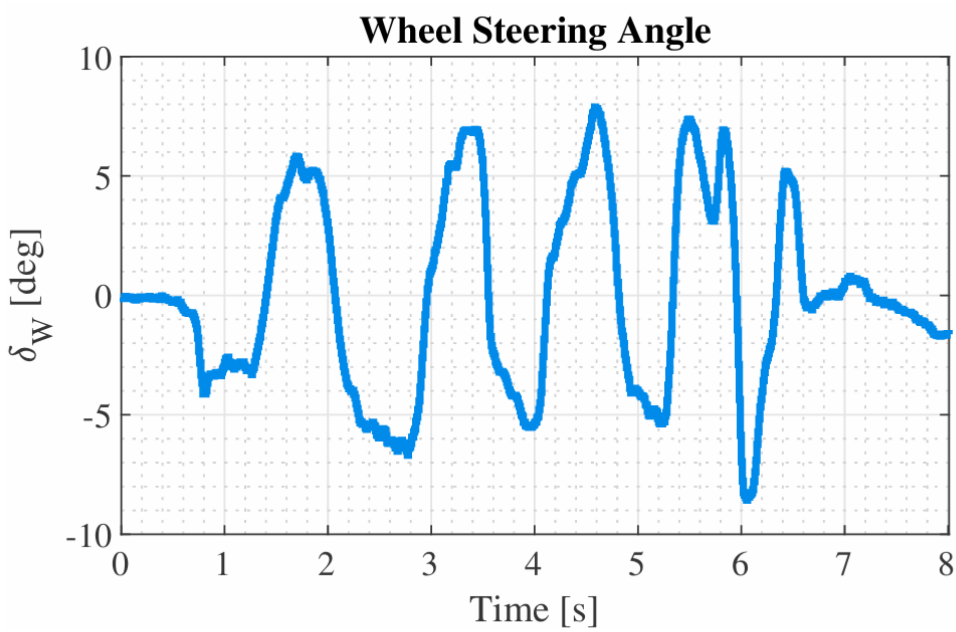

Figure 42: Sine sweep steering maneuver trial test

In our case, the maximum power had been fixed to 10, 20 and 30 kW, without torque constraints. This was done to have a more or less constant speed to try to evaluate the transfer function of the vehicle at these speeds and then interpolate the parameters for the intermediate values.

The tests performed did not give any result from this point of view, due to the limited available space on the straights of the racetrack (both as width and length), resulting in too few data and at too high variation of frequency. Another problem was due to the fact that the driver is not able to perform very high frequency steering maneuvers if the track is limited due to the fear of spinning the vehicle and performs counter-steering actions as in fig.42. These problems are even worse when the vehicle speed increases.

These maneuver has been used instead as test for validation of the internal model of the EKF and TV and test maneuvers for the real estimation.

4.2.2 Constant Radius Cornering

Constant radius cornering maneuvers are standard maneuvers to assess the steady-state lateral performance and balance of vehicles. Usually set of CRC are performed with variable turning radius, to allow different maximum speeds and steering angles and better characterize the vehicle. The usual turning radius ranges from 20 up to 100 m, to simulate tight turns or highway behavior.

On a test track is practically impossible to find a place to run CRC test, especially if that track is not conceived with test purposes. Given the reduced dimension of our test vehicle and also the final application, the turn radius can be much smaller with respect to road vehicles, reducing vehicle speed and risk.

The chosen layout is presented in fig.43, this is not very satisfactory since the limit speed is of around 45 km/h, but in the end it simulates pretty well one circle of a skidpad track. The allowed maximum turning radius of that layout is 10 m, found in the mid path of the circular crown.

Figure 43: CRC layout

Figure 44: CRC onboard view

CRC maneuver will be extremely useful while comparing the internal models of EKF and TV.

4.3 Traditional EKF

The Extended Kalman Filter is analyzed, to understand wether its performance can be enhanced in some way. The EKF have been simulated in open loop, fed with the needed track data and compare with the ground truth established by the sideslip angle sensor.

4.3.1 Results - The problem of tire temperature

The following results represent the performance of the estimator on maneuvers like: slalom, DLC, sine sweep steering and a track lap. They are presented in terms of time series of sideslip angle β, Yaw Rate r, vehicle measured longitudinal speed V_x, wheel steering angle δ_W, longitudinal acceleration a_x, lateral acceleration a_y, reported in a GG-plot for the track lap. The different contributions of the sideslip estimator, as explained in section 2.2, are reported in figures 45,46,47 and 48.

Looking at the time series, it is easy to notice that the dynamic contribution is not satisfactory. Nonetheless, the combined contribution gives good results in the sine sweep and the track lap, which are the most complicated working situations. The goodness of the combined estimation in these two tests is related mainly to the kinematic estimation, which is fairly reliable in these maneuvers but is also spoiling the result in the other tests.

The fundamental problem is related to the dynamic estimator, the EKF, that is not reliable enough. The source of this mismatch will be found in the internal model of the estimator: this model cannot take into account the real grip condition in which the car is found to be working. The majority of the test were performed under low grip, due to very low tire working temperature.

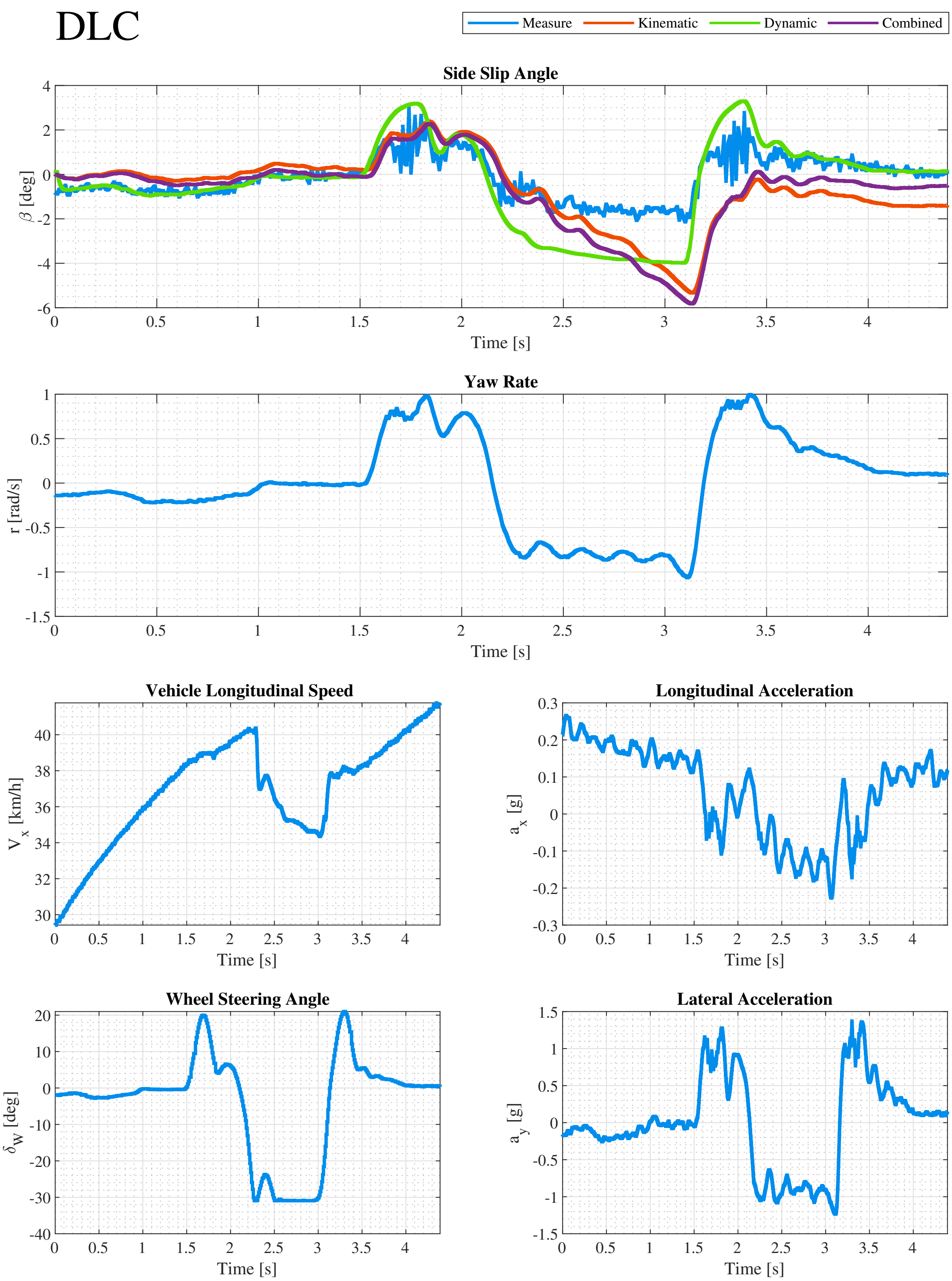

Figure 45: Sideslip estimation performance - DLC

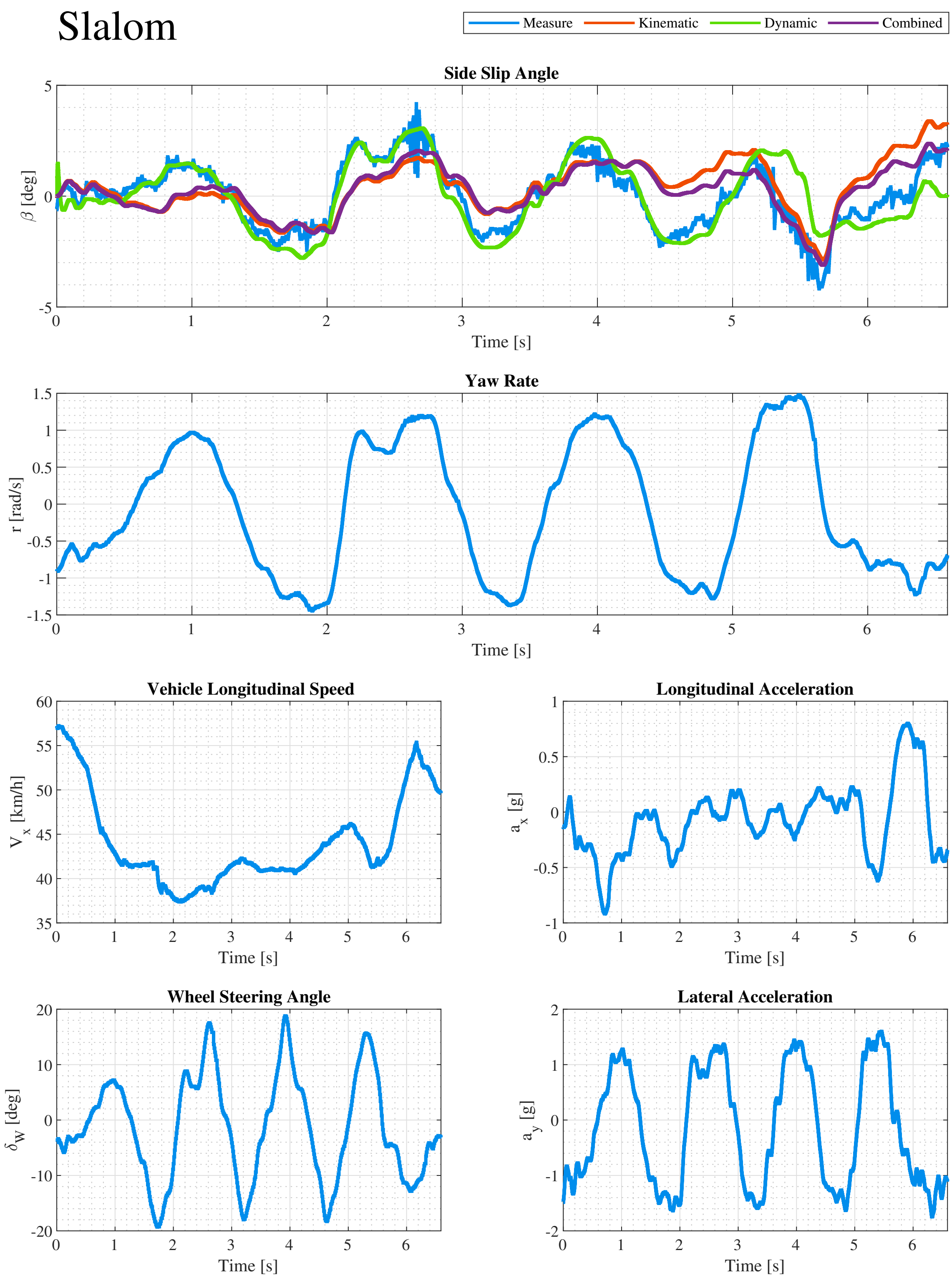

Figure 46: Sideslip estimation performance - slalom

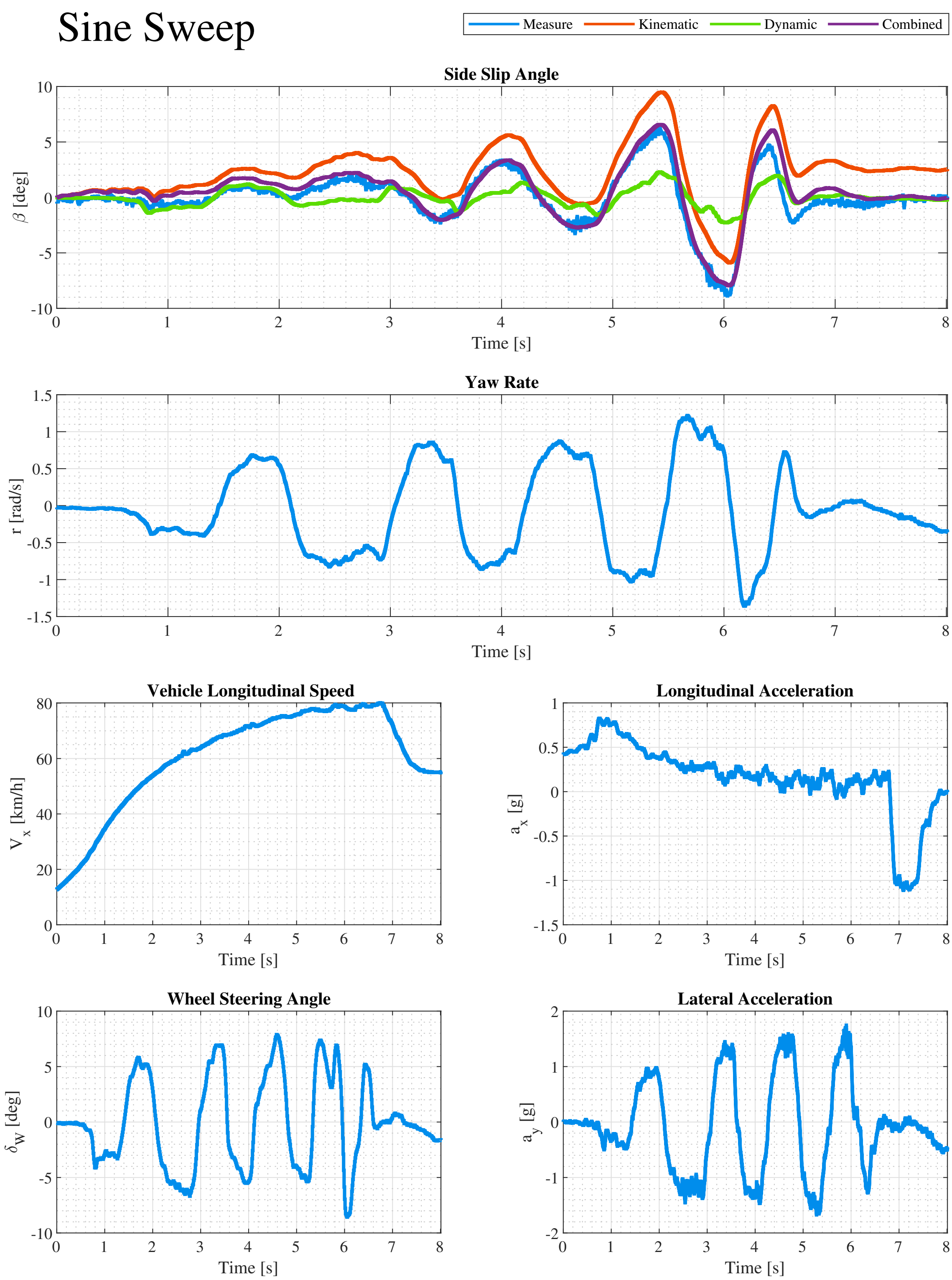

Figure 47: Sideslip estimation performance - sine sweep steering

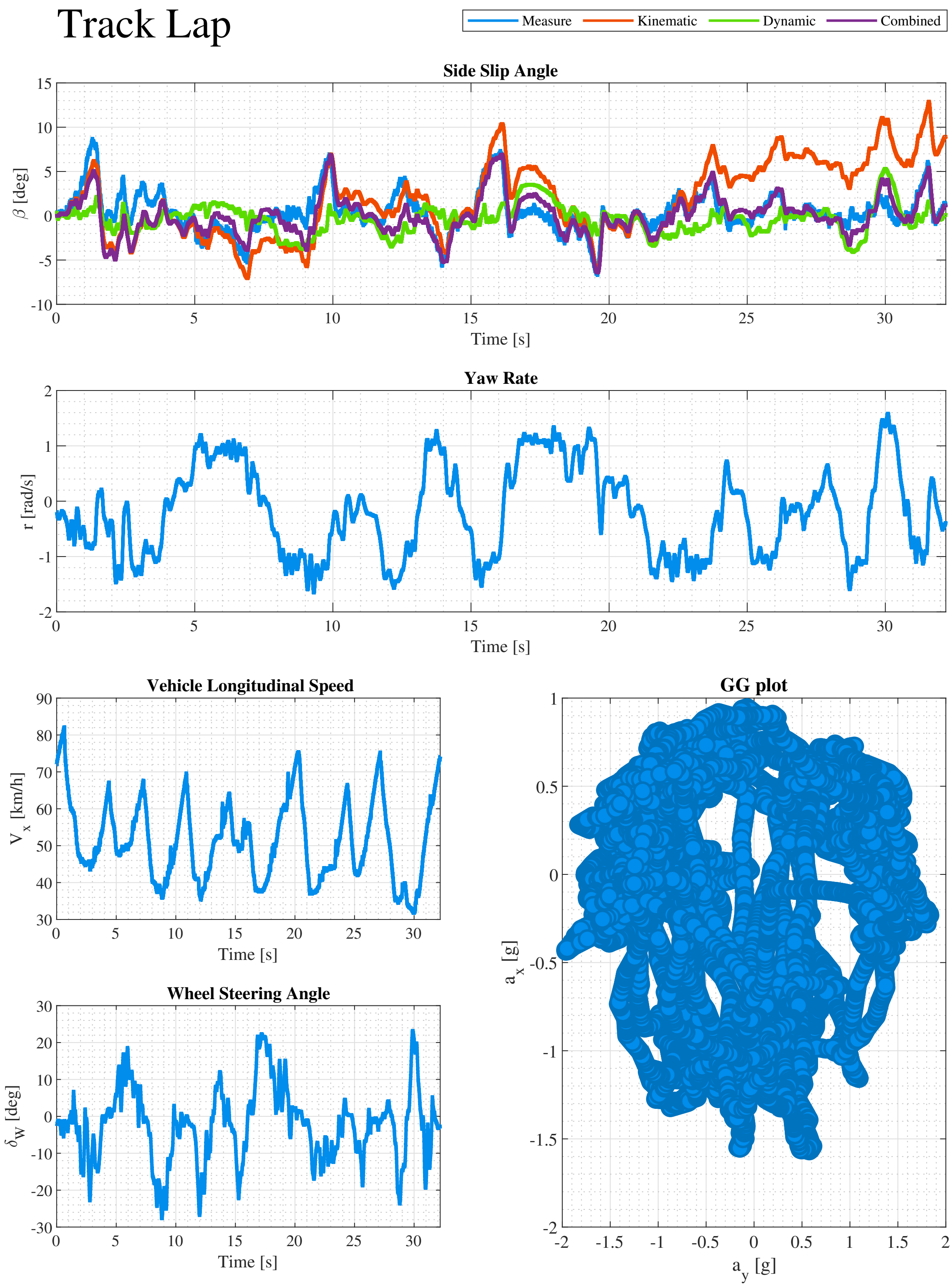

Figure 48: Sideslip estimation performance - Track lap

4.3.2 The internal model

The internal model is tested in open loop fed with real track data as V_x and δ_W from CRC, DLC and slalom maneuvers. The resulting Yaw Rate and sideslip angle are compared to the ground truth respectively from the IMU and the Kistler sensor. The results are shown in figures 49,50 and 51.

The original model overestimates by far the lateral capability of the vehicle during DLC and slalom, as can be seen from the difference in yaw rate peak values. It is more difficult to understand the behavior of the sideslip, since during kinematic conditions it theoretically is in phase with the steering and in dynamic conditions it progressively changes sign. What we can say is that when the grip is increased, the the sideslip angle becomes nearer to kinematic conditions.

It is evident that is not just a matter of tuning grip coefficient once for all. If the tire model is adapted for low grip situations, as in DLC and slalom maneuver, then it is not reliable for high grip maneuvers, as the CRC. This is remarked by the fact that the low grip model is not able to perform completely the CRC maneuver, since a strong oversteer leads to a loss of control before reaching the real car limit. Since the test track is the same, the absolute track grip should be the same, moreover the track and air temperatures at which the data is recorded is very similar between all the maneuvers.

It seems that the variable that is not taken into account is the tire temperature: higher tire temperature allow to reach higher lateral accelerations, higher corner speeds, due to higher grip, as can be seen in fig.52.

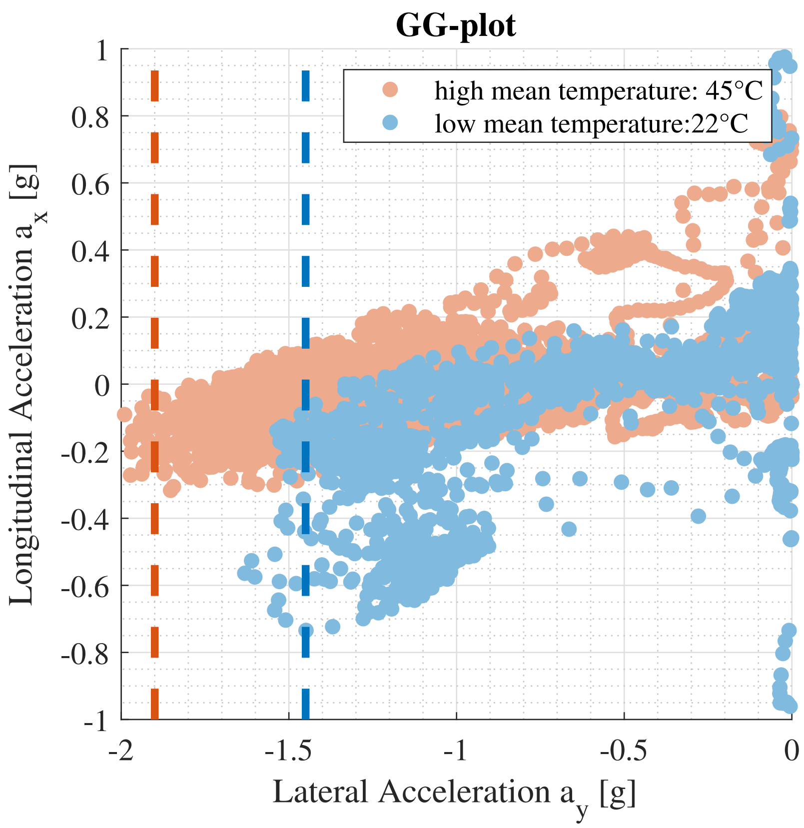

Figure 52: Low temperature vs High temperature GG plot

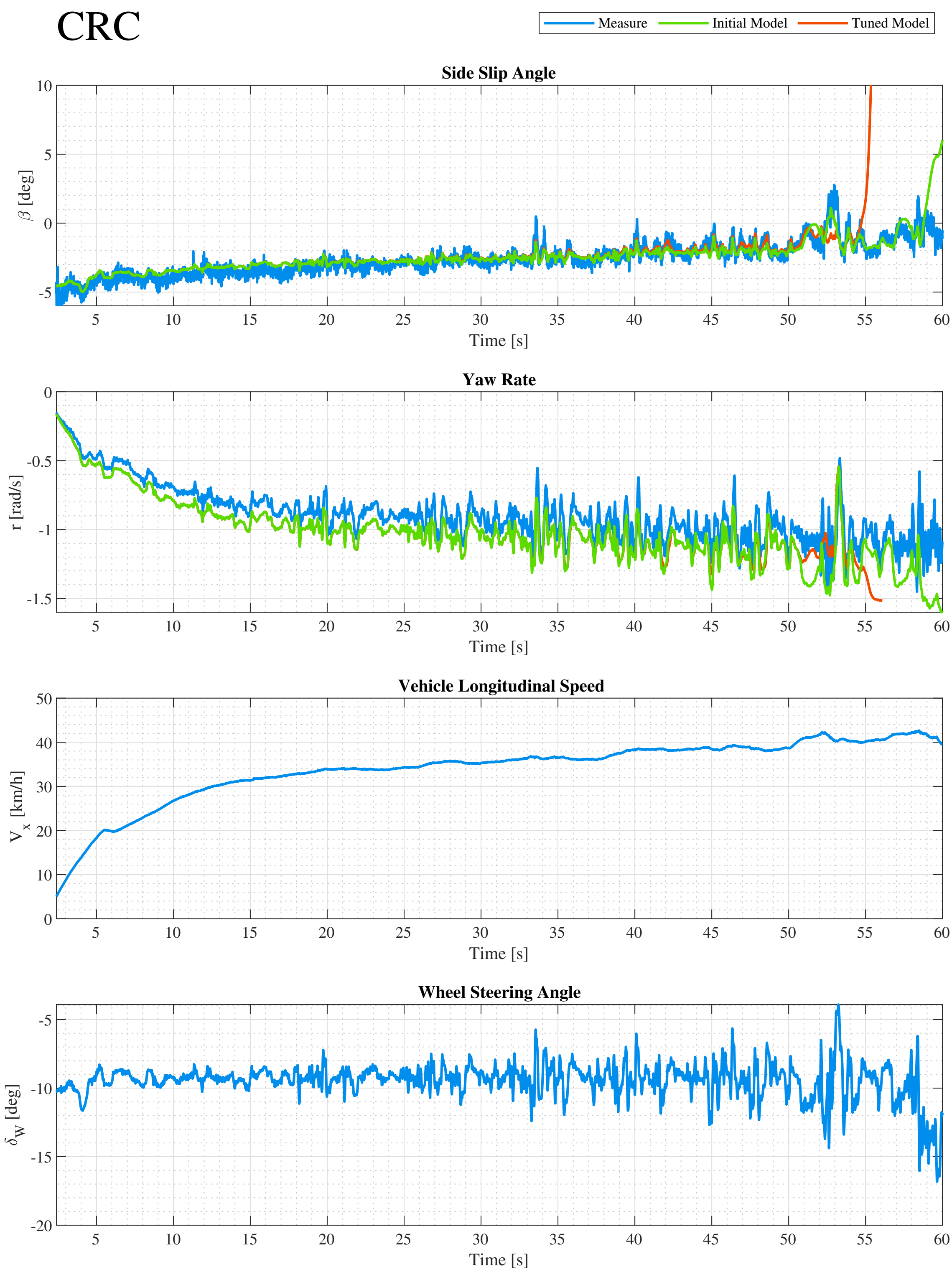

Figure 49: Internal model tests - CRC

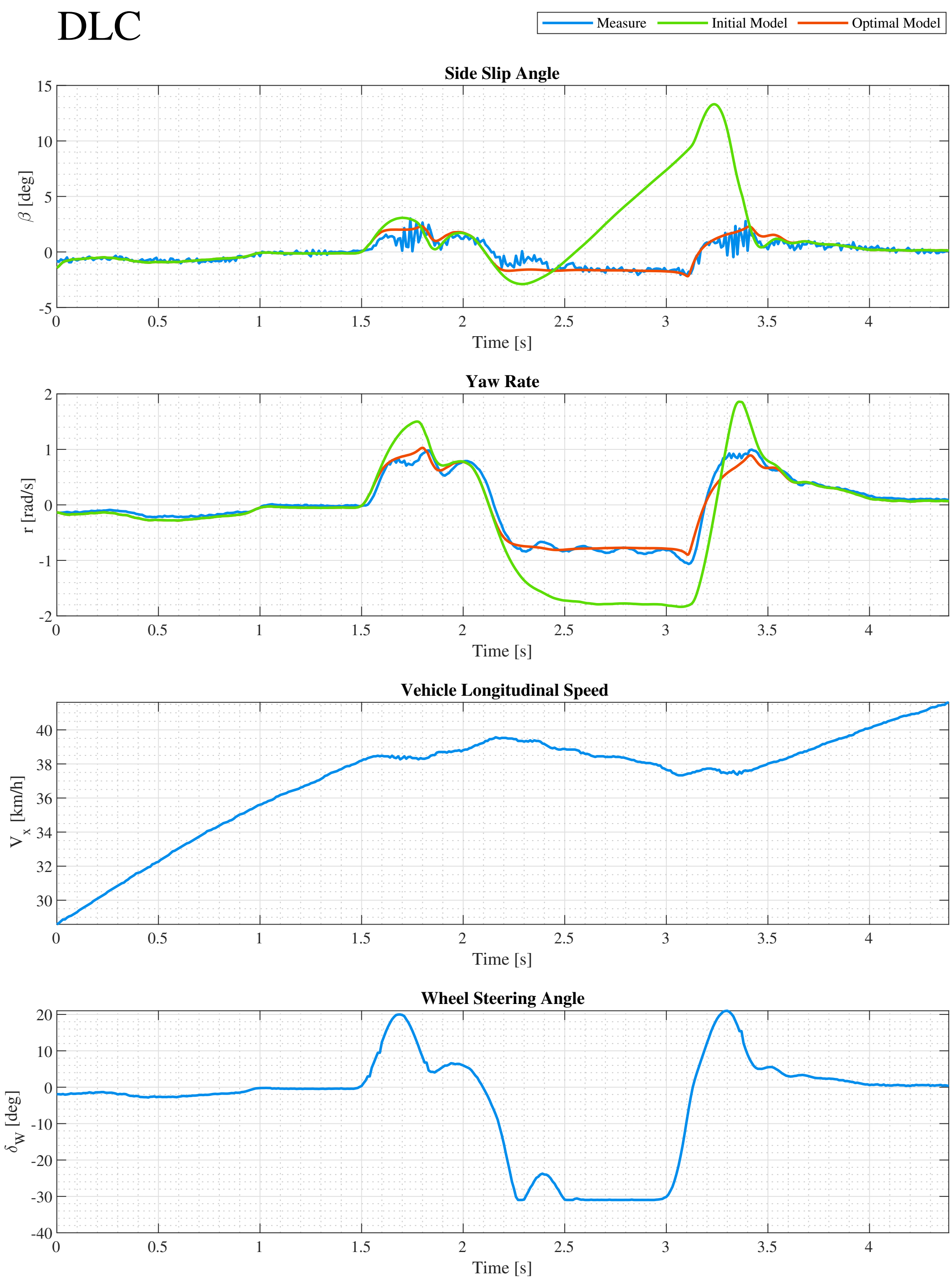

Figure 50: Internal model tests - DLC

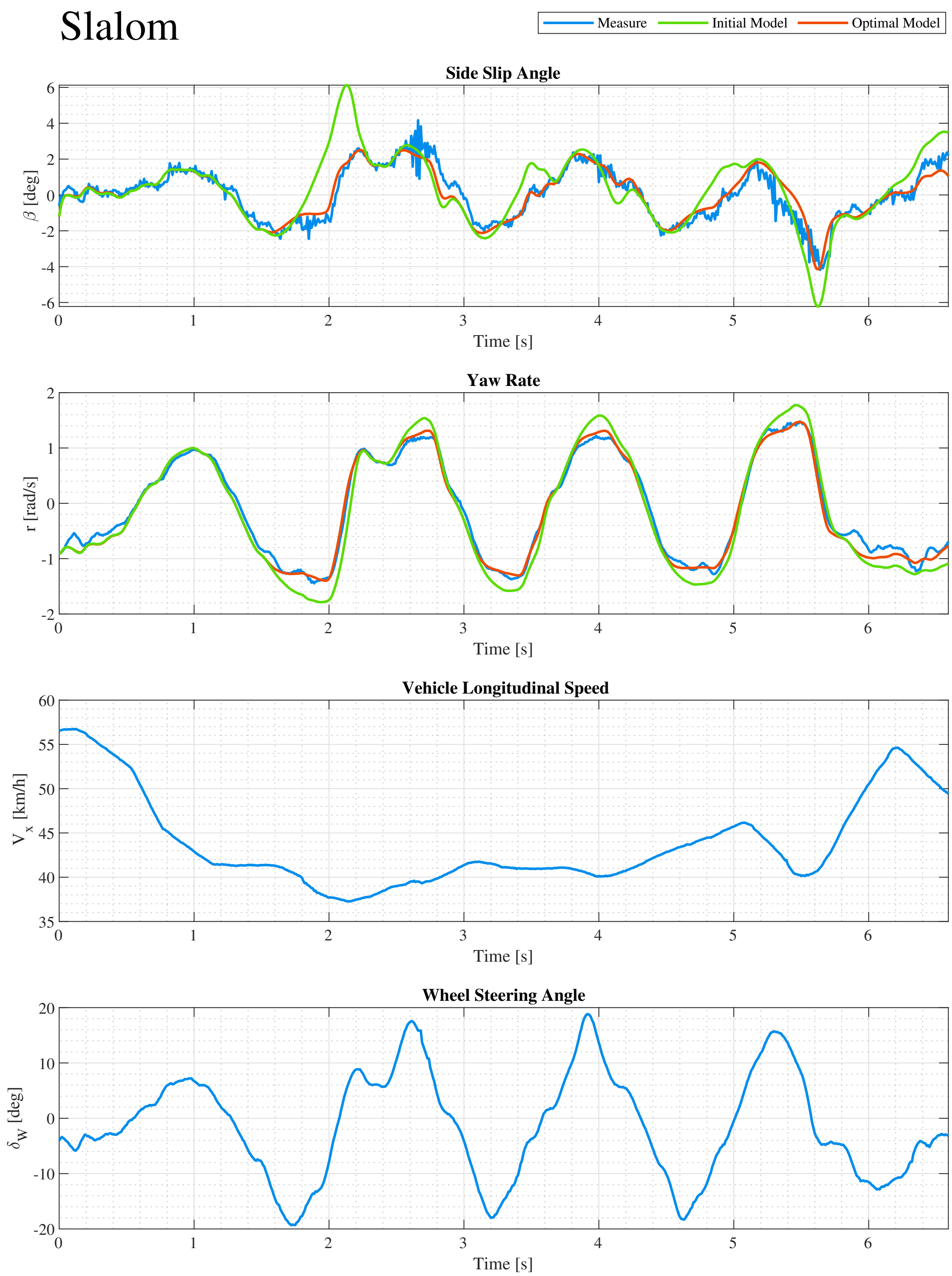

Figure 51: Internal model tests - Slalom

4.3.3 Temperature Model Validation

The next problem is how to estimate the temperature effect, having at our disposal track data only. Two main datasets have been used for this purpose: lower tire temperature complete track laps and the CRC maneuver.

The scatter plot in fig.53 represents the axle lateral forces from the low tire temperature track laps, colored with respect to the estimated vertical axle force that is function of longitudinal acceleration and vehicle speed because of aerodynamics. These laps are characterized by low longitudinal acceleration since the requested torque is lowered by traction control or by the driver that is waiting for the tires to warm up. With a certain amount of caution, can give some reference values to tune a Pacejka model seen at vehicle level.

In this case, the vehicle Pacejka forces are found using the same sideslip angle for left and right tire, assuming a vertical axle force $F_{z,axle}$ to be equally split between the two tires on the same axle. The sum of the two so obtained lateral forces is F_y. [16].

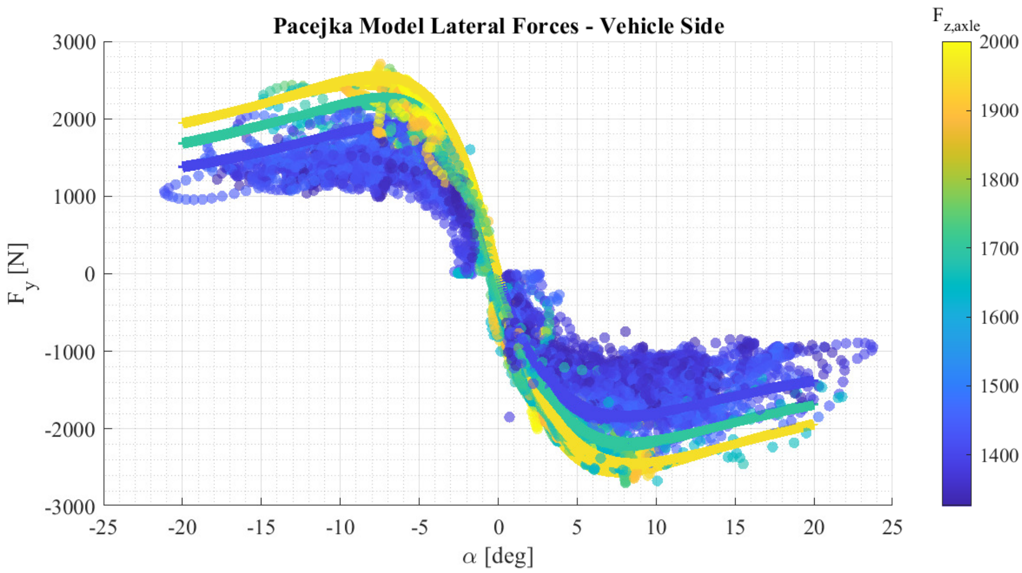

Figure 53: Axle lateral forces scatter plot vs vehicle Pacejka model

Lateral forces are calculated as in 27 and 28 in section 2.2.4. The sideslip angle of the axle is calculated as in eq.32 and 33.

$$\alpha_f = arctan(\frac{V_y + r\ a}{V_x}) - \delta_W \tag{32}$$

$$\alpha_r = arctan(\frac{V_y - r\ b}{V_x}) \tag{33}$$

From this plot we can already observe one possible temperature effect: being the test track run in clockwise direction, the left wheels are more loaded and they heat up faster. This produces an asymmetry in the force distributions that is evident when compared to a symmetric model like the introduced Pacejka. It can be seen that, for negative sideslip angles, the model that is more or less correctly fitting in the opposite semi-plane, is pretty overestimating the lateral force for the same vertical axle force.

When comparing this data with the CRC we come across another problem: during CRC the vertical force on the axle will be pretty much constant due to very low longitudinal accelerations and low speeds. This implies that the colormap based on $F_{z,axle}$ will lose meaning. A more meaningful indicator will therefore be the maximum vertical force on the axle, since we can expect that a high contribution of the axle lateral force will be addressed by the most loaded tire.

If the corner radius is assumed to be constant, as in a CRC, there is a precise relation between the maximum vertical force on between the wheels of the same axle, the minimum vertical force and vehicle speed.

$$F_{z,max,i} = A_{Fz} + (B_{Fz} + C_{Fz})\, V^2 \tag{34}$$

where

$$A_{Fz} = \frac{m\, g\, p_i}{2} \;\; ; \;\; B_{Fz} = \frac{\rho\, S\, C_z\, k_i}{4} \;\; ; \;\; C_{Fz} = \frac{m\, h_{CG}\, p_i}{R\, t} \tag{35}$$

In eq.35, p_i is the front-rear weight repartition, ρ is the air density, k_i is the front-rear aerodynamic repartition, R is the turn radius and t is the vehicle track width. In other words. A_{Fz} is the term that takes into account the static weight distribution independent on the speed. B_{Fz} takes into account the aerodynamic load and is related to the square of the speed. C_{Fz} is related to lateral load transfer, dependent on the lateral acceleration that, at fixed turn radius, is dependent on the square of the speed as well. In this way we can write eq.36 and 37.

$$V = \sqrt{\frac{F_{z,max} - A}{B + C}} \tag{36}$$

$$F_{z,min,i} = A_{Fz} + (B_{Fz} - C_{Fz})\, V^2 \tag{37}$$

In conclusion, we can say that we can fix $F_{z,max,i}$, for a known corner radius retrieve V, and $F_{z,min,i}$, calculate the the lateral force produced by the inner and outer wheel considering the calculated vertical forces and a series of side slip angles, assumed equal between left and right. Summing the two contributions, we get the lateral axle force for a fixed $F_{z,max,i}$. This is performed to obtain the plot in fig.54, in which the solid lines represent the vehicle-side Pacejka model rear axle lateral force colored with respect to $F_{z,max,r}$. The scatter plot represents the CRC track estimated rear axle lateral force colored with respect to $F_{z,max,r}$. The dashed line represents the Pacejka model optimized for low grip applications as in fig.53.

It is optimal to observe that for low values of $F_{z,max,r}$, the vehicle-side Pacejka model shows an equivalent cornering stiffness that is higher with respect to higher $F_{z,max,r}$ values. This is coherent with a tire cornering that saturates over a certain vertical force value, in other words, the lateral load transfer is lowering the cornering stiffness of the axle since the most loaded tire works more and more in a saturation region.
Coherently with these results, a new Pacejka model is introduced inside the vehicle model that has variable coefficients with respect to temperature. It is important to notice that the temperature affected parameters are not in generally the maximum cornering stiffness, but more often the lateral peak friction coefficient and the saturation characteristic of the Lateral force with respect to the sideslip angle.

In fig.55 are reported the relative changes of the Pacejka parameters according to a linear relation with temperature, found with an interpolation procedure. This

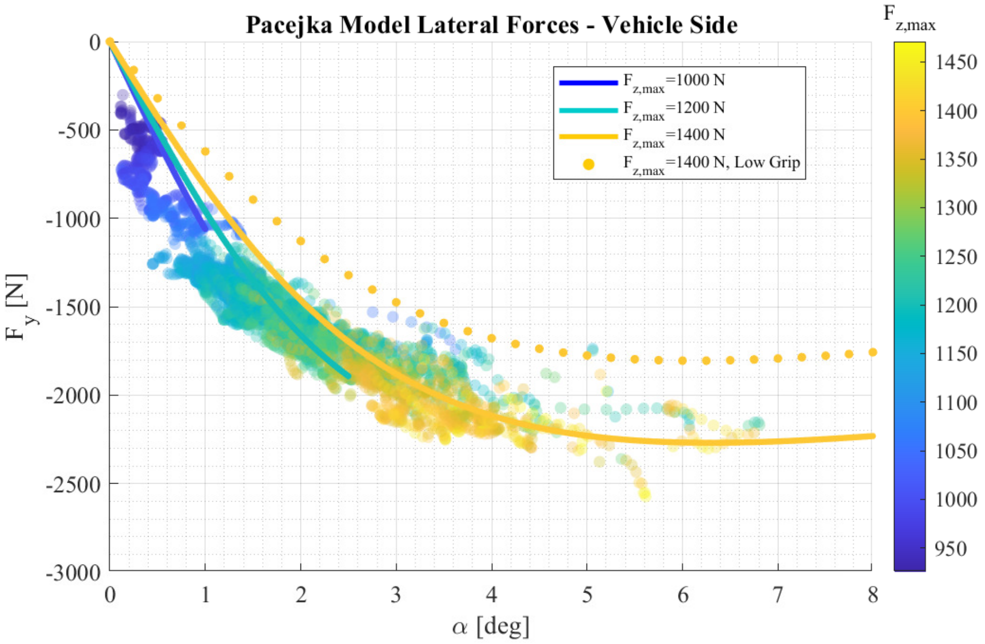

Figure 54: Axle lateral forces vs vehicle Pacejka model at fixed $F_{z,max,i}$

procedure was performed knowing the tire temperatures at which the maneuver was executed and a first estimation of the new parameter, this was found with manual tuning of the parameters. Starting from the estimate given by the model depicted in fig.54, the parameters have been tuned with open loop simulations fed with real track data, trying to minimize the discrepancies between measured sideslip and yaw rate with respect to simulated. This optimization was performed on three maneuvers: DLC, slalom and CRC. The reference temperature was chosen to be 60°C, so that the nominal parameters are found for that tire temperature.

The equations of the temperature adaptive model are the following.

$$dT_1 = (T_1 - T_0)/T_0 \tag{38}$$

$$Cy = pcy1 * (1 + PTY2. * dT_1) \tag{39}$$

$$dfz = (F_z - F_{z,0})/(F_{z,0}) \tag{40}$$

$$mupy = (pDy1 + pDy2 * dfz) * (1 - pDy3 * sin(\gamma)) \tag{41}$$

$$Dy = mupy * Fz * (1 + PTY3. * dT1) \tag{42}$$

$$Ey = (pEy1 + pEy2 * dfz) * (1 - (pEy3 + pExy4 * (sin(\gamma))^2)) \tag{43}$$

$$Kya0 = F_{z,0} * pky1 * sin(2 * atan(F_z/(pky2 * F_{z,0}))) \tag{44}$$

$$Kya = Kya0 * (1 - pky3 * (sin(\gamma))^2) \tag{45}$$

$$By = Kya/(Cy1 * Dy) \tag{46}$$

$$F_y = Dy * sin(Cy1 * atan(By * (1 - Ey) * \alpha + Ey * atan(By * \alpha))) \tag{47}$$

with γ as the camber angle, $T_0 = 60°C$ and $PTY2, PTY3$ are the interpolated coefficients.

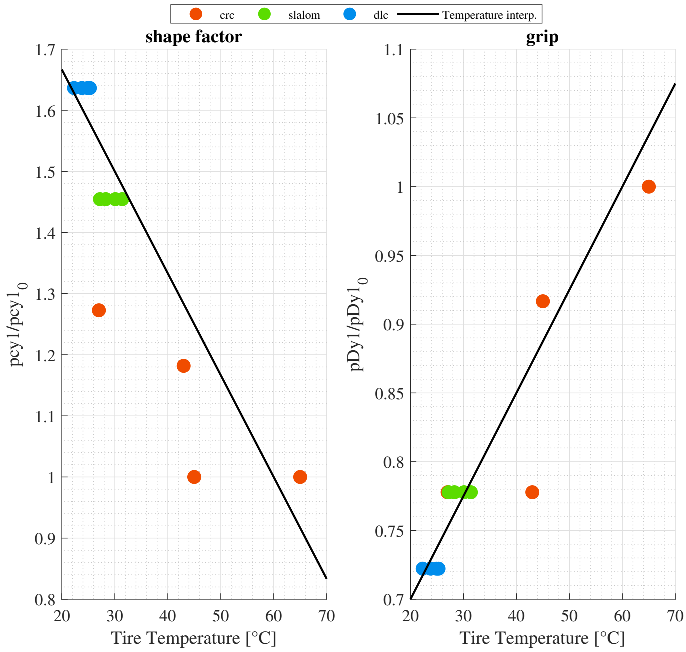

Figure 55: Pacejka coefficient variation with tire temperature

In theory, a better approximation would be parabolic, showing a peak value. For temperatures higher than the one guaranteeing best performance, thermal degradation should happen. Unfortunately no data in this region have been recorded.

The final vehicle model is fed with the measured temperatures used to adapt the Pacejka model, simulations are performed to assess the performance of this temperature adaptive model through all the maneuvers. Results are reported in terms described in 4.3.2 in fig.56, 57 and 58 and with a bar chart reporting the Goodness of fit (NRMSE), the rms error and the max absolute error, both for yaw rate and sideslip angle in fig.60.

It can be pointed out that being this model an interpolation between different other models, its precision to the specific case is not as high as the specific tuning. The advantage of this adaptive model is that it is just one general model that works in a broader range of situations, as stated by the cumulative errors in the bar chart. Low temperature optimized model errors are missing in the cumulative values since they cannot be calculated properly: with a low temperature tuned model applied to the CRC, the simulation ends due to divergency of the state of the vehicle before the actual end of the maneuver, hence the error cannot be calculated.

It can be seen in fig.58 that the temperature model is also beneficial for the CRC, since a little reduction of grip must be taken into account due to the inner wheels very low temperatures, caused by the fact that the car is turning for a lot of time only in one direction.

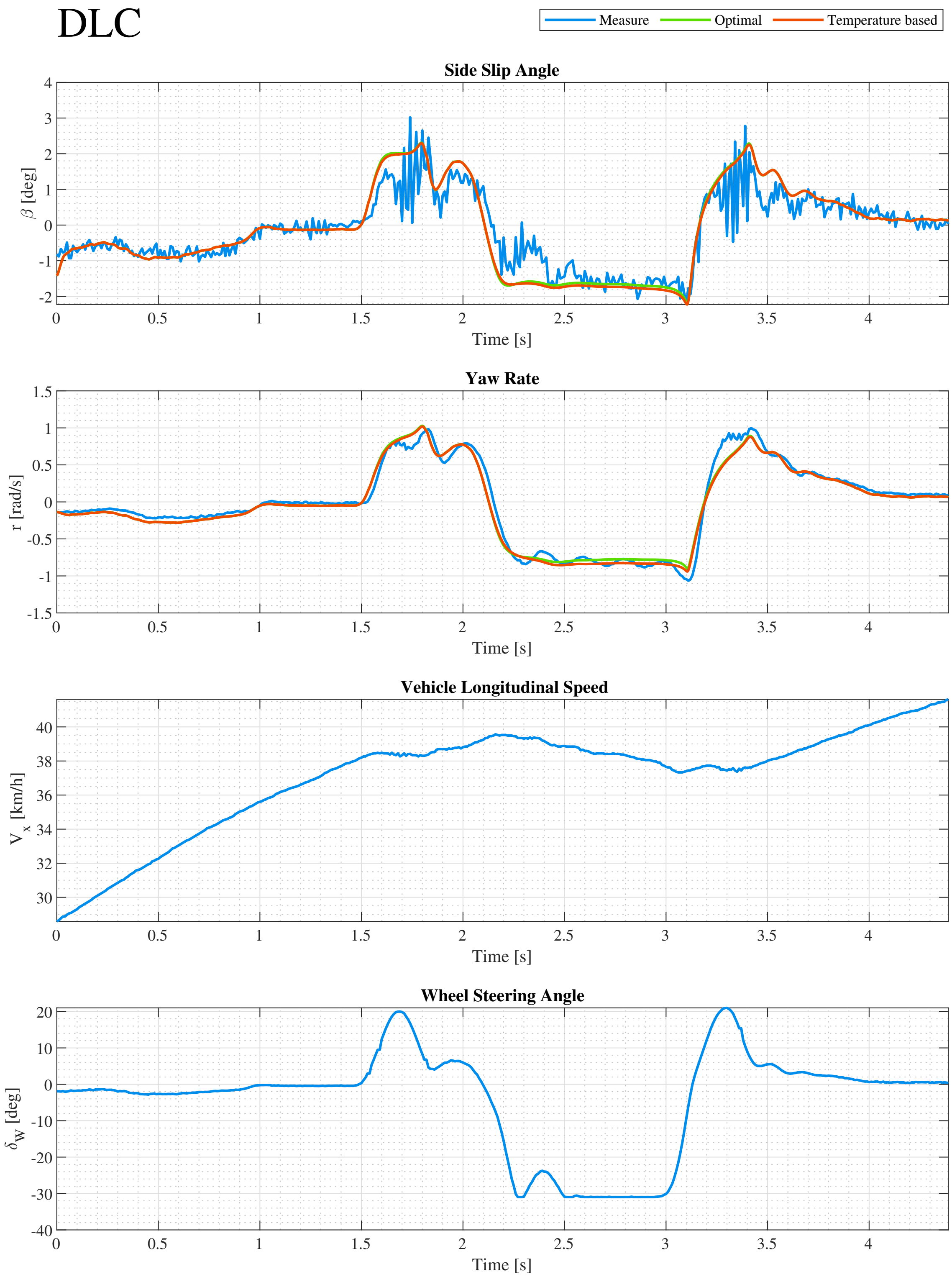

Figure 56: Temperature adaptive model tests - DLC

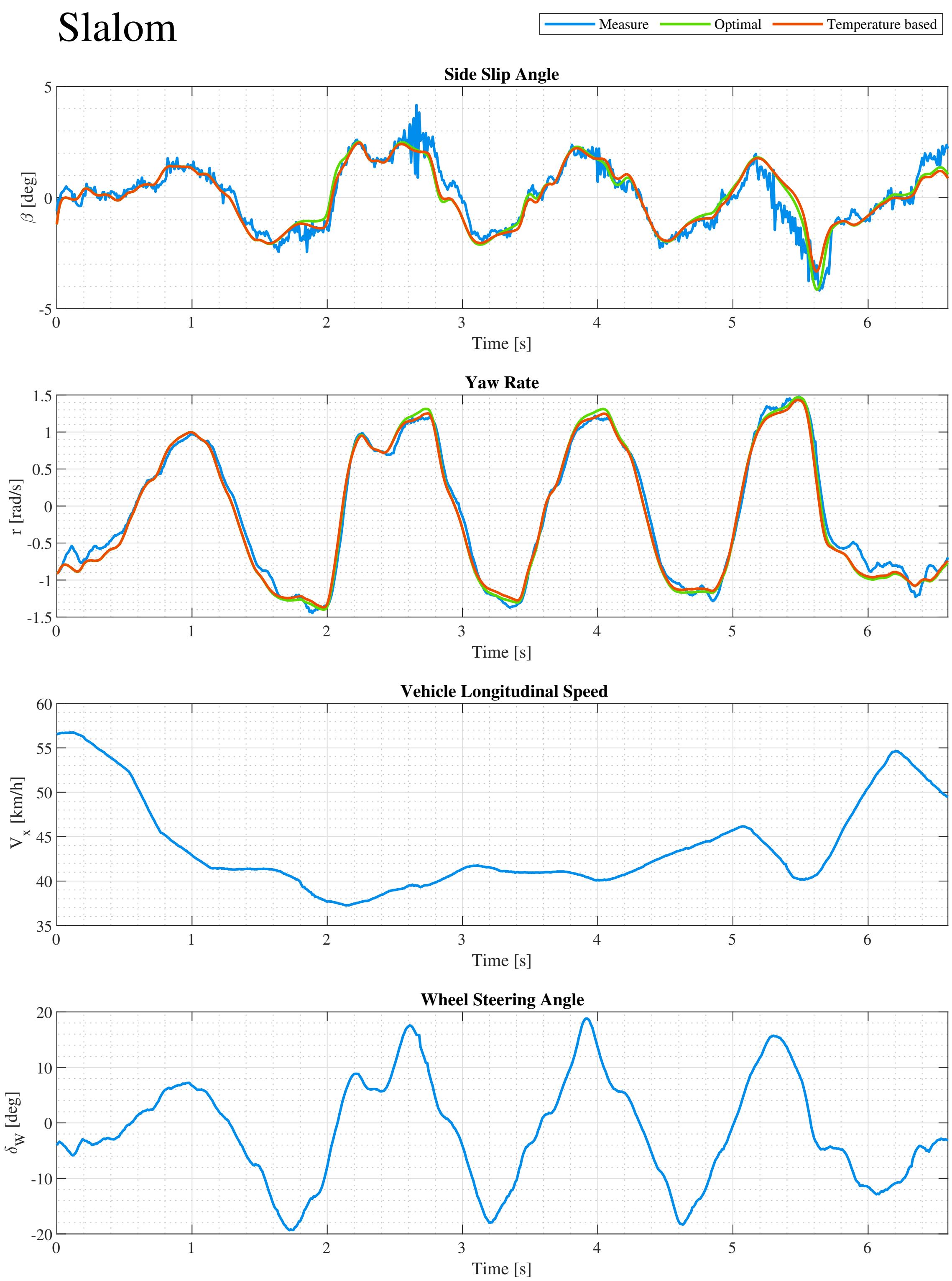

Figure 57: Temperature adaptive model tests - Slalom

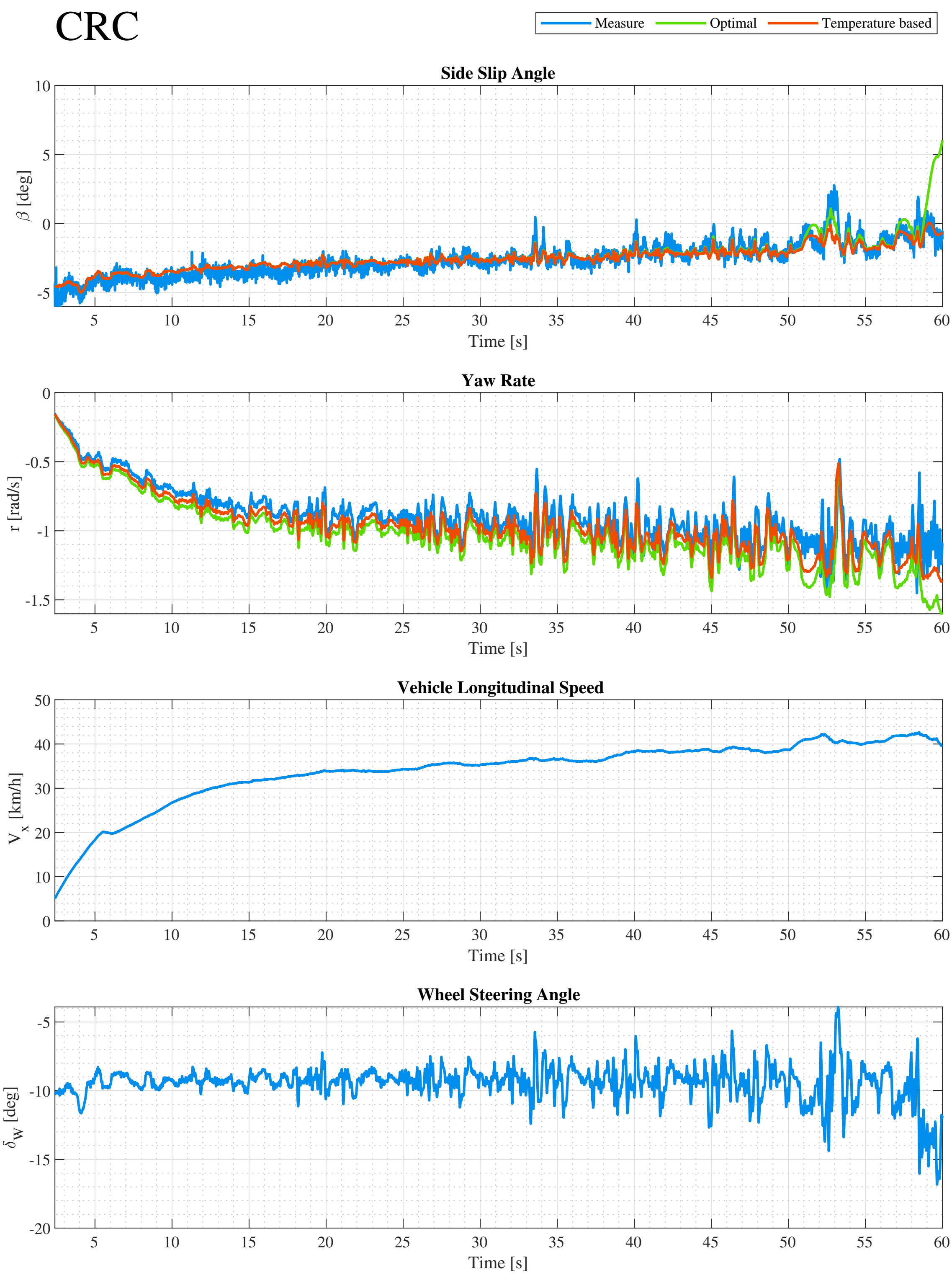

Figure 58: Temperature adaptive model tests - CRC

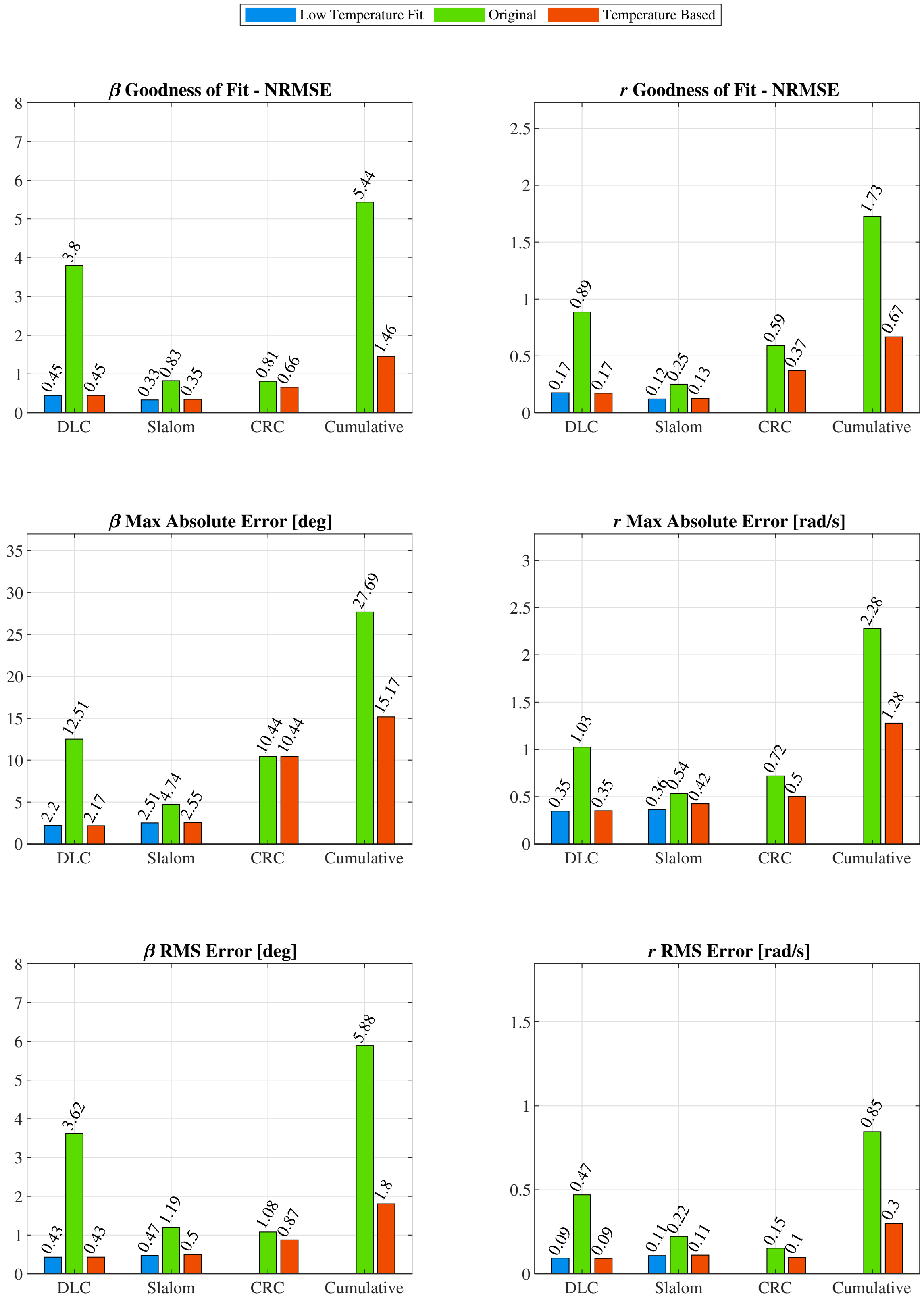

Figure 59: Temperature model error bar chart

4.3.4 Limits of this approach

The methodology used in this work works for the studied maneuvers and track, but is not portable to other track since the grip that is estimated is the sum of two contributions: track grip and tire grip. It is always the interaction between tire and road that gives the real amount of force. A much better way of estimating temperature coefficients would be to exploit tire testing machines directly, then the overall grip can be adjusted on track by a quick trial-error procedure looking at the accelerations.

Ideally it would be possible to extract tire parameters directly from the acquired data with an optimization algorithm. This is not very meaningful since there are constraints that the optimizer cannot take into account, it is better to leave this work to a human operator that can act with the experience and reason to tune the parameters, trying to avoid over-fitting on the data.

A huge disadvantage of this procedure is linked to the fact that lateral and vertical forces are not directly measured on suspension arms by strain gauges or load cells, this means that the real lateral force expressed by a single tire cannot be found unless some stringent assumption on the lateral friction coefficient are made, this is why fig.54 and 53 are reported as forces at vehicle or axle level and not at tire level.

4.3.5 Yaw Moment Diagram

The Yaw Moment Diagram is a standard approach to evaluate vehicle performance in terms of control and stability [15]. It represents the yaw moment, as the moment of the tire forces at the ground level versus the lateral acceleration for constant iso-lines of driver steering input and vehicle side-slip angle and it is useful to evaluate the transient behavior of the vehicle.

Of course, the size of this diagram depends strictly on the grip and the capability to change the rotation of the vehicle, both will depend on many parameters such as suspension stiffness or the anti-roll bar stiffness, but in our case study they depend mainly on tire temperature, that affects the tire model previously found, and vehicle speed, that involves the aerodynamics.

The following picture represents the YMD of the test vehicle with the torque vectoring control switched off.

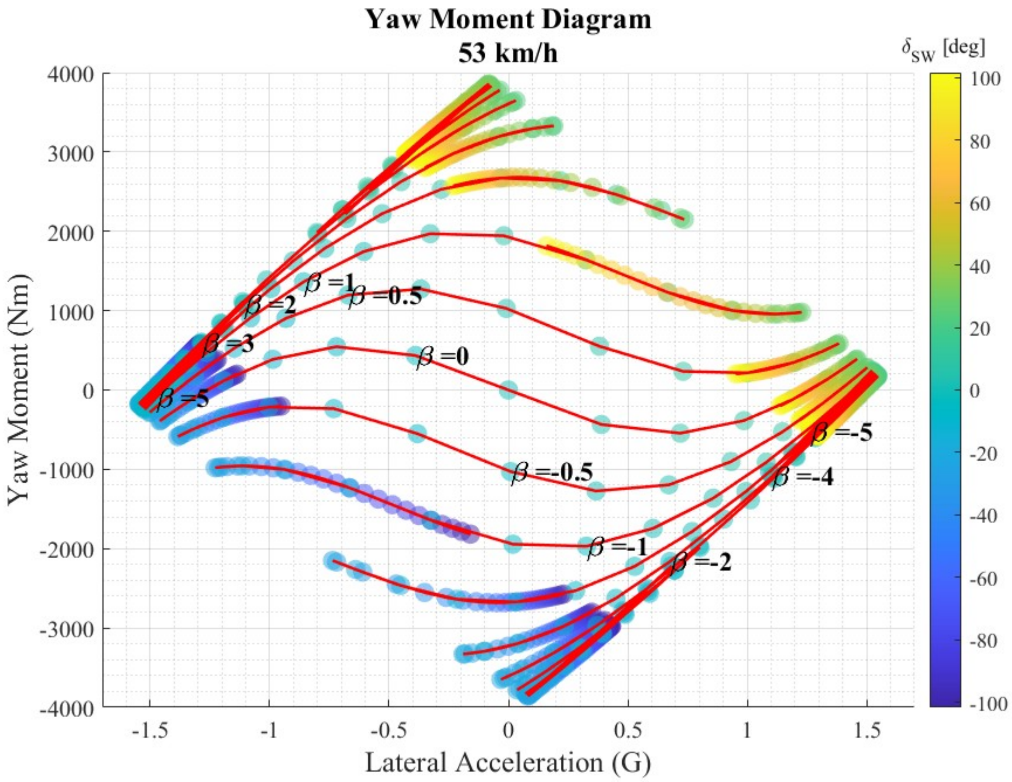

Figure 60: YMD representative of a DLC maneuver : tire temperature 30 °C

From this picture we can clearly see that the vehicle lacks of proper control from steering angles above around 50 deg. This is due to the fact that, adding more steering angle in the vehicle that is already in a limit condition will increase the front wheels' sideslip angles. Since the front wheels are already in saturation, an increase in sideslip angle will cause a decrease in lateral force that will compromise the lateral grip of the car.

From this picture we can see that the understeering is in the end due to both tire characteristic and the increase of steering angle. The maximum performance behavior is found in the oversteering region of the diagram (Yaw Moment and lateral acceleration of the same sign).

If tire temperature increases, this saturation effects decreases.

4.4 Temperature Enhanced EKF - Results

Based on the previous discussion, the internal model of the EKF has been enhanced with temperature coefficients. The new model is tested as was done in section4.3.1. The results are reported in terms of timeseries of notorious signals (in figures 61, 62, 63, 64, 65 and 66) and in terms of Goodnees of Fit (NRMSE), maximum absolute error and rms error with respect to sideslip angle (fig.67). The considered maneuvers for this evaluation are the one previously used and, in addition, one more DLC and one more slalom.

The tire temperature for each maneuver was measured at the end of the maneuver itself, these data are reported in table 7.

Tire	*DLC* 1	*DLC* 2	*Slalom* 1	*Slalom* 2	*CRC*	*Steering sine sweep*	*Track lap*
FL	24.8	24.9	30.1	22.0	44.7	20.4	46.5
FR	22.3	22.3	27.2	18.6	26.8	20.2	45.1
RL	24.5	25.3	31.4	22.8	65.2	20.6	49.0
RR	23.7	23.8	28.3	22.2	43.9	20.7	48.0

Table 7: Table with tire temperature for the analyzed maneuver, in [°C]

It must be pointed out that the correct tuning of the filters downstream of the kinematic and dynamic estimation changes with depending on the maneuver. This is due to the fact that in some maneuver is normal that the dynamic estimation is not exhaustive, while in others it is pretty reliable. Now that the internal model is reliable for pure lateral maneuvers and adaptive filtering can be adopted.

From the bar chart in fig.67, it can be seen that in all the maneuvers there is a reduction of the error, even in minimal, so we can assess that the temperature has a positive contribution to the internal model of an estimator in order to increase its performance.

One good thing about the new estimation is that, also during more challenging maneuvers, peak estimated values are nearer to the measured ground truth. This is good news for scope of this estimator that must track well the extreme working conditions to provide correct information to the TV algorithm that uses this information only when a certain sideslip angle is reached.

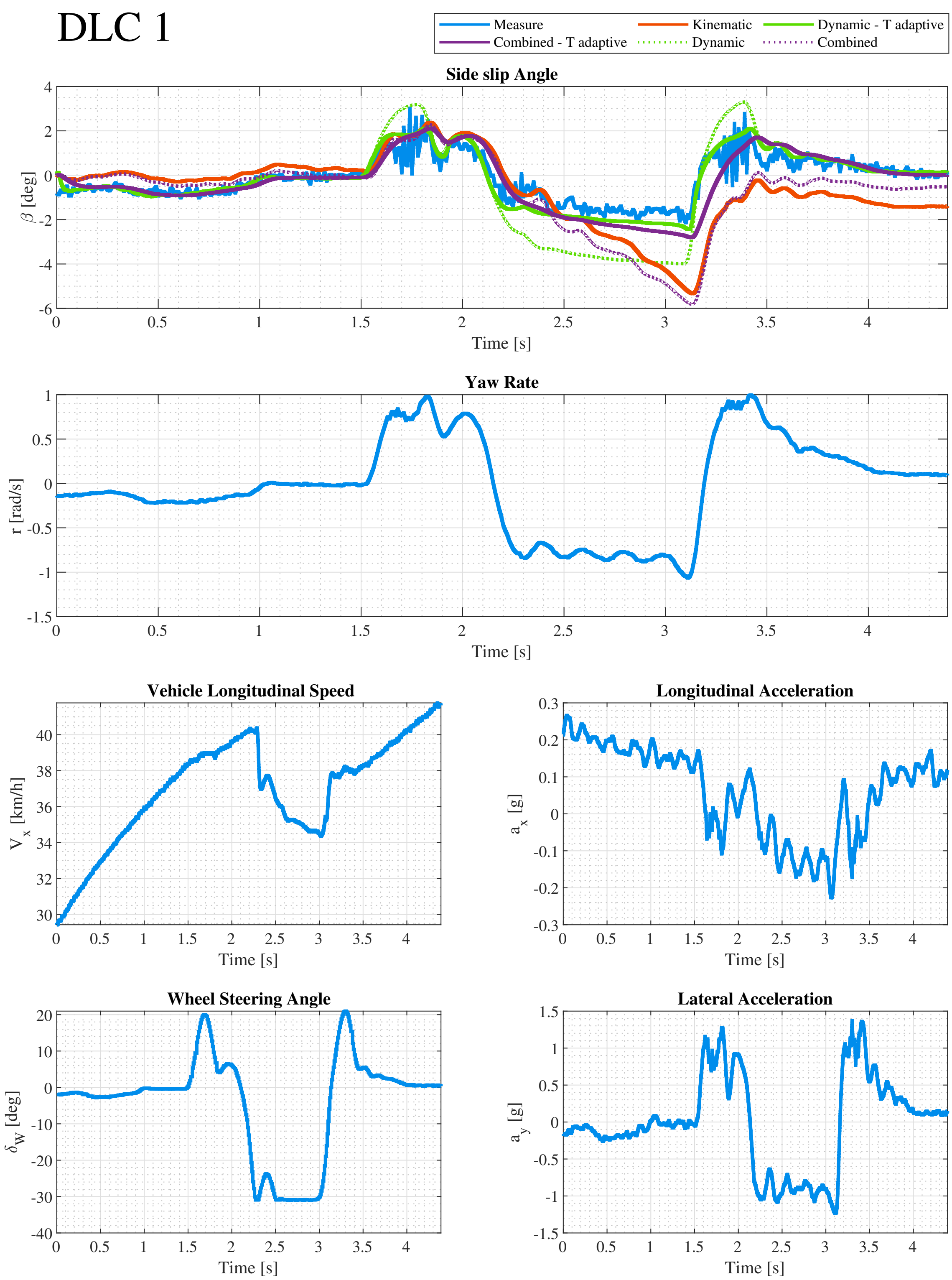

Figure 61: Sideslip enhanced estimation performance - DLC1

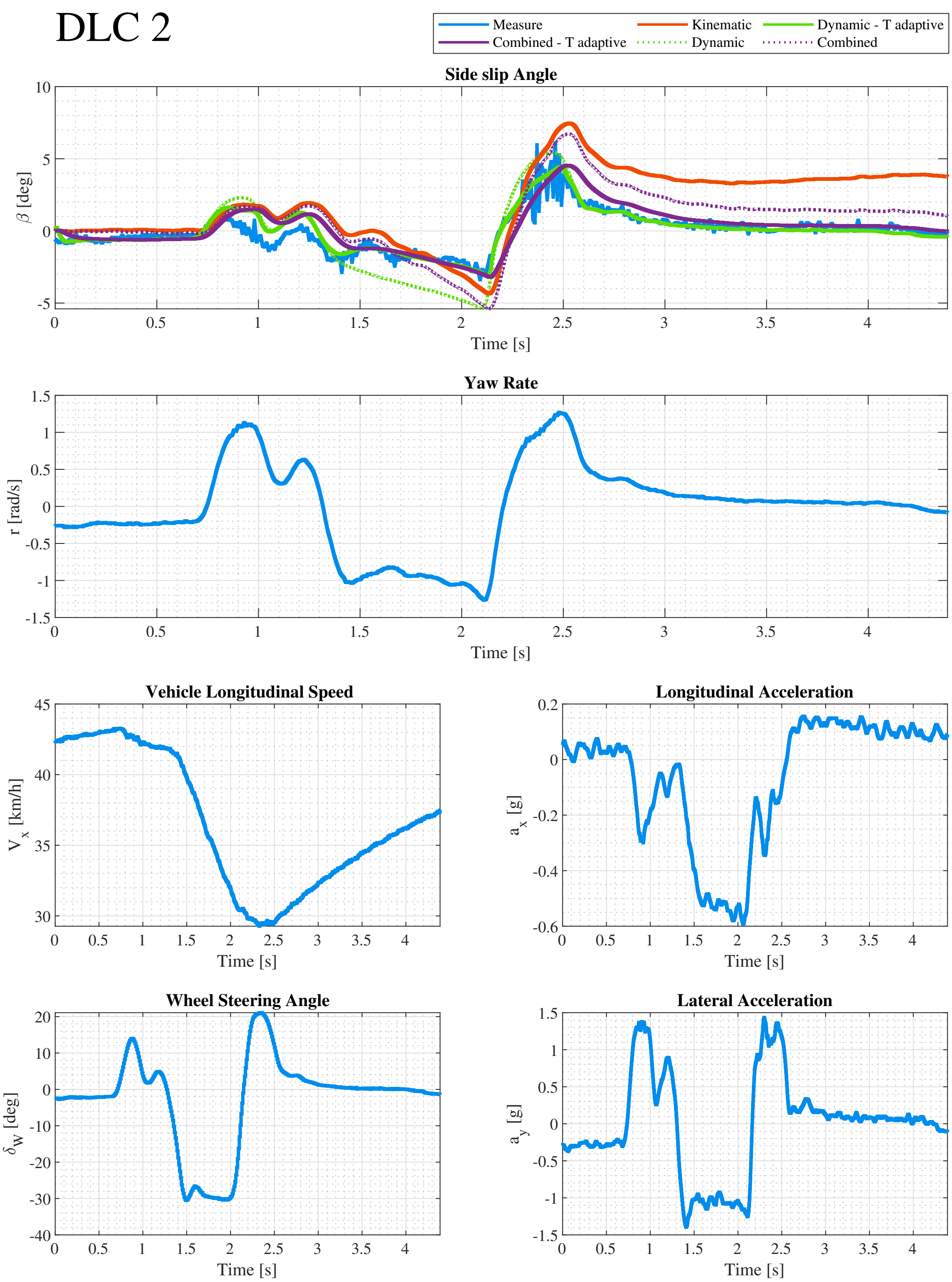

Figure 62: Sideslip enhanced estimation performance - DLC2

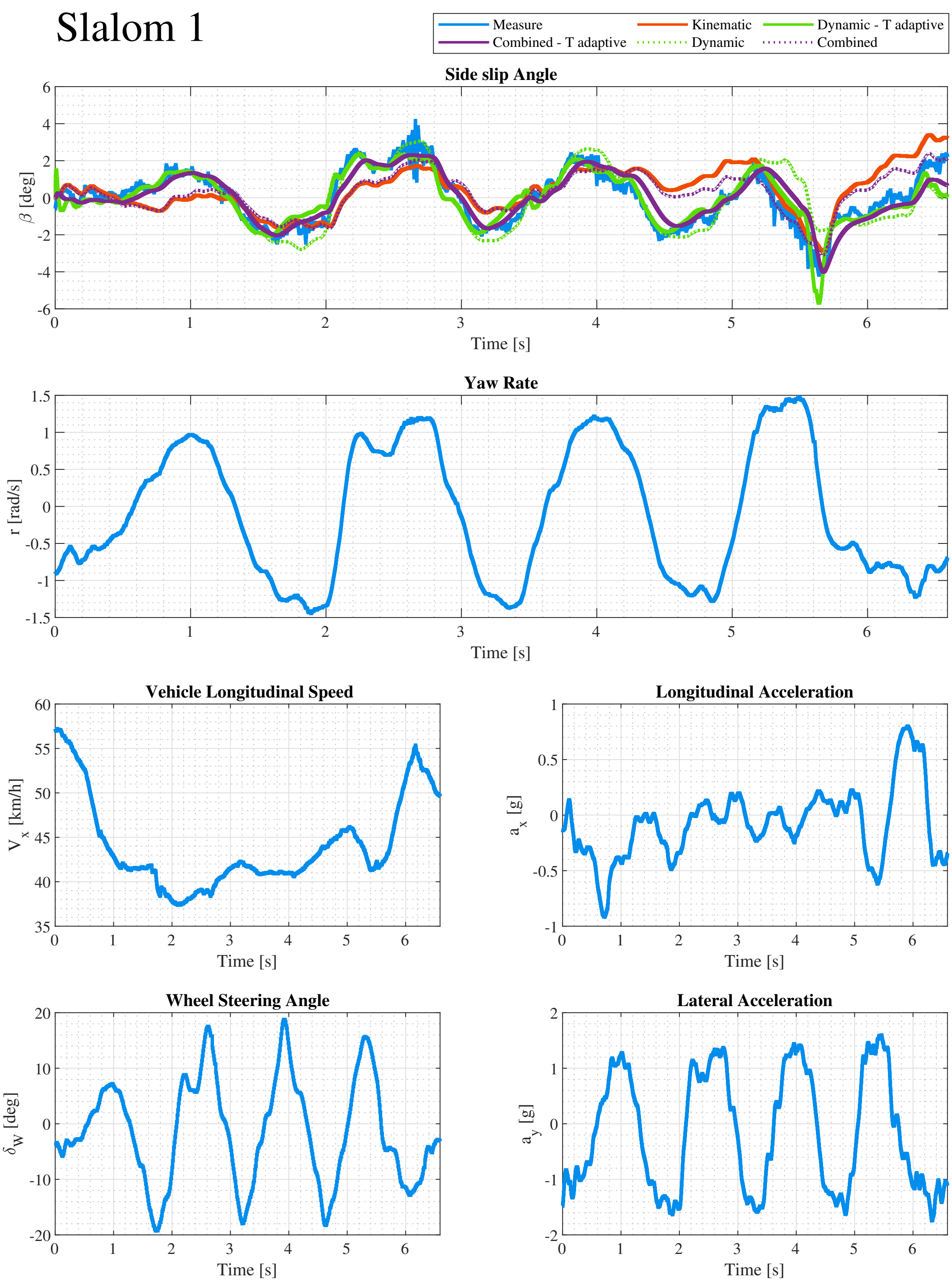

Figure 63: Sideslip enhanced estimation performance - Slalom1

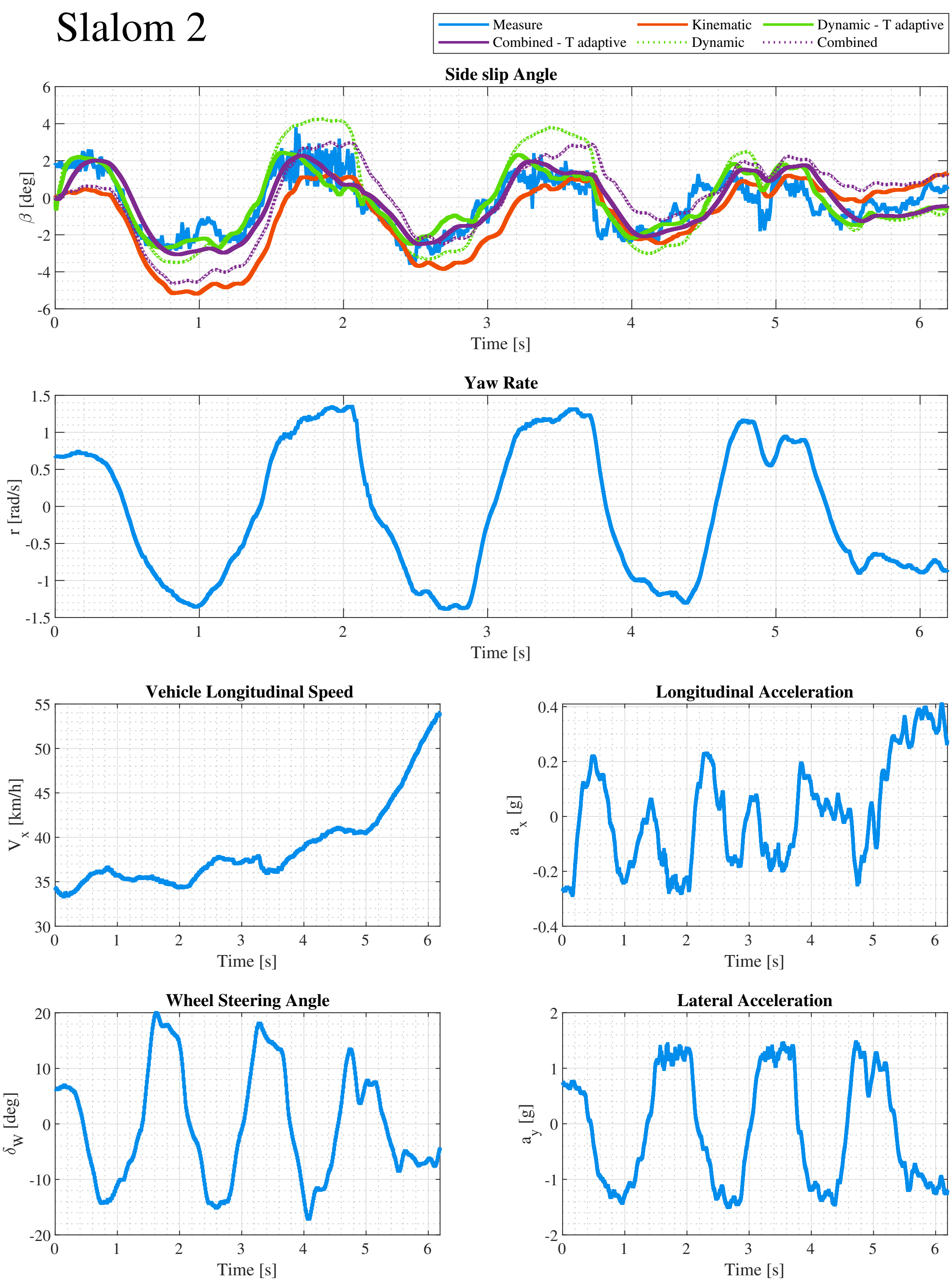

Figure 64: Sideslip enhanced estimation performance - Slalom2

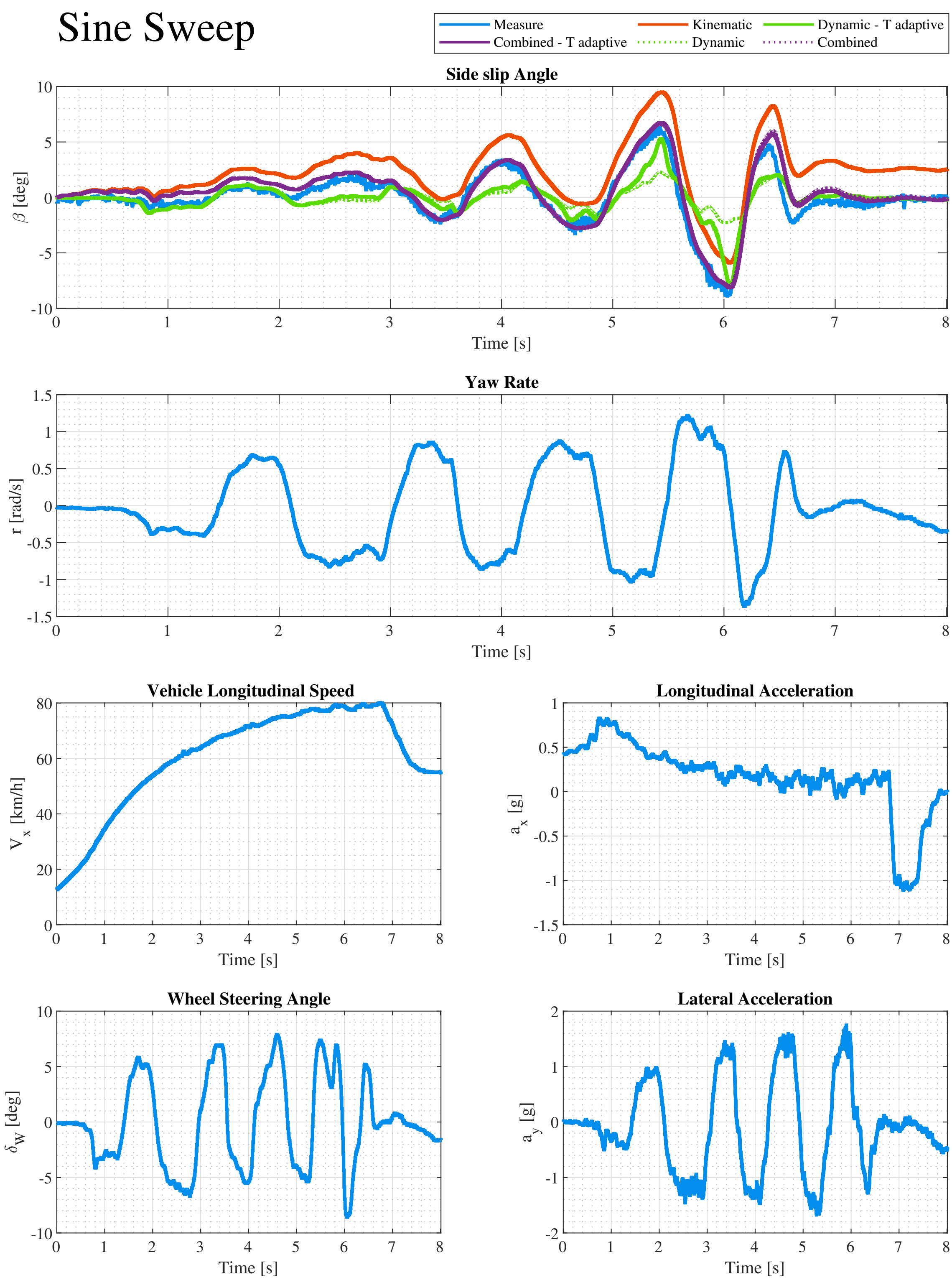

Figure 65: Sideslip enhanced estimation performance - Sine sweep steering

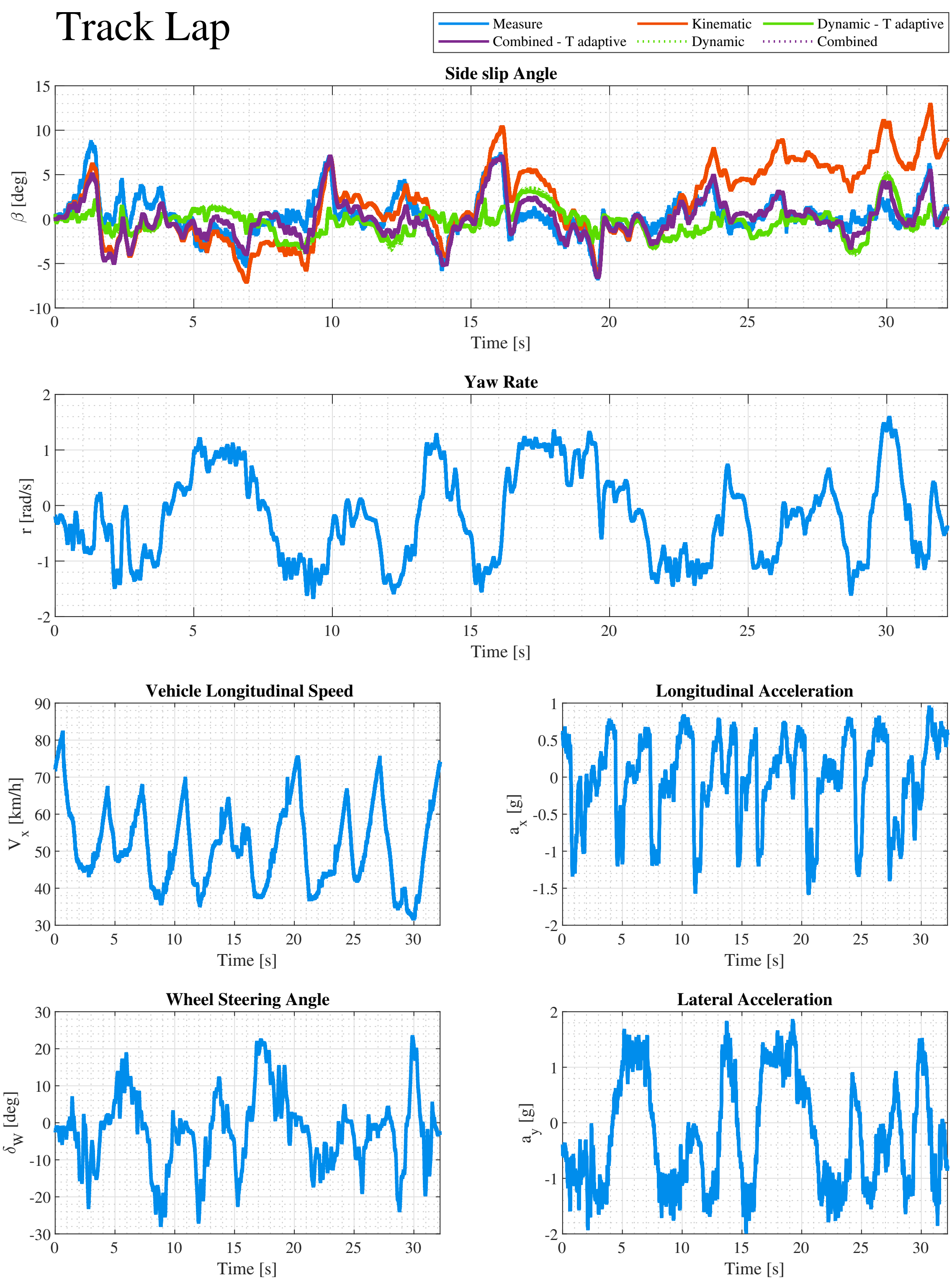

Figure 66: Sideslip enhanced estimation performance - Track lap

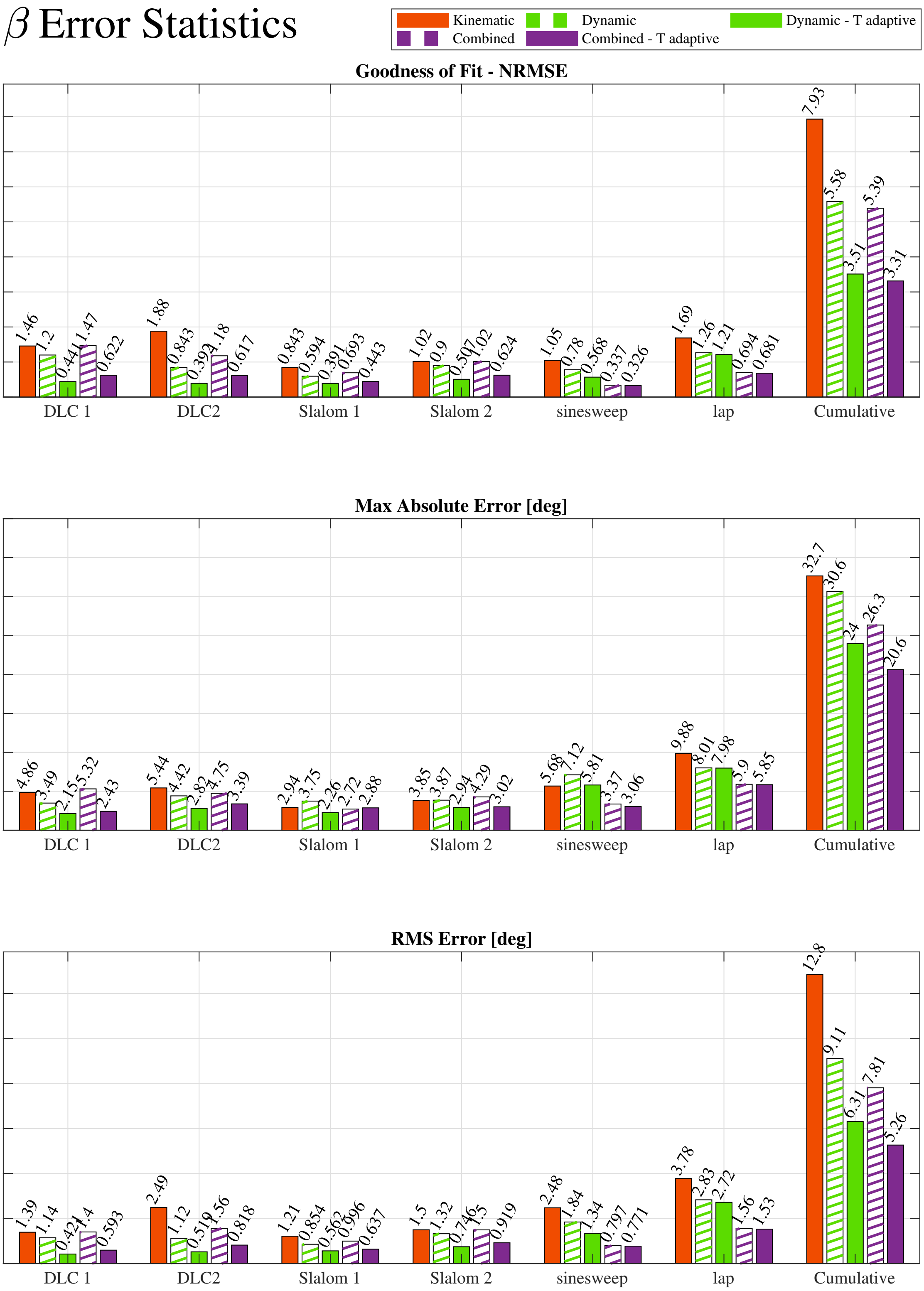

Figure 67: Sideslip estimation performance - bar chart KPI

The reasons why steering sine sweep and track lap are still challenging situations for the EKF can be the following:

- The traction force during these two maneuvers is not negligible. According to the elliptical approximation there must be a decrement in lateral performance when a longitudinal ground force is expressed. This is why during braking maneuvers and especially during wheel locks the estimation is not reliable. It can be clearly seen from the longitudinal acceleration plot during a track lap that the time spent at low longitudinal acceleration is negligible compared to the remaining.
- Both track lap and sine sweep steering are characterized by higher speeds with respect to DLC and slalom. This might have something to do with aerodynamics, that are not validated on track but only in wind tunnel.
- Both track lap and sine sweep steering excite the vehicle with higher steering frequencies, this is also a consequence of the higher speeds. At higher frequencies the behavior of the suspension system and the vertical bouncing of the tire becomes more relevant, especially if low pressures are used inside the tires. All these are not modeled inside the EKF.

5 Conclusions and future works

5.1 Torque Vectoring

5.1.1 Track test of Feed Forward controller

Due to a malfunction in the map selection system implemented in the steering wheel, the feedforward controller was always off during the track validation. New test session are planned to asses the performance of this controller that must work in parallel with the already validated feedback architecture.

5.1.2 Track test with new temperature based model

The torque vectoring algorithm uses the very same model implemented in EKF. Another test campaign must be performed in order to assess the controller behavior with the enhanced internal model, hoping in another increment in performance that is expected when an internal model of an optimal controller matches even better the characteristic of the plant.

5.1.3 Develop a model for wet operation, grip estimation

Based on this work, the adaptability of controllers to track conditions must be analyzed. An online grip estimation algorithm can be implemented in order to adapt the control output based on the 'measured' condition, without modeling which is the cause of that condition.

5.2 Side slip estimation

5.2.1 Dynamic and combined estimation blend

Dynamic an Kinematic estimation has revealed to be a life saver when it comes to more complex maneuvers. Nonetheless, there might be situations in which the dynamic only contribution is a better estimator than combined, as it was seen in DLC maneuvers and Slalom maneuvers. The same behavior is expected to happen during skidpad disciplines, in which the car runs under very low torque input in almost pure lateral operation.

A possible suggestion to address this problem can be to develop a rule based function that switches between the dynamic estimation and the combined estimation depending on the longitudinal acceleration , or even better the torque request or the longitudinal slip) and on the yaw rate derivative. Longitudinal slip is an indicator that tells us how much far we are from the pure lateral conditions, hence the higher the longitudinal speed and the higher the weight on the combined estimations. The yaw rate derivative is a symptom of both strong oversteering, if the derivative is coherent with the steering signal or understeering if the derivative has the opposite sign with respect to steering angle. Both these conditions are characterized by a loss of total grip of the vehicle, due to a high loss in grip at front or rear axle. As a matter of fact, if a strong loss of grip happens at the rear axle, no lateral force can counterbalance the centrifugal force apart from the yaw inertia of the vehicle. In the end, a suggestion can be to compute the absolute value of the yaw acceleration and the higher it is, the higher is the weight given to the combined estimation.

5.2.2 Possible implementation of a longitudinal model

The implementation of a longitudinal model, in order to have a combined lateral-longitudinal model, inside the EKF or TV is risky. Taken into account the high frequency nature of the slip, this might decrease the performance due to unwanted oscillatory behavior cause by high sensitivity of the tire Pacejka model to low longitudinal slip values. Maybe a pseudo-longitudinal-lateral model can be implemented while being fed by the commanded torques, that at least are known a priori and shouldn't be estimated.

Moreover, longitudinal slip must be estimated or measured. If the vehicle speed is measured somehow, sensors or gps, then the estimation of the longitudinal slip considering the rotational speed of the wheels can be performed and can give good results. If, instead, the vehicle speed is estimated considering the wheel speed, as it is done in 1.5.14, the wheel slip is hard to retrieve with the needed precision.

References

[1] Giancarlo Genta;Lorenzo Morello. The automotive chassis, volume 1, second edition. 2020.

[2] Giancarlo Genta;Lorenzo Morello. The automotive chassis, volume 2, second edition. 2020.

[3] Luca Massano; Raffaele Manca; Andrea Tonoli. Slip controller development for an electric 4wd formula student race car. 2023.

[4] Luis M. Castellanos Molina; Raffaele Manca; Shailesh Hegde; Nicola Amati ; Andrea Tonoli. Predictive handling limits monitoring and agility improvement with torque vectoring on a rear in-wheel drive electric vehicle. 2023.

[5] Federico Battaglino; Stefano Favelli; Andrea Tonoli. Slip controller development for an electric 4wd formula student race car. 2022.

[6] Angelo Bonfitto; Stefano Feraco; Marco Rossini; Francesco Carlomagno. Fuzzy logic method for the speed estimation in all-wheel drive electric racing vehicles. 2021.

[7] Michele Asperti; Michele Vignati; Edoardo Sabboni. Ontorque vectoring control: Review and comparison of state-of-the-art approaches. 2024.

[8] Tommaso Goggia; Aldo Sorniotti; Leonardo De Novellis; Antonella Ferrara; Patrick Gruber; Johan Theunissen; Dirk Steenbeke;Bernhard Knauder;Josef Zehetner. Integral sliding mode for the torque-vectoring control of fully electric vehicles: Theoretical design and experimental assessment. 2015.

[9] Alberto Parra; Davide Tavernini; Patrick Gruber; Aldo Sorniotti. On nonlinear model predictive control for energy-efficient torque-vectoring. 2022.

[10] A. Beliautsou, V.; Fedorova. Development of torque vectoring controller tuned with neural networks. 2022.

[11] Damrongrit (Neng) Piyabongkarn; Rajesh Rajamani; John A. Grogg; and Jae Y. Lew. Development and experimental evaluation of a slip angle estimator for vehicle stability control. 2009.

[12] Greg Welch; Gary Bishop. An introduction to the kalman filter. 2001.

[13] Attila Widner; Viktor Tihanyi; Tamàs tettamanti. Framework for vehicle dynamics model validation. 2022.

[14] Derek Seward. Race car design. 2014.

[15] Douglas L. Milliken illiam F. Milliken. Race car vehicle dynamics. 1994.

[16] H.B.Pacejka. Tyre and vehicle dynamics. 2002.